DEVELOPMENT AND CHARACTERISATION OF PLA/PBS-NANOCELLULOSE COMPOSITE SCAFFOLDS FOR CULTURING HEPATOCYTES-DERIVED HUMAN UMBILICAL CORD WHARTON'S JELLY MESENCHYMAL STEM CELLS

PONGSATORN POOPISUT

A Thesis Submitted in Partial Fulfillment of the Requirements for the
Degree of Doctoral of Philosophy in Biotechnology
Suranaree University of Technology
Academic Year 2024

การพัฒนาและการวิเคราะห์ลักษณะของโครงเลี้ยงเซลล์ที่ขึ้นรูปจาก PLA/PBS-นาโนเซลลูโลสสำหรับการเลี้ยงเซลล์ตับที่เปลี่ยนจากเซลล์ต้นกำเนิดมีเซ็นไคม์จากเนื้อเยื่อวาร์ตันเจลลี่ของสายสะดือมนุษย์

นายพงศธร ภูพิศุทธิ์

วิทยานิพนธ์นี้เป็นส่วนหนึ่งของการศึกษาตามหลักสูตรปริญญาปรัชญาดุษฎีบัณฑิต
สาขาวิชาเทคโนโลยีชีวภาพ
มหาวิทยาลัยเทคโนโลยีสุรนารี
ปีการศึกษา 2567

DEVELOPMENT AND CHARACTERISATION OF PLA/PBS–NANOCELLULOSE COMPOSITE SCAFFOLDS FOR CULTURING HEPATOCYTES-DERIVED HUMAN UMBILICAL CORD WHARTON'S JELLY MESENCHYMAL STEM CELLS

Suranaree University of Technology has approved this thesis submitted in partial fulfillment of the requirements for the Degree of Doctor of Philosophy.

Thesis Examining Committee

.....

(Assoc. Prof. Dr. Prakit Sukyai)
Chairperson

.....

(Assoc. Prof. Dr. Apichat Boontawan)
Member (Thesis Advisor)

Kanjana Thumanu
.....

(Dr. Kanjana Thumanu)
Member (Thesis Co-advisor)

.....

(Prof. Dr. Rangsun Parnpai)
Member

.....

(Assoc. Prof. Dr. Mariena Ketudat-Cairns)
Member

.....

(Assoc. Prof. Dr. Yupaporn Ruksakulpiwat)
Vice Rector for Academic Affairs
and Quality Assurance

.....

(Prof. Dr. Neung Teaumroong)
Dean of Institute of Agricultural
Technology

พงศธร ภูพิศุทธิ์: การพัฒนาและการวิเคราะห์ลักษณะของโครงเลี้ยงเซลล์ที่ขึ้นรูปจาก PLA/PBS-นาโนเซลลูโลสสำหรับการเลี้ยงเซลล์ตับที่เปลี่ยนจากเซลล์ต้นกำเนิดมีเซ็นไคม์จากเนื้อเยื่อวาร์ตันเจลลี่ของสายสะดือมนุษย์ อาจารย์ที่ปรึกษา: รศ.ดร.อภิชาติ บุญทาวัน, 104 หน้า.

คำสำคัญ: โครงเลี้ยงเซลล์/นาโนเซลลูโลส/PLA/PBS/เซลล์ตับ/เซลล์ต้นกำเนิดมีเซ็นไคม์จากเนื้อเยื่อวาร์ตันเจลลี่.

วัสดุคอมโพสิตที่มีคุณสมบัติเฉพาะตัวเป็นที่ต้องการมากขึ้น สำหรับการใช้งานด้านวิศวกรรมเนื้อเยื่อ งานนี้มุ่งเป้าไปที่การผลิตโครงเลี้ยงเซลล์จากวัสดุชีวภาพผสมนาโนเซลลูโลสเพื่อใช้สำหรับวิจัยวิศวกรรมเนื้อเยื่อตับ ซึ่งกากชานอ้อยจะถูกใช้เป็นวัตถุดิบเริ่มต้นสำหรับการสกัดนาโนเซลลูโลส โดยผสมผสานการลดขนาดด้วยแรงดันสูง (30,000 psi, 15 รอบ) และย่อยด้วยเอนไซม์ความเข้มข้น 7% นาโนเซลลูโลสที่ได้มีขนาดเฉลี่ย 278.9 นาโนเมตร ดัชนีการกระจายตัว (PDI) 0.752 และดัชนีความเป็นผลึก 50.00% จากนั้นนาโนเซลลูโลสนี้จะถูกผสมกับพลาสติกชีวภาพโพลีแลกติกแอซิด (PLA) และโพลีบิวทิลีนซักซิเนต (PBS) สำหรับการผลิตโครงเลี้ยงเซลล์โดยเทคนิคการผลิตฟิล์มบาง อัตราส่วนของวัสดุคอมโพสิตได้รับการปรับให้เหมาะสมโดยใช้วิธีการพื้นผิวการตอบสนอง (RSM) ส่งผลให้ได้องค์ประกอบที่เหมาะสมคือ PLA 65.00%, PBS 26.82% และนาโนเซลลูโลส 8.18% ตามน้ำหนัก การประเมินความเป็นพิษต่อเซลล์ในหลอดทดลองของโครงเลี้ยงเซลล์ที่ปรับให้เหมาะสมแสดงให้เห็นความสามารถในการมีชีวิตของเซลล์โดยเฉลี่ยสูงถึง 96.65% นอกจากนี้ เซลล์ต้นกำเนิดมีเซนไคจากวุ้นวาร์ตันของมนุษย์ (hWJ-MSCs) ที่เพาะเลี้ยงบนโครงยึดแสดงให้เห็นถึงศักยภาพในการพัฒนาไปเป็นกลุ่มเซลล์ตับในช่วงเวลา 17 วัน งานวิจัยนี้ถือเป็นก้าวแรกที่สำคัญในการพัฒนาโครงเลี้ยงเซลล์ใหม่ที่ใช้เซลลูโลสเป็นฐานสำหรับการประยุกต์ใช้ทางวิศวกรรมเนื้อเยื่อตับ

สาขาเทคโนโลยีชีวภาพ ลายมือชื่อนักศึกษา.....

ปีการศึกษา 2567 ลายมือชื่ออาจารย์ที่ปรึกษา.....

ลายมือชื่ออาจารย์ที่ปรึกษาร่วม Kanjana Thumanu.....

PONGSATORN POOPISUT: DEVELOPMENT AND CHARACTERISATION OF PLA/PBS–NANOCELLULOSE COMPOSITE SCAFFOLDS FOR CULTURING HEPATOCYTES-DERIVED HUMAN UMBILICAL CORD WHARTON'S JELLY MESENCHYMAL STEM CELLS. THESIS ADVISOR: ASSOC. PROF. APICHAT BOONTAWAN, Ph.D., 104 PP.

Keywords: scaffolds/nanocellulose/PLA/PBS/hepatocytes/Wharton's jelly mesenchymal stem cells.

Composite materials with tailored properties are increasingly sought after for tissue engineering applications. This work aimed to fabricate a nanocellulose-based biopolymer scaffold specifically designed for liver tissue engineering. Natural sugarcane bagasse was used as the raw material for nanocellulose extraction, employing a synergistic approach that combined high-pressure homogenization (30,000 psi, 15 cycles) and enzymatic digestion (7% enzyme concentration). The resulting nanocellulose exhibited an average size of 278.9 nm, a polydispersity index (PDI) of 0.752, and a crystallinity index of 50.0%. Subsequently, this optimized nanocellulose was blended with poly lactic acid (PLA) and poly butylene succinate (PBS), for scaffold production using a film casting technique. The composite material ratio was meticulously optimized using response surface methodology (RSM), leading to an optimal composition of 65.00 wt% PLA, 26.82 wt% PBS, and 8.18 wt% nanocellulose. In vitro cytotoxicity evaluation of the optimized scaffold revealed a high average cell viability of 96.65%. Furthermore, human Wharton's Jelly Mesenchymal Stem Cells (hWJ-MSCs) seeded onto the scaffold exhibited the potential to differentiate towards a hepatocyte lineage over a 17 days period. This work represents a significant initial step towards the development of novel nanocellulose-based scaffolds for liver tissue engineering applications

School of Biotechnology

Academic Year 2024

Student's Signature.....

Advisor's Signature.....

Co-Advisor's Signature. Kanjana Thumanu

ACKNOWLEDGEMENTS

I would like to express my deepest and most sincere gratitude to my research advisor, Assoc. Prof. Dr. Apichat Boontawan. His guidance throughout this research journey has been invaluable. He provided me with the opportunity to conduct this research and equipped me with the methodology to carry it out and present the findings with utmost clarity. Working and learning under his mentorship has been a great privilege and honor.

Besides my advisor, I would like to thank my thesis co-advisor, Dr. Kanjana Thumanu, for her continuous support throughout my PhD studies and research.

I am grateful to the Embryo Technology and Stem Cell Research Center for their support in facilitating this research. I would also like to extend my thanks to Prof. Dr. Rangsun Parnpai for his genuine support within the Embryo Technology and Stem Cell Research Center, which significantly contributed to the successful completion of this thesis.

My sincere thanks also go to my friends and research colleagues for their constant encouragement.

Finally, I would like to express my gratitude to all those who have directly or indirectly supported me in completing this research work.

PONGSATORN POOPISUT

CONTENTS

Page

CONTENTS (Continued)

Page

CONTENTS (Continued)

Page

LIST OF TABLES

Table **Page**

LIST OF FIGURES

Figure **Page**

LIST OF FIGURES (Continued)

Figure **Page**

LIST OF FIGURES (Continued)

Figure **Page**

LIST OF ABBREVIATIONS

PLA	=	Poly Lactic Acid
PBS	=	Poly Butylene Succinate
CNF	=	Cellulose Nanofibrils
CNC	=	Cellulose Nanocrystals
BNC	=	Bacterial Nanocellulose
TEMPO	=	2,2,6,6-tetramethylpiperidine-1-oxyl
OPEFB	=	Oil Palm Empty Fruit Bunches
TEM	=	Transmission Electron Microscopy
SEM	=	Scanning Electron Microscope
XRD	=	X-Ray Diffractometer
FTIR	=	Fourier-Transform Infrared Spectroscopy
MSCs	=	Mesenchymal stem cells
RO	=	Reverse Osmosis
NMP	=	N-methyl pyrrolidone
hWJ-MSCs	=	Human Wharton's Jelly mesenchymal stem cells
MTT	=	3-(4,5-dimethylthiazol-2-yl)-2,5-diphenyl tetrazolium bromide
AFP	=	Alpha-fetoprotein
CK18	=	Cytokeratin 18
ALB	=	Albumin
PFA	=	Paraformaldehyde
FESEM	=	Field emission scanning electron microscopy
PDI	=	Polydispersity index
PCA	=	Principal component analysis
FTIR	=	Fourier Transform Infrared
CI	=	Crystallinity Index
TGA	=	Thermogravimetric analysis
DSC	=	Differential scanning calorimetry

CHAPTER I
INTRODUCTION

1.1 Significance of study

Sugarcane production plays a vital role in the global sugar industry, reaching approximately 1.9 billion metric tons in 2022 for sugar extraction (Food and Agriculture Organization of the United Nations, 2023). However, processing generates a significant by-product, sugarcane bagasse, which accounts for roughly 30% of the sugarcane stalk's dry weight (Molina-Cortés, A., Quimbaya, M., Toro-Gomez, A., & Tobar-Tosse, F., 2023). Traditionally, bagasse has been used for on-site electricity generation within sugar factories. However, exploring alternative applications is crucial for efficient waste management and resource utilization.

Nanocellulose, a high-value material derived from renewable resources, offers a promising solution for sugarcane bagasse valorization. Nanocellulose production from bagasse can not only reduce waste generation within the sugar industry but also unlock new avenues for material development. Nanocellulose possesses remarkable properties, including biodegradability, lightweight structure, and cost-effectiveness, making it highly desirable in various fields. Notably, the nanocellulose market has witnessed significant growth, reaching nearly USD 146.7 million in 2019, with a projected industry trend of 21.4% growth from 2020 to 2026 (Kiran, 2020). The versatility of nanocellulose extends to diverse applications, including electronics (generators, solar cells, touch sensors), consumer goods (computers, mobile phones), and the healthcare sector (biomedical engineering, tissue engineering) (Kiran, 2020)

This study investigates the utilization of sugarcane bagasse as a raw material for nanocellulose production using a combined approach of high-pressure homogenization pretreatment and enzymatic processing. The extracted nanocellulose will then be blended with PLA/PBS to develop biopolymer scaffolds for tissue engineering applications.

1.2 Research objective

1.2.1 To investigate the effect of co-operated high-pressure homogenization with enzymatic hydrolysis on the size reduction of nanocellulose derived from sugarcane bagasse.

1.2.2 To optimize the ratio of PLA, PBS, and nanocellulose for the production of biocompatible scaffolds with desired mechanical properties suitable for tissue engineering applications.

1.2.3 To develop a bio-scaffold incorporating optimized PLA/PBS and nanocellulose composite for artificial liver bioreactor application.

1.3 Research hypothesis

1.3.1 Sugarcane bagasse, due to its high cellulose content, is a suitable raw material for producing nanocellulose with desired properties for tissue engineering applications.

1.3.2 Co-operated high-pressure homogenization combined with enzymatic hydrolysis will significantly reduce the size of nanocellulose particles derived from sugarcane bagasse compared to using these techniques individually.

1.3.3 Incorporation of nanocellulose into biopolymer scaffolds will increase their hydrophilicity compared to scaffolds without nanocellulose.

1.3.4 Biopolymer scaffolds containing optimized ratios of PLA, PBS, and nanocellulose will exhibit superior mechanical properties, and hydrophilicity compared to scaffolds with non-optimized ratios, making them more suitable for tissue engineering applications.

1.4 Scope and limitation of study

This study investigates the potential of sugarcane bagasse as a raw material for nanocellulose production for tissue engineering applications. Nanocellulose will be isolated from pretreated sugarcane bagasse using a combined approach of high-pressure homogenization and enzymatic hydrolysis. The structure and properties of the extracted nanocellulose will be characterized. Subsequently, the nanocellulose will be blended with PLA and PBS in various ratios to develop biocompatible scaffolds

for tissue engineering. The optimal ratio of PLA, PBS, and nanocellulose in the scaffold will be determined based on its properties. Finally, the biocompatibility of the optimized scaffold will be evaluated using in vitro cell culture with human Wharton's jelly-derived mesenchymal stem cells (hWJ-MSCs) undergoing differentiation towards hepatocyte lineage on the scaffold.

1.5 Expected results

1.5.1 The combined application of high-pressure homogenization and enzymatic hydrolysis is expected to significantly reduce the size of nanocellulose particles derived from sugarcane bagasse compared to using these techniques individually.

1.5.2 Incorporation of nanocellulose into biopolymer scaffolds is anticipated to increase their hydrophilicity, as measured by water contact angle analysis.

1.5.3 The optimized nanocellulose-based biopolymer scaffolds are expected to exhibit minimal cytotoxicity towards hWJ-MSCs as assessed by cell viability assays like MTT assay

1.5.4 This study aims to evaluate the potential of the optimized scaffold to support the differentiation of hWJ-MSCs towards the hepatocyte lineage.

CHAPTER II

LITERATURE REVIEW

2.1 Lignocellulosic material

Lignocellulosic materials, derived from plant biomass, represent a vast and renewable resource with significant potential for the production of biofuels, biochemicals, and biomaterials. These materials are primarily composed of cellulose, hemicellulose, and lignin, forming a complex and recalcitrant structure. A comprehensive understanding of their composition, structure, and properties is crucial for developing efficient and sustainable utilization strategies.

2.1.1 Main component of lignocellulose

Lignocellulosic materials are composed of three primary components:

2.1.1.1 Cellulose is the most abundant biopolymer on Earth, primarily found in plant cell walls, algae, and some bacteria, consisting of β-D-glucose units linked by β-1,4-glycosidic bonds (Klemm et al., 2005) as show in figure 2.1a It is a crucial structural component that provides mechanical strength and stability to plant tissues. The structure of cellulose consists of linear chains of glucose molecules arranged in a highly ordered manner, forming crystalline and amorphous regions (fig 2.1b) (Moon et al., 2011). The crystalline domains contribute to its mechanical strength, while the amorphous regions provide flexibility and facilitate enzymatic hydrolysis. Cellulose chains are stabilized by extensive intra- and intermolecular hydrogen bonding, which influences its solubility and processability (Habibi et al., 2010). Understanding the hierarchical structure of cellulose is essential for tailoring its properties for various applications, including nanocellulose production, biodegradable materials, and biomedical scaffolds (Dufresne, 2012). Recent studies have focused on modifying cellulose structure through chemical and enzymatic treatments to enhance its functionality and expand its industrial applications.

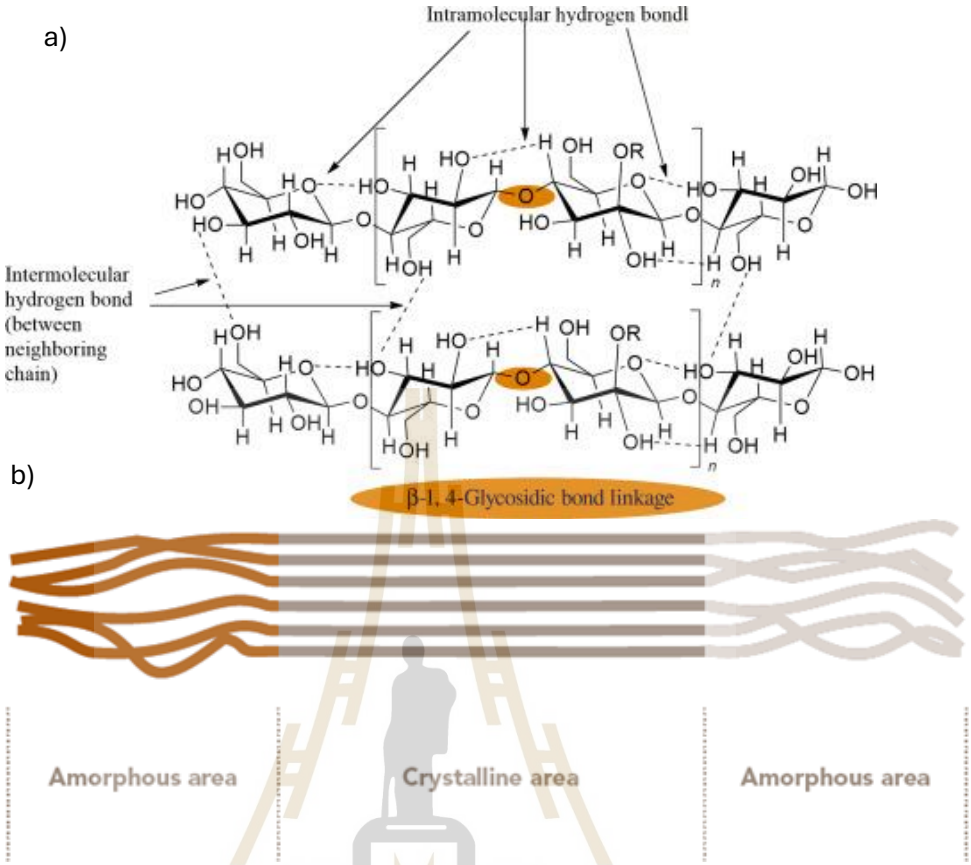

Figure 2.1 Chemical structure of cellulose a) β-D-glucose units linked by β-1,4-glycosidic bonds., b) crystalline and amorphous regions.

Cellulose exists in two primary polymorphic forms: Cellulose I (native cellulose) and Cellulose II (regenerated cellulose). Cellulose I, the naturally occurring form found in plants, bacteria, and algae, consists of parallel β-1,4-linked glucan chains and is highly crystalline, mechanically strong, but difficult to dissolve. It exists in two subtypes: Cellulose Iα, which has a triclinic crystal structure and is predominantly found in bacteria and algae (Sugiyama et al., 1991) as shown in figure 2.2 (a, c) and Cellulose Iβ, which has a monoclinic structure and is primarily present in higher plants and tunicates (Nishiyama et al., 2002) as shown in figure 2.2 (b, d). Due to its superior mechanical properties, Cellulose I plays a crucial role in the production of nanocellulose, which is widely applied in biomedical materials and advanced composites.

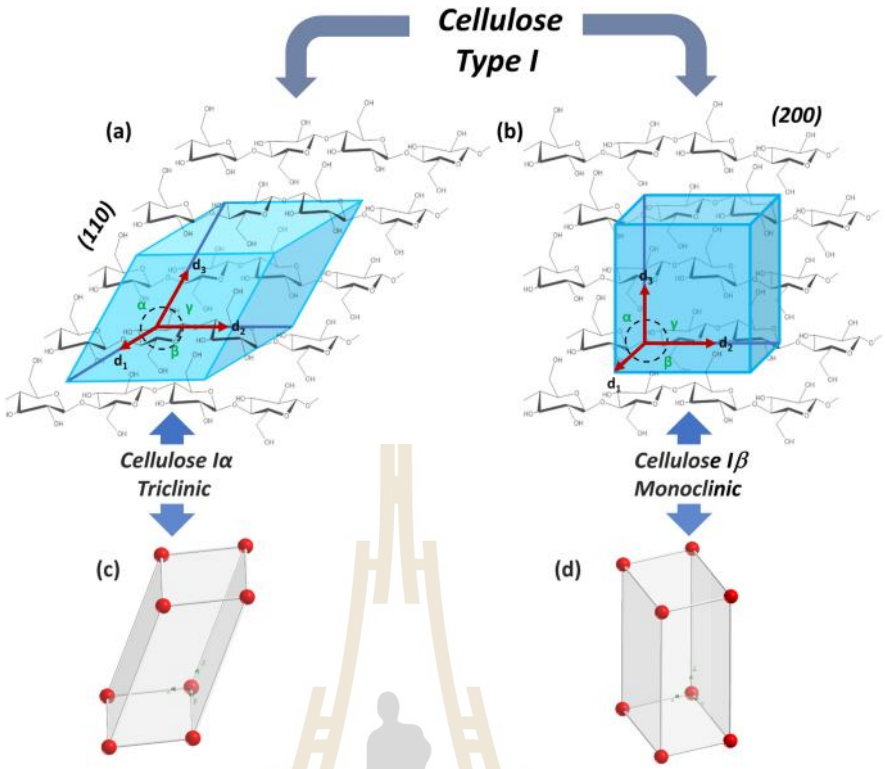

Figure 2.2 Primary polymorphic forms a) Cellulose Iα, b) Cellulose Iβ ,and crystal structure ; c) triclinic pattern , d) monoclinic pattern(Hernández-Varela, J.D. et al., 2021)

Cellulose II, formed through mercerization or regeneration, features an antiparallel chain arrangement with stronger hydrogen bonding, making it the most thermodynamically stable form of cellulose (O'Sullivan, 1997). Unlike Cellulose I, which is naturally occurring, Cellulose II is more soluble, accessible to enzymatic hydrolysis, and easier to process, making it preferable for industrial applications such as biofuel production and textiles (Marrinan and Mann, 1956). The chemical structures of cellulose I and cellulose II were compared, as shown in figure 2.3. Its enhanced solubility and processability contribute to its widespread use in sustainable materials, pharmaceuticals, and advanced cellulose-based composites.

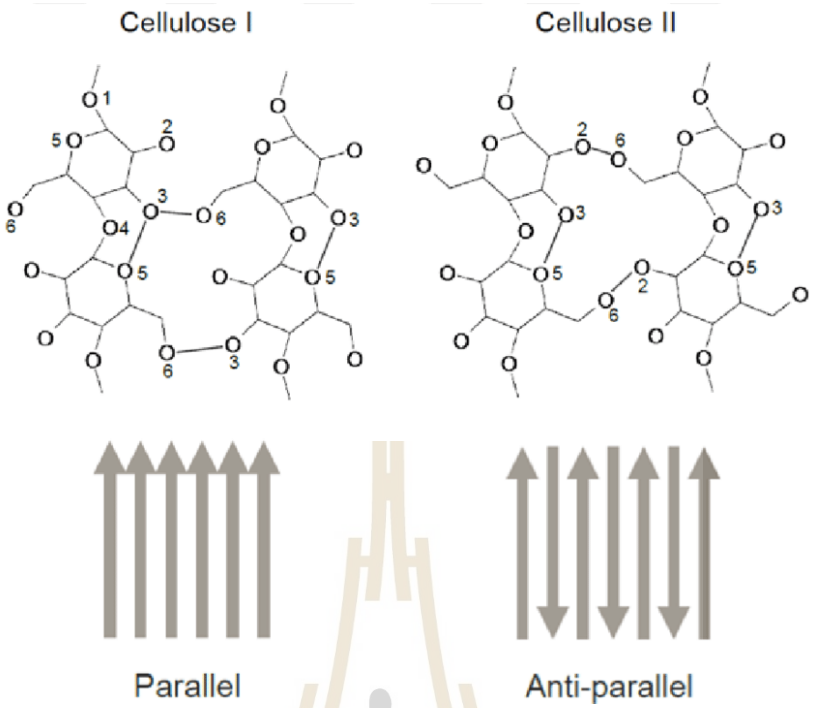

Figure 2.3 Comparison of chemical structures cellulose I and cellulose II (Kushan E., 2020)

2.1.1.2 Hemicellulose is a heterogeneous polysaccharide that, unlike cellulose, consists of branched chains of various sugar monomers (fig 2.4 a-e) such as xylose, mannose, arabinose, and galactose (Scheller and Ulvskov, 2010). It forms a matrix with cellulose and lignin in plant cell walls, providing flexibility and linking structural components. The amorphous nature of hemicellulose makes it more susceptible to hydrolysis compared to cellulose, allowing for easier breakdown in biorefinery processes (Peng et al., 2012). The composition and structure of hemicellulose vary among plant species, with xylans being the predominant type in hardwoods and glucomannans in softwoods. Due to its hydrophilic nature, hemicellulose has potential applications in biodegradable films, food additives, and biofuels, where structural modifications improve its processability and functional properties (Ebringerová, 2006).

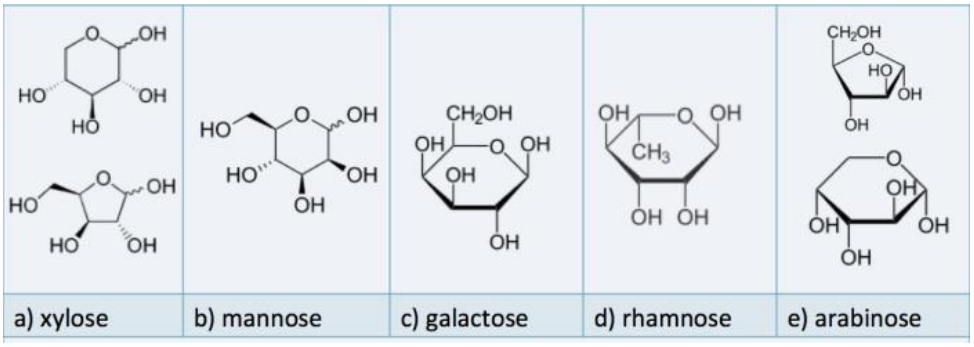

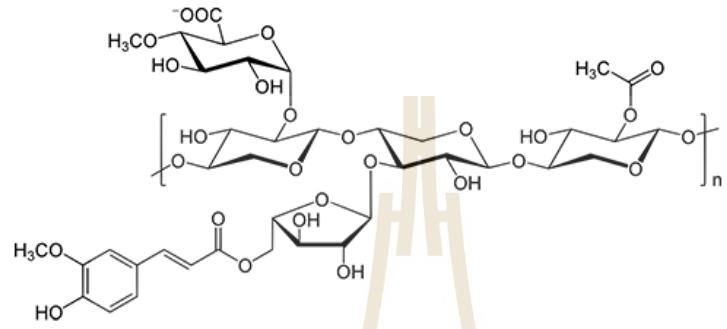

f)

Figure 2.4 various sugar monomers a) xylose, b) mannose, c) galactose, d) rhamnose, e) arabinose and f) structure of hemicellulose (xylan) (Pennsylvania State University, 2024).

2.1.1.3 Lignin is an amorphous, highly branched aromatic polymer as shown in Fig 2.5 that provides rigidity and hydrophobicity to the plant cell wall (Boerjan, Ralph, and Baucher, 2003). Composed mainly of phenylpropanoid units, such as guaiacyl (G), syringyl (S), and p-hydroxyphenyl (H) monomers, lignin acts as a binding agent between cellulose and hemicellulose, offering structural support and resistance against microbial degradation (Ralph et al., 2004). Its complex and heterogeneous structure makes lignin difficult to degrade, posing challenges in biomass processing and biofuel production. However, lignin has significant potential for valorization, including applications in bioplastics, adhesives, and carbon-based materials (Laurichesse and Avérous, 2014). Ongoing research focuses on efficient lignin extraction and modification strategies to enhance its functionality and integration into various industries.

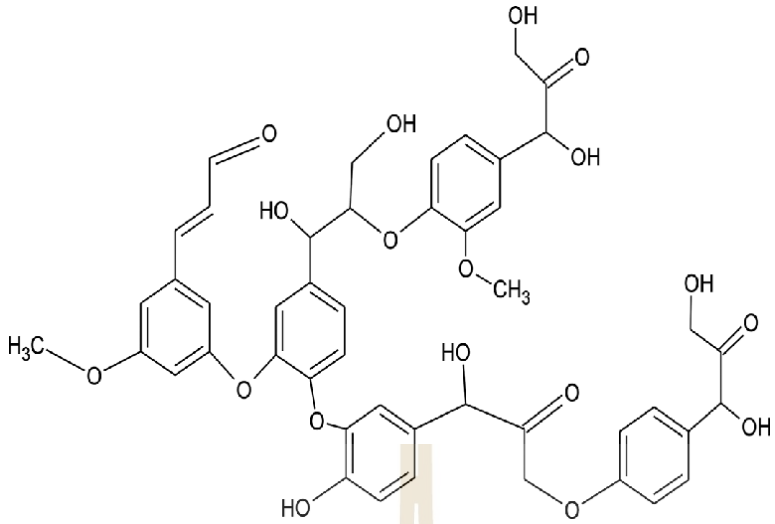

Figure 2.5 Chemical structure of lignin (Mahmood et al. 2018)

2.1.2 Structural Interactions and Recalcitrance

Lignocellulosic materials exhibit significant structural recalcitrance due to the intricate interactions between cellulose, hemicellulose, and lignin as shown in Fig 2.6 which hinder enzymatic hydrolysis and biomass conversion (Zhao et al., 2012). The crystalline nature of cellulose, the complex branching of hemicellulose, and the hydrophobic, cross-linked lignin network create a rigid, protective barrier that resists microbial and enzymatic degradation (Himmel et al., 2007). Lignin, in particular, acts as a physical shield around cellulose microfibrils, limiting enzyme accessibility and contributing to biomass recalcitrance (Li et al., 2014). Additionally, strong covalent and non-covalent interactions between lignin and polysaccharides, such as ester and ether linkages, further enhance this resistance (Rahikainen et al., 2013). Various pretreatment strategies, including chemical, enzymatic, and mechanical processes, have been explored to disrupt these interactions and enhance the efficiency of lignocellulosic biomass conversion into biofuels and biochemicals (Sun and Cheng, 2002). Understanding these structural interactions is crucial for optimizing biomass deconstruction methods and improving the cost-effectiveness of lignocellulosic biorefineries.

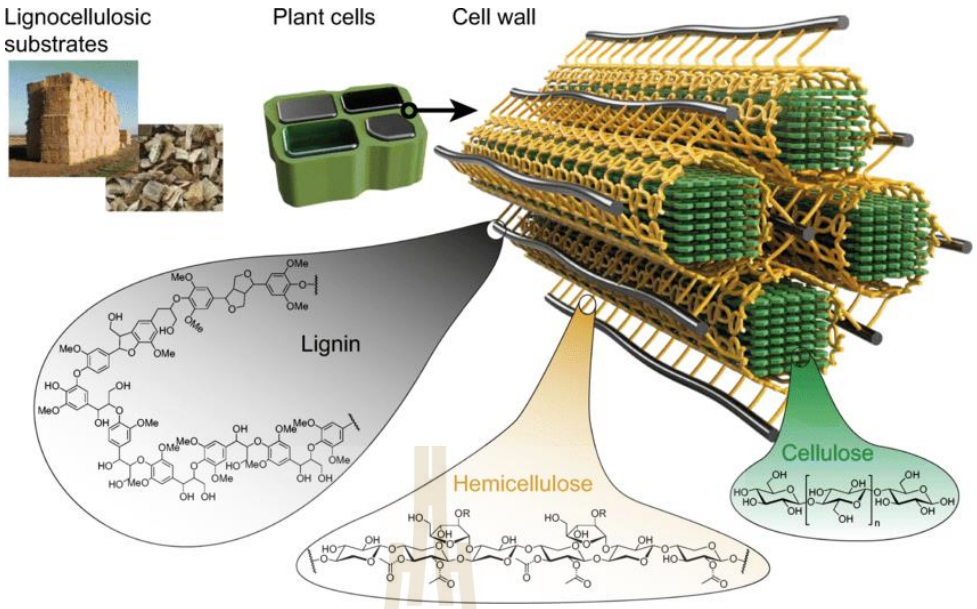

Figure 2.6 Components and structure of lignocellulosic materials (Brethauer et al., 2020)

2.1.3 Pretreatment and Bioconversion Strategies

Effective pretreatment and bioconversion strategies are crucial for overcoming the recalcitrance of lignocellulosic biomass, enhancing enzymatic hydrolysis, and improving the efficiency of biofuel and biochemical production (Mosier et al., 2005). Pretreatment methods include physical (e.g., milling and grinding), chemical (e.g., acid, alkaline, and organosolv treatments), physicochemical (e.g., steam explosion and liquid hot water), and biological approaches (e.g., microbial and enzymatic treatments) (Alvira et al., 2010). These strategies aim to break down the complex lignocellulosic structure by disrupting lignin-carbohydrate linkages, increasing cellulose accessibility, and reducing hemicellulose complexity (Mood et al., 2013). Bioconversion processes, such as enzymatic saccharification and microbial fermentation, play a key role in transforming pretreated biomass into fermentable sugars and valuable bio-products (Chandra et al., 2007). Recent advancements in consolidated bioprocessing (CBP), genetic engineering of microorganisms, and enzyme cocktail optimization have further improved conversion efficiency and economic feasibility (Lynd et al., 2008). Continued research on integrating pretreatment and bioconversion strategies is essential to advancing sustainable bioenergy and bioproduct industries.

2.1.4 Industrial Applications

Biomass for industrial applications is sourced from agricultural residues (such as straw, husks, and bagasse), forestry waste (including wood chips, sawdust, and bark), dedicated energy crops (like switchgrass and miscanthus), and organic waste (municipal solid waste, animal manure, and food waste). These feedstocks serve as raw materials for bio-based products, including biofuels, bioplastics, and biofertilizers. However, their availability and sustainability depend on land use, climate conditions, and advancements in biomass processing technologies. As industries emphasize renewable resources, optimizing biomass utilization is crucial for enhancing energy production, reducing carbon emissions, and promoting eco-friendly material development (U.S. Department of Energy, 2024; National Renewable Energy Laboratory, 2024).

Lignocellulosic materials have widespread industrial applications, ranging from biofuels and biochemicals to composite materials and biomedical products. The conversion of lignocellulosic biomass into bioethanol, biodiesel, and biogas offers a renewable alternative to fossil fuels, contributing to sustainable energy solutions (Ragauskas et al., 2006). In addition, lignocellulose-derived nanocellulose and lignin-based materials are used in packaging, coatings, and environmentally friendly plastics (Dufresne, 2012). The pharmaceutical and biomedical fields have also explored the use of lignocellulosic materials in drug delivery systems, wound dressings, and tissue engineering scaffolds due to their biocompatibility and mechanical strength (Chinga, 2018). Furthermore, lignocellulosic byproducts serve as animal feed, soil conditioners, and raw materials for high-value chemicals such as furfural, levulinic acid, and biopolymers (Zoghlami and Paës, 2019). With ongoing research and advancements in processing technologies, lignocellulosic materials continue to emerge as versatile, sustainable resources across multiple industries as shown in figure 2.7.

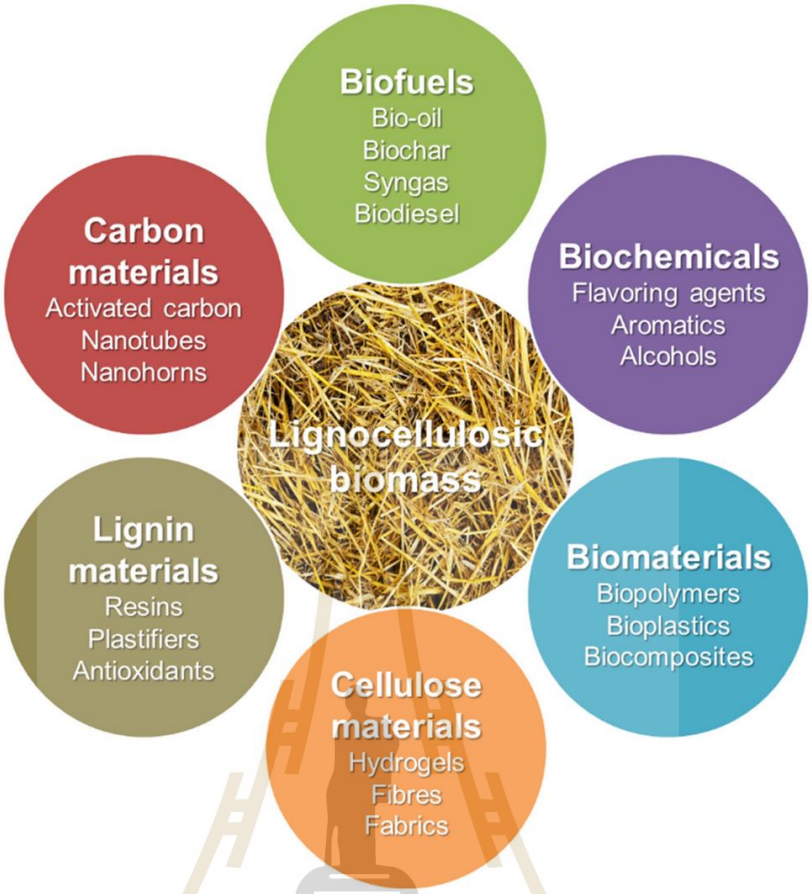

Figure 2.7 different industrially relevant bioproducts (Okolie *et al*., 2021)

2.2 Nanocellulose based Biopolymers

2.2.1 Nanocellulose

In the realm of biopolymers, cellulose stands out as the most abundant, forming a major structural component of plant cell walls. It's a linear homopolysaccharide composed of β-glucose units linked by 1,4-glycosidic bonds. When cellulose undergoes specific processing techniques, it can be broken down into nanoscale structures known as nanocellulose. Nanocellulose generally has at least one dimension in the range of 1-100 nm.

Cellulose exhibits a hierarchical structure, ranging from the macroscopic level down to the nanoscale. As depicted in Figure 2.8(A), cellulose fibers are composed of bundles of smaller fibrils. These fibrils further comprise crystalline and amorphous regions, as illustrated in Figure 2.8(B). Crystalline regions feature a highly ordered arrangement of cellulose chains, contributing to the material's stiffness and strength.

Conversely, amorphous regions exhibit a less organized structure, influencing the flexibility of cellulose (Phanthong *et al*., 2018).

Nanocellulose refers to cellulose broken down into nanoscale structures, typically with at least one dimension in the range of 1-100 nm. This nanoscale reduction significantly impacts the physical and mechanical properties of cellulose, offering improved characteristics compared to its bulk form. Nanocellulose was categorized into three main types:

- Cellulose Nanofibrils (CNF): These possess high aspect ratios (length-to-diameter) and excellent flexibility. CNFs are typically extracted using mechanical processes.
- Cellulose Nanocrystals (CNC): CNCs are highly crystalline and possess rod-like structures. They are often obtained through chemical treatment methods.
- Bacterial Nanocellulose (BNC): BNC is produced by specific bacteria and exhibits high purity and excellent biocompatibility.

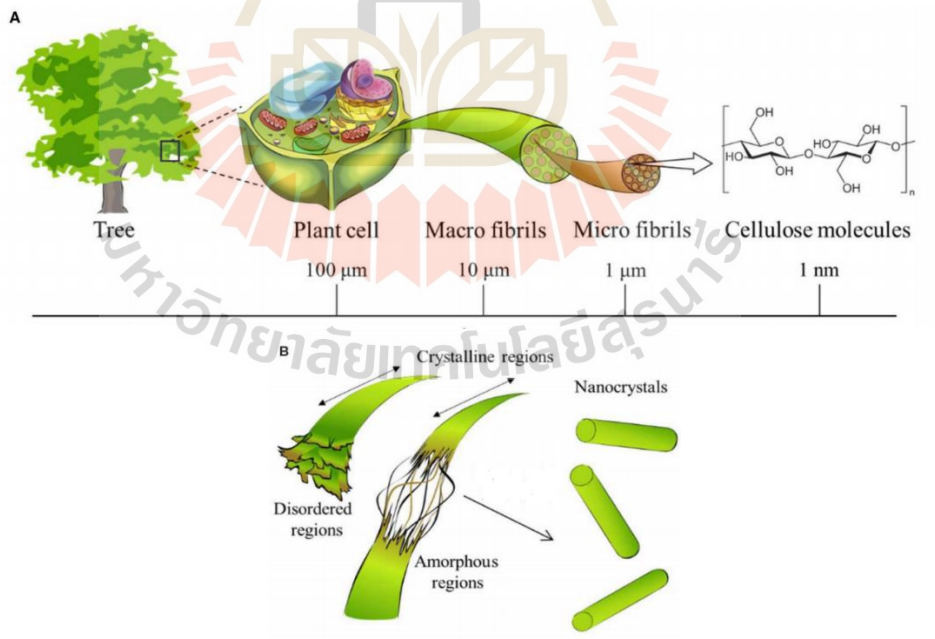

Figure 2.8 Cellulose contained in plants or trees has a hierarchical structure from the meter to the nanometer scale, as shown in (A). The crystalline and amorphous regions of cellulose is shown in (B) (Trache *et al*., 2020)

While all types of nanocellulose share a similar chemical composition (β-1,4-glycosidic linked glucose units), they differ in morphology (shape), particle size, and crystallinity due to variations in source material and extraction methods (Phanthong *et al*., 2018). These differences influence their specific properties and potential applications. The structure of nanocellulose was illustrated using transmission electron microscopy (TEM) and scanning electron microscopy (SEM), as shown in Figure 2.9 These techniques allow for the visualization of the morphology and size distribution of the nanocellulose particles. The key characteristics of different nanocellulose types was summarized in table 2.1, including their production methods and size ranges.

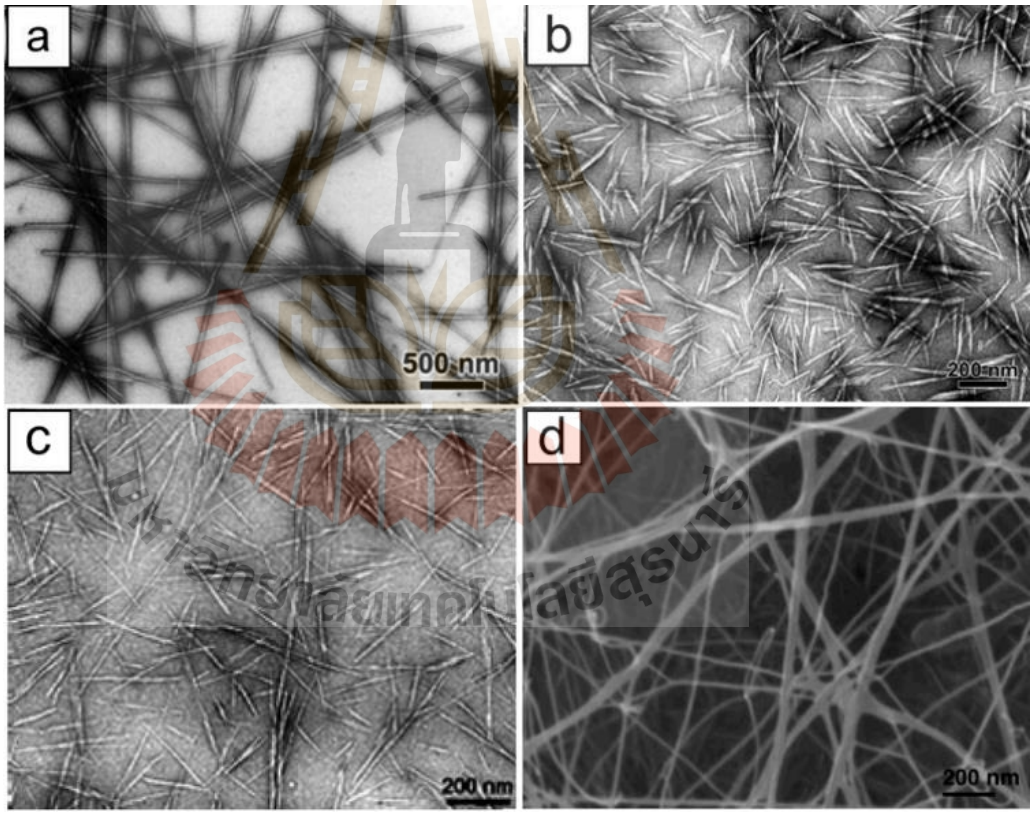

Figure 2.9 TEM images of a dried dispersion of cellulose nanocrystals (CNC) derived from (a) tunicate, (b) ramie, and (c) sisal, and (d) SEM image of nanofibrils of bacterial cellulose (BC) (Parry, 2016).

Table 2.1 Type of nanocelluloses, method of production and sizes (Parry, 2016).

Types of nanocelluloses	Typical sources	Method of production	Average Dimensions
Cellulose nanocrystals (CNC)	Wood, cotton, tunicate, ramie, bacterial cellulose, bamboo	Acid Hydrolysis	Diameter 3-50 nm Length: 30nm to -300 nm (wood and cotton based) 100 nm to several microns (tunicate and bacterial cellulose based)
Nanofibrillated Cellulose (NFC)	Wood, cotton, potato hemp, flax	High pressure homogenization, Microfluidization, Grinding, Cryocrushing	Diameter 5-60 nm Length: several microns regardless of the cellulose source
Bacterial Cellulose (BC)	*Acetobacter/ Glucobacter xylinum*	Biosynthesis of glucose and alcohol	Diameter 10-100 nm Length: Mostly several tens of micrometers up to a mm.

Sugarcane bagasse, a fibrous by-product generated during sugarcane processing, represents a significant portion of agricultural waste. This residue is a complex lignocellulosic material with a composition of approximately 35-45% cellulose, 26.2-35.8% hemicellulose, 11.4-25.2% lignin, and 2.9-14.4% other components (Chandel et al., 2012). Traditionally, sugarcane residues have found applications in ethanol production, paper and board manufacturing, animal feed, and electricity generation. However, due to its high cellulose content, sugarcane bagasse emerges as a promising and sustainable feedstock for nanocellulose production.

2.2.1.1 Chemical methods for nanocellulose extraction

Chemical methods are widely employed for nanocellulose extraction, with acid hydrolysis being a prominent technique. Sulfuric acid is frequently used, as exemplified by the hydrolysis of sugarcane bagasse with 50% sulfuric acid at a 1:25 cellulose-to-acid ratio, at 40°C for 10 minutes (Trache et al., 2020; Wulandari et al., 2016). Other acids, such as hydrochloric acid, can also be utilized, as demonstrated by the extraction of nanocellulose from ramie fibers using various concentrations (6, 8, and 10 M) at 45°C for 70 minutes with a 1:20 g/ml cellulose-to-acid ratio (Akbar et al., 2020). Additionally, organic acids like citric acid are gaining traction in biorefinery approaches. (Bondancia et al.,2020) reported a maximum CNC yield of 23% (diameter: 9 nm, length: 215 nm) after a 6-hour reaction at 120°C. While dialysis remains the primary method for acid removal and nanocellulose purification, its lengthy processing

time is a disadvantage. TEMPO-mediated oxidation presents an alternative chemical approach. (Hastuti et al., 2019) successfully derived cellulose nanofibers from oil palm empty fruit bunches (OPEFB) using a TEMPO/NaBr/NaClO system at pH 10 and room temperature for 2 hours. However, a major drawback associated with chemical methods is the generation of wastewater from the washing process, requiring proper treatment and disposal practices for environmental sustainability.

2.2.1.2 Mechanical methods for nanocellulose extraction

Mechanical processes utilize high shear forces to break down cellulose fibers into nanofibrils. Common techniques include ball milling, ultrasonication, and high-pressure homogenization.

- Ball Milling: This method employs a rotating jar containing milling balls of various sizes. The cellulose material gets crushed and refined due to collisions between the balls and the jar walls (Trache et al., 2020; Phanthong et al., 2016). Ball milling can be used in combination with mild acid hydrolysis or as a pretreatment step for enzymatic nanocellulose production (Squinca et al., 2020).
- Ultrasonication: This technique utilizes sound waves to generate cavitation (bubble formation and collapse) within the cellulose suspension. The resulting high-energy forces contribute to the defibrillation of cellulose fibers (Phanthong et al., 2018). Ultrasonication often serves as an assisting technique, frequently combined with chemical methods (acid hydrolysis or oxidation) for nanocellulose production (Perdoch et al., 2020).
- High-Pressure Homogenization: This method involves forcing a cellulose slurry through a narrow chamber at high pressure. The intense shear forces generated within the fluid effectively cleave cellulose microfibrils into nanofibrils (Phanthong et al., 2018). As an example, nanocellulose was successfully isolated from soy pulp using high-pressure homogenization at pressures ranging from 100-140 MPa for three passes (Wu et al., 2020).

2.2.1.3 Enzymatic Hydrolysis for Nanocellulose Production

Enzymatic hydrolysis offers a promising bio-based approach for nanocellulose extraction. This method utilizes enzymes to selectively break down

non-cellulosic components in lignocellulosic biomass, such as sugarcane bagasse and straw. Compared to chemical methods, enzymatic hydrolysis provides a more environmentally friendly alternative with minimal environmental impact and reduced energy consumption. Several enzymes are employed in enzymatic hydrolysis for nanocellulose production. Key enzymes include:

- Endoglucanase: This enzyme cleaves cellulose chains internally, increasing accessibility for other enzymes.
- Beta-glucosidase: This enzyme breaks down cellobiose, a disaccharide byproduct of cellulose hydrolysis, into glucose monomers.
- Xylanase: This enzyme degrades xylan, a hemicellulose component present in lignocellulosic biomass, facilitating the isolation of cellulose.

The effectiveness of enzymatic hydrolysis depends on various factors, including enzyme loading, reaction time, and temperature. Studies have reported successful nanocellulose production using commercial enzyme cocktails at temperatures around 50°C and reaction times ranging from 42 to 96 hours (Martelli et al., 2016; Squinca et al., 2020). Pretreatment of lignocellulosic biomass can significantly enhance the efficiency of enzymatic hydrolysis. Ball milling, for example, has been shown to improve the accessibility of cellulose to enzymes, leading to higher nanocellulose yields (Squinca et al., 2020). Enzymatic hydrolysis can achieve moderate yields of nanocellulose. Studies have demonstrated yields of approximately 11.3% and 12% for sugarcane bagasse and straw, respectively, after a 96-hour enzymatic hydrolysis process (de Aguiar et al., 2020) as shown in figure 2.10.

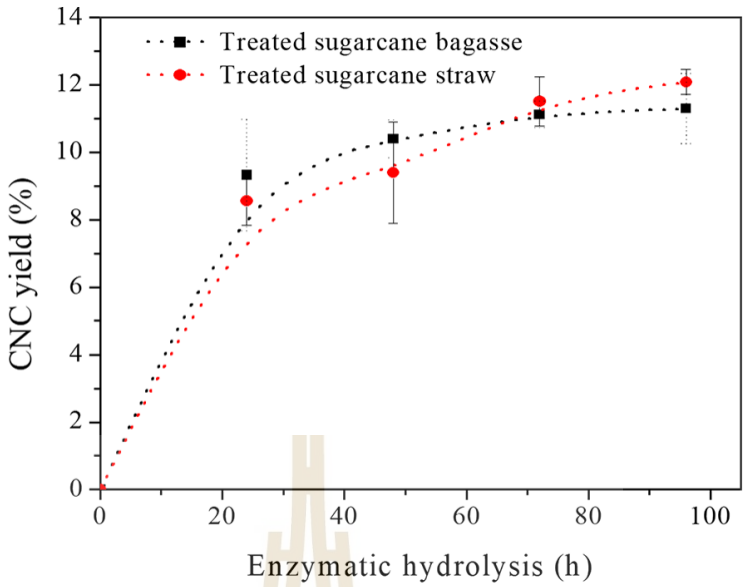

Figure 2.10 Yields of enzymatic nanocellulose from treated sugarcane bagasse and straw, using 10% (w/v) solids loading and enzyme 10 mg protein/g of solid at 50 °C. (de Aguiar *et al*., 2020)

2.2.1.4 Bacterial Nanocellulose Production

Bacterial nanocellulose (BNC) offers a unique route for nanocellulose production through a bioprocess mediated by specific bacteria. Unlike other extraction methods that rely on harsh chemicals or intensive mechanical forces, BNC production leverages fermentation, a generally more environmentally friendly approach. Notably, *Gluconacetobacter xylinus* (formerly known as *Acetobacter xylinum*) stands out as a highly efficient and non-pathogenic bacterium for producing cellulose nanofibrils.

The cultivation of *G. xylinus* for BNC production typically employs Hestrin & Schramm (HS) medium. This medium provides an optimal environment for bacterial growth and cellulose production. HS medium is formulated with glucose as the primary carbon source, fueling the metabolic processes of the bacteria. Additionally, a combination of peptone and yeast extract serves as a rich source of nitrogen, essential for bacterial growth and cellulose biosynthesis. The fermentation process usually adopts a stationary phase approach, allowing the bacteria to maximize cellulose production within a defined timeframe. Fermentation times typically range from 4 to 15 days, depending on the desired yield and targeted properties of the BNC.

The specific details of BNC production and corresponding fermentation times using HS medium can be found in Table 2.2.

Table 2.2 Bacterial nanocellulose (BNC) production in Hestrin & Schramm (HS) medium (Corujo *et al.*, 2016)

strain	fermentation time (day)	production (g/L)
Komagataeibacter hansenii MCM B-967	7	0.3
Gluconacetobacter xylinus ATCC 10788	7	0.4
Komagataeibacter sp. PAP1	7	1.2
Komagataeibacter sucrofermentans DSM 15973	15	1.2
Gluconacetobacter hansenii UAC09	7	1.5
Gluconacetobacter medellinenses	13	1.9
Gluconacetobacter sacchari	4	2.5-2.7

2.2.2 Polylactic acid

Lactic acid is a versatile molecule found naturally in organisms. Its unique chemical structure, featuring hydroxyl and carbonyl groups, comprises three forms as shown in Figure 2.11 This structure makes lactic acid a valuable precursor for other compounds. Notably, its pure L and D forms are particularly in demand. Most importantly, L-lactic acid serves as the foundation for poly(lactic acid), a useful polymer with various industrial applications.

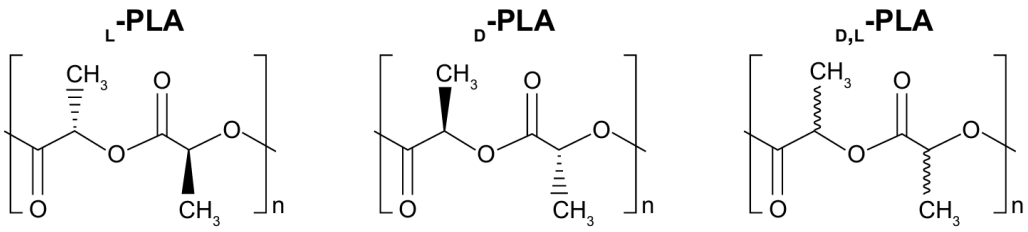

Figure 2.11 Structure of poly(lactic acid) isomers (L-PLA, D-PLA, D,L-PLA) (Song et al., 2018)

Lactic acid bacteria can be categorized into two primary groups based on their fermentation products: homofermenters and heterofermenters. Homofermenters specialize in lactic acid production, efficiently converting glucose into lactate via the glycolysis pathway and utilizing enzymes like lactate dehydrogenase for this primary output (Castañeda et al., 2023). Conversely, heterofermenters exhibit greater metabolic versatility, utilizing glucose to generate a wider range of products including acetic acid, carbon dioxide, and ethanol alongside some lactic acid (Castañeda et al.). For example:

Homofermenters: Preferred for industrial production of high-purity lactic acid used in plastics, food additives, and pharmaceuticals. They are also essential for yogurt production.

Heterofermenters: Used in various food fermentations like sourdough bread, kimchi, sauerkraut, and some sausages. Their ability to produce flavor compounds and tolerate some oxygen makes them suitable for these applications.

Polylactic acid (PLA) possesses a unique combination of properties ideal for industrial applications. The physical properties of PLA were summarized in Table 2.3. Moreover, PLA offers excellent transparency, low-temperature stability, and resistance to grease and oil. Importantly, these properties can be strategically manipulated by adjusting D-content and molecular weight (Ranakoti et al., 2022). For example, increasing molecular weight enhances strength but reduces crystallinity. The ratio of D- and L-content directly influences crystallinity and biodegradation.

Table 2.3 Physical properties of PLA (Ranakoti et al., 2022)

Property	Values
Specific Gravity	1–1.5
Surface Energy (dynes)	36–40
Melting Temperature (°C)	140–210
Molecular Weight (Daltons)	Approx. 1.6 × 105
Melt Flow Index (g/10 min)	4–22
Crystallinity (%)	5–35
Glass Transition Temperature (°C)	50–75

The degradation is crucial for the long-term effects of PLA materials. In the field of biomedicine, a slow degradation rate of PLA is a drawback. Therefore, blending PLA with other materials has been used to develop properties. However, achieving the ideal balance between degradation speed, strength, and other properties for safe tissue growth and implant function remains a challenge.

2.2.3 Polybutylene succinate

Polybutylene succinate (PBS), a commercially available biodegradable and sustainable bioplastic since 1993, has attracted continuous research efforts to develop eco-friendly fermentation methods using microorganisms as an alternative feedstock (Rafiqah et al., 2021). PBS was synthesized through polycondensation of succinic acid (or dimethyl succinate) with 1,4-butanediol (BDO). The flowchart of PBS production was presented in Figure 2.12 Polybutylene succinate (PBS) synthesis involves a two-step process:

- Esterification/Transesterification: This step reacts succinic acid (or dimethyl succinate) with BDO (with a slight BDO excess) to form oligomers. The reaction occurs at 160-190°C under nitrogen and removes water (or methanol) as a byproduct.
- Polycondensation: The oligomers undergo further reaction at higher temperatures (220-240°C) and high vacuum to remove BDO and form high-molecular-weight PBS. Various catalysts like tin(II) chloride, distannoxane, and titanium-based catalysts are used in this step.

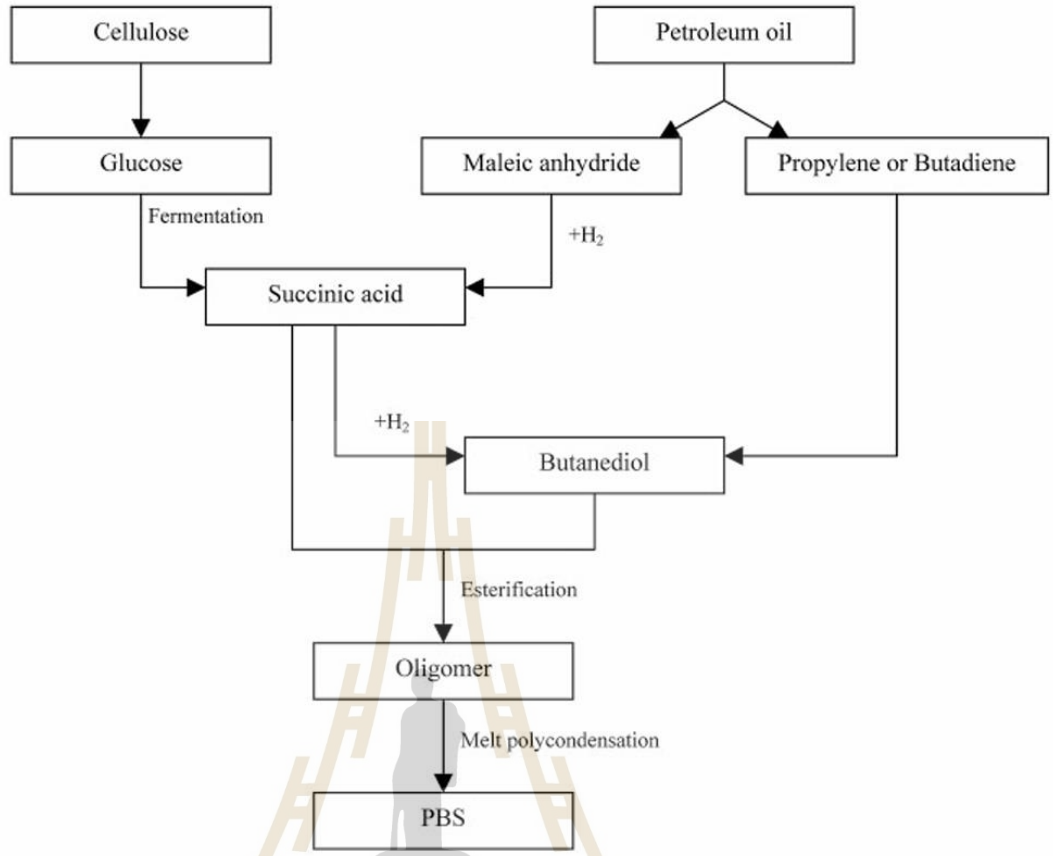

Figure 2.12 PBS production flowchart (Xu and Guo, 2010)

PBS is a versatile bioplastic with a semi-crystalline structure, making it desirable for various applications. It exhibits good elongation and properties as shown in Table 2.4. However, PBS degrades in water and lacks some properties like softness. To mitigate these limitations, PBS is often blended with other materials.

Table 2.4 Physical properties of PBS (Su et al., 2019).

properties	PBS
Glass transition temperature (°C)	-32
Melting point (°C)	114
Heat distortion temperature (°C)	97
Modulus of elasticity (MPa)	550-700
Tensile strength (MPa)	34
Elongation at break (%)	560

2.2.4 Properties of nanocellulose based biopolymer

Nanocellulose has attracted great interest in the preparation of nanocomposites with polymer matrices due to its interesting properties. Nanocellulose-based biopolymers exhibit exceptional mechanical strength, high surface area, and tunable rheological properties, making them suitable for a wide range of applications (Dufresne, 2012). These biopolymers demonstrate remarkable biodegradability, biocompatibility, and non-toxicity, which are essential for biomedical applications such as wound healing, drug delivery, and tissue engineering (Kargarzadeh et al., 2017). Additionally, nanocellulose enhances the thermal stability and barrier properties of polymer matrices, improving their performance in packaging and coatings (Eyholzer et al., 2010). The high aspect ratio and hydroxyl-rich surface of nanocellulose allow for chemical modifications that tailor its functionality for specific industrial needs (Lin & Dufresne, 2014). Ongoing research focuses on optimizing nanocellulose integration into composite materials to expand its commercial viability and sustainable applications (Trache et al., 2020).

Mechanical testing studies on nanocellulose-reinforced biopolymers have demonstrated significant property enhancements across various research efforts. In PLA composites, tensile strength increases by 21% with 5 wt% cellulose nanofibrils (CNF) (Jonoobi et al.,2010)., while tensile strength achieved a 54% improvement using 1 wt% cellulose nanocrystals (CNC) with surfactant (Fortunati, et al., 2012). More dramatic results were observed in modulus and strength (up to 58% and 210%, respectively) with well-dispersed CNC (Wang and Drzal, 2012). However, cellulose nanofibrils CNF led to higher strength and modulus than CNC at the same fiber concentration (Xu et al., 2016). For PBS matrices, even more substantial improvements were recorded, and the tensile modulus increased with the addition of CNF or CNC (Lin et al.2011). Overall, these studies highlight the effectiveness of nanocellulose as a reinforcing agent for biopolymers. Relatively low concentrations of nanocellulose (typically 1-5 wt%) can substantially enhance mechanical properties, particularly modulus. This reinforces the potential of nanocellulose-reinforced biopolymers for various applications, including packaging, biomedical devices, and tissue engineering.

2.2 Tissue engineering

2.2.1 Key Components of Tissue Engineering

2.2.1.1 Stem cells

Stem cells are categorized by potency, which determines their ability to differentiate into various cell types, as summarized in Table 2.5. Totipotent stem cells (e.g., zygote) can develop into any body or extraembryonic cell, while pluripotent stem cells (e.g., ESCs, iPSCs) can generate all body cells but not placenta. Multipotent stem cells (e.g., MSCs, HSCs) differentiate into a limited range of related cells, making them valuable for tissue engineering, especially for bone, cartilage, and blood. Oligopotent stem cells (e.g., myeloid and lymphoid progenitors) give rise to only a few specific cell types, while unipotent stem cells (e.g., muscle satellite cells) specialize in a single cell type but retain self-renewal properties. Pluripotent stem cells offer the highest potential but pose tumor risks, whereas multipotent stem cells are safer and widely used in regenerative medicine.

Table 2.5 types of stem cell

Potency	Differentiation Potential	Examples	Applications	Limitations
Totipotent	All body + extraembryonic cells	Zygote, Morula	Early development studies	Ethical issues, rare
Pluripotent	All body cells (not placenta)	ESCs, iPSCs	Organoids, regenerative medicine	Tumor risk, ethical concerns
Multipotent	Multiple related cell types	MSCs, HSCs, NSCs	Bone, cartilage, blood cell engineering	Limited differentiation
Oligopotent	Few related cell types	Myeloid, Lymphoid progenitors	Blood/immune cell therapy	Very restricted potential
Unipotent	One specific cell type	Satellite cells, Epidermal cells	Skin grafts, muscle repair	Least versatile

Stem cells are undifferentiated cells with the ability to self-renew and differentiate into specialized cell types, making them a cornerstone of regenerative medicine and tissue engineering (Singh et al., 2021). They are categorized into embryonic stem cells (ESCs), adult stem cells, and induced pluripotent stem cells (iPSCs). ESCs, derived from the inner cell mass of blastocysts, possess pluripotency, allowing them to differentiate into all three germ layers (Thomson et al., 1998). Adult stem cells, such as mesenchymal stem cells (MSCs) and hematopoietic stem cells (HSCs), are multipotent and primarily contribute to tissue repair and homeostasis (Pittenger et al., 1999). iPSCs, generated by reprogramming somatic cells through the introduction of key transcription factors, provide an ethical alternative to ESCs with promising applications in disease modeling and personalized medicine (Takahashi & Yamanaka, 2006). Stem cells have demonstrated potential in treating neurodegenerative disorders, cardiovascular diseases, and musculoskeletal injuries through their regenerative properties and immunomodulatory effects (Trounson & McDonald, 2015). However, challenges such as tumorigenic risks, immune rejection, and standardization of differentiation protocols remain significant barriers to clinical translation (Bianco et al., 2013). Advances in biomaterials, gene editing, and 3D bioprinting continue to drive innovations in stem cell-based therapies, paving the way for more effective regenerative medicine strategies.

2.2.1.1.1 Mesenchymal stem cells (MSCs)

Mesenchymal stem cells (MSCs) are a type of adult stem cell possessing the unique ability to differentiate into various cell types of mesenchymal origin, such as bone, cartilage, and fat cells. This multipotency makes them a promising tool in regenerative medicine. Additionally, MSCs exhibit immunomodulatory properties, meaning they can interact with the immune system in a way that minimizes rejection by the recipient's body. A diverse array of tissues, including bone marrow, umbilical cord, and adipose tissue, were identified as suitable sources for MSC isolation (Figure 2.13). Moreover, The isolation process typically involves a density gradient separation for bone marrow, adipose, and blood-derived MSCs, while enzymatic digestion with collagenase was used for other tissues (Table 2.6).

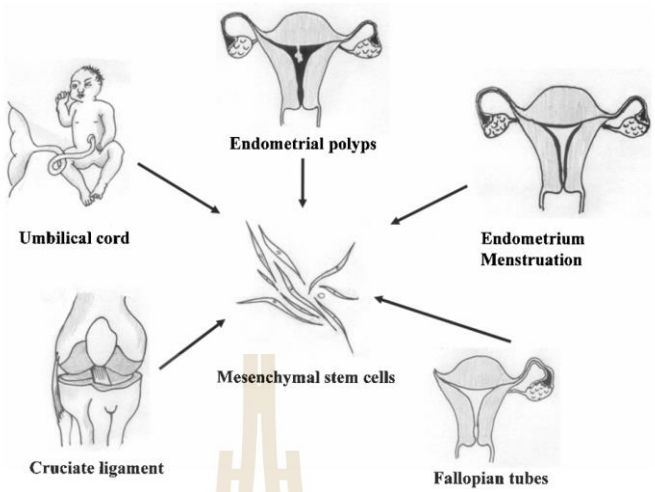

Figure 2.13 Various sources of MSCs (Ding, Shyu, and Lin, 2011)

Table 2.6 The isolation process of MSCs (Ullah, Subbarao and Rho, 2015)

Source	Method of isolation
Bone marrow	Ficoll density gradient method Novel marrow filter device
Adipose tissue	Digestion method Membrane filtration method
Amniotic fluid and membrane	Density gradient method Digestion method
Dental tissues	Digestion method
Endometrium	Digestion method
Limb bud	Digestion method
Peripheral blood	Ficoll density gradient
Placenta and fetal membrane	Digestion method
Salivary gland	Digestion method(Ringer solution)
Skin and foreskin	Digestion method
Sub amniotic umbilical cord lining membrane	Digestion method
Synovial fluid	Ficoll density gradient method
Wharton's jelly	Enzymatic digestion method

Wharton's Jelly, a component of the umbilical cord matrix, was identified as a source for MSCs. Wharton's Jelly Cell (WJC) have been proven to differentiate into neuronal and glial cells in vitro. Moreover, these cells can migrate to the site of injury and differentiate into neuronal and glial cells in stroke rats. When compared to bone marrow-derived MSCs, WJ-derived MSCs are characterized by faster growth and greater expansion potential (Ding, Shyu, and Lin, 2011). The suitability of WJ-derived MSCs as an alternative source for various therapeutic applications was proposed, highlighting the necessity for further investigation through long-term clinical trials. However, the multipotency of MSCs makes them a promising candidate for future clinical applications in various diseases, warranting further research on their differentiation, transplantation, and immune response.

2.2.1.2 Biomaterial scaffold

Biomaterial scaffolds play a crucial role in tissue engineering by providing a three-dimensional (3D) framework that supports cell attachment, proliferation, and differentiation, mimicking the extracellular matrix (ECM) to facilitate tissue regeneration (O'Brien, 2011). These scaffolds can be fabricated from natural biomaterials such as collagen, gelatin, chitosan, and alginate, or synthetic polymers like polylactic acid (PLA), polycaprolactone (PCL), and poly(lactic-co-glycolic acid) (PLGA) (Hutmacher, 2000). The choice of scaffold material influences properties such as biodegradability, mechanical strength, and biocompatibility, which are essential for successful tissue integration (Murphy et al., 2010).

Numerous materials have been explored as scaffolds for tissue engineering applications. To achieve optimal functionality, a critical aspect is the close match between the scaffold and the newly generated tissue. Various scaffolds, derived from a wide range of biomaterials, have been developed to promote the regeneration of different tissues and organs within the body. When designing or evaluating the suitability of a scaffold for tissue engineering, several key considerations are paramount: biocompatibility, biodegradability, and mechanical properties (O'Brien, 2011).

- Biocompatibility: Biocompatibility, a material's ability to elicit a favorable host response in a specific application (i.e., non-toxic and non-

immunogenic) (Anderson, 2012), is crucial for scaffold design. A biocompatible scaffold should primarily support cell attachment, normal function, migration (both on the surface and throughout the scaffold), and proliferation before the cells start laying down new extracellular matrix (O'Brien, 2011). Factors influencing biocompatibility include the material's chemistry, scaffold structure, and morphology. Additionally, the biomaterial synthesis process, the scaffold manufacturing method, and the sterilization conditions can significantly impact biocompatibility.

- Biodegradability: Furthermore, the scaffold should exhibit biodegradability to allow cells to produce their own extracellular matrix and allow their byproducts to be safely eliminated (O'Brien, 2011).
- Mechanical Properties: Ideally, the scaffold's mechanical properties should match those of the targeted implantation site. The scaffold must possess sufficient mechanical strength to withstand surgical manipulation during implantation. However, achieving high strength often comes at the expense of reduced porosity, another crucial property for optimal cell function (O'Brien, 2011).

A critical aspect of designing scaffolds for tissue engineering applications was achieved a close match between the mechanical properties of the scaffold and the targeted implantation site. Sufficient mechanical strength was necessitated for the scaffolds to endure surgical manipulation during implantation. However, an inherent trade-off was identified, whereby high strength could only be achieved at the expense of reduced porosity, another crucial parameter for optimal cellular function within the scaffold (O'Brien, 2011).

Advanced fabrication techniques, including electrospinning, 3D bioprinting, and freeze-drying, have been employed to create scaffolds with controlled porosity and architecture, enhancing cellular infiltration and vascularization (Jakab et al., 2010). Research focuses on functionalizing biomaterial scaffolds with bioactive molecules, growth factors, and nanomaterials to improve their regenerative potential (Dvir et al., 2011). Despite significant progress, challenges remain in optimizing scaffold degradation rates, mechanical properties, and immune responses for clinical applications (Liu et al., 2016). Future advancements in biomaterials and scaffold fabrication technologies hold great promise for developing personalized and bioactive scaffolds for tissue engineering and regenerative medicine.

2.2.1.3 Bioactive Molecules

Bioactive molecules play a critical role in biomedical applications by modulating cellular behavior, promoting tissue regeneration, and enhancing the functionality of biomaterials (Langer and Tirrell, 2004). These molecules include growth factors, peptides, cytokines, and small molecules that influence cell proliferation, differentiation, and extracellular matrix synthesis (Lutolf and Hubbell, 2005). Growth factors such as vascular endothelial growth factor (VEGF), transforming growth factor-beta (TGF-β), and bone morphogenetic proteins (BMPs) have been extensively used in tissue engineering to stimulate angiogenesis, osteogenesis, and wound healing (Chen et al., 2007). Bioactive molecules can be incorporated into scaffolds via surface modifications, chemical conjugation, or controlled release systems to ensure localized and sustained therapeutic effects (Lee et al., 2011). Advances in nanotechnology and biomaterials have enabled the development of smart delivery systems, including nanoparticles and hydrogels, that improve the bioavailability and stability of these molecules (Yoo et al., 2011). Despite their therapeutic potential, challenges such as degradation kinetics, immune responses, and precise dose control must be addressed for clinical translation. Future research focuses on optimizing bioactive molecule delivery strategies to enhance regenerative medicine and targeted therapies.

2.2.2 Applications of nanocellulose based biopolymer in Tissue Engineering

Tissue engineering focuses on creating functional tissues to repair or replace damaged organs in the body. Each tissue type serves a specific purpose. For example, skin provides a protective barrier, bones and cartilage offer structural support, and the pancreas plays a crucial role in biochemical production. In tissue engineering, a patient's own cells are often cultured in a lab environment and then seeded onto specially designed scaffolds. These cultured scaffolds are then implanted into the patient's body, where the scaffolds serve as a template for the cells to grow and differentiate into the desired tissue.

A diverse array of natural and synthetic polymers were investigated for the fabrication of scaffolds for tissue regeneration. Each polymer offered distinct advantages in terms of mechanical strength and structural form.

Common scaffold architectures included sponge-like structures, fibrous matrices, and gel-type constructs suitable for cell culture (Sridhar et al., 2011). When selecting biopolymers for scaffold production, paramount considerations were placed on biocompatibility, biodegradability, and the ability to achieve the desired mechanical properties.

Nanocellulose-based scaffolds have emerged as promising materials for tissue engineering due to their unique properties. These properties include biocompatibility, water absorption and retention, optical transparency, and suitable chemo-mechanical characteristics. Nanocellulose scaffolds offer potential applications in repairing, improving, or replacing various damaged tissues and organs, including skin, blood vessels, nerves, skeletal muscle, heart, liver, and those in the field of ophthalmology (Luo et al., 2019).

Cellulose nanocrystals was incorporated with polyvinyl alcohol (PVA) to create tissue engineering scaffolds. The impact of these scaffolds on human skin cells in a laboratory setting was subsequently evaluated (Lam et al., 2017). Additionally, cellulose nanofibrils (CNFs) was blended with gelatin (gel) and cross-linked for application in bone tissue engineering. The structure of these cross-linked scaffolds was analyzed using scanning electron microscopy (SEM), and a 3D model was generated by microcomputed tomography (m-CT) (Figure 2.14).

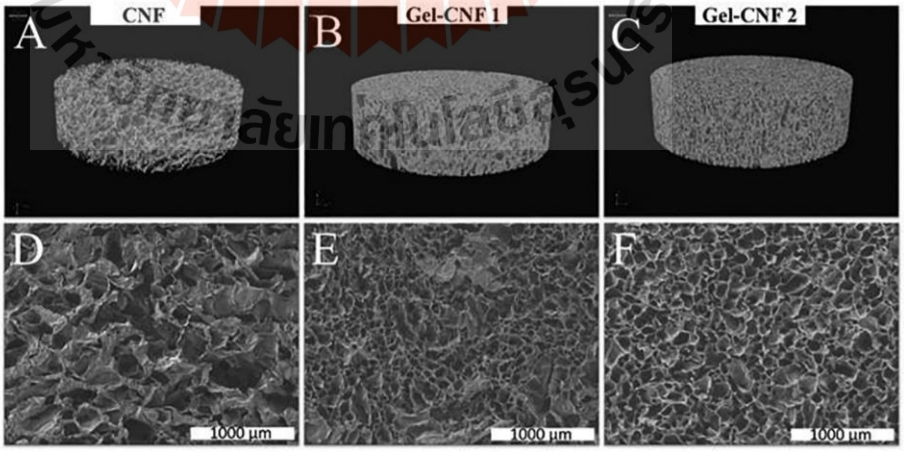

Figure 2.14 Structural surface characterization by m-CT (A-C) and SEM (D-F) (Carlström *et al.,* 2020).

Polylactic acid (PLA) emerged as a prominent biopolymer classified within the aliphatic polyester family. Notably, PLA could be derived from sustainable resources such as sugarcane, corn, and potatoes. Electrospinning was employed to create PLA-based scaffolds and their blends, finding various applications in the medical field, as detailed in Table 2.7. Additionally, studies reported that the properties of the solvent used in electrospinning PLA fibers, such as boiling point, viscosity, conductivity, and surface tension, significantly affect the process efficiency, morphology, and diameter distribution of the resulting PLA nanofibers (Figure 2.15).

Table 2.7 Details of various electrospun based PLA for biomedical applications. (Kanmaz *et al*., 2018)

Polymers and Blends	Molecular	Solvents weight (g/mol)	Average fiber diameter (nm)	Fillers	Application
PLA	200,000	DMAc and CHL	971 ± 274	Cur	Wound healing
PLLA and PVDF	90,000	DMAc and AC	2,290 – 4,620	Cur and Enro	Wound healing
PLGA	120,000-190,000	Trifluoroethanol and CHL	777 ± 249	Ciprofloxacin and sodium alginate	Wound healing
PLLA	300,000	DCM	3000-5000	DMOG and DS	Wound healing
PLGA	75,000	1,1,1,3,3,3-hexafluoro-2-propanol (HFIP)	~1,000	-	Cardiac
PLGA	110,000	HFIP	720 ± 350	Elastin and collagen	Cardiac
PLA	75,000-120,000	DMF, DCM and methanol	~556	Dipyridamole	Cardiac
PLLA	100,000	HFIP	100–500	Laminin	Nerve
PLLA	100,000	HFIP and hexamethyl-disilazane (HMDS)	860 ± 110	Coll and HA	Bone
(PPDO:PLLA:-PEG)	42,000	DMF and DMC	~1,400	-	Skin
PLA and PEVA	205,000	CHL and methanol	1,000–3,000	Tetracycline	Drug release
PLLA	-	CHL, 1,2-dichlorethane and ethyl acetate	290 - 539	Cyclosporine A (CsA)	Drug release
PLA	470,000	DMF and DCM	549.7 ± 153.1	Graphene oxide (GO) and rhodamine B	Drug release
PLLA and chitosan	low molecular weight	AC and DCM	2 760 ± 720	-	Dental

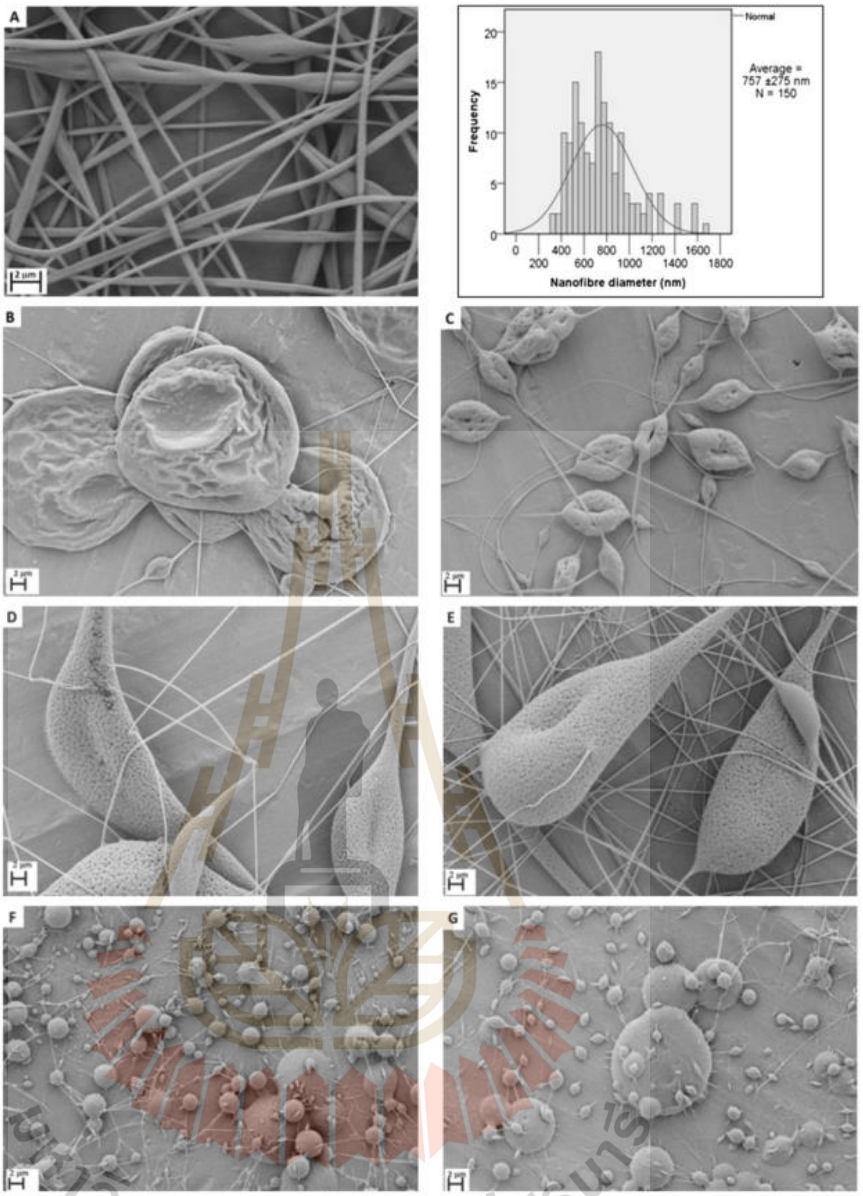

Figure 2.15 Effect of single solvent systems on nanofibre morphology: scanning electron micrographs of PLA nanofibres from solutions of 10% (w/v) of PLA in: (a) acetone with nanofibre diameter distribution, (b) 1,4-dioxane, (c) tetrahydrofuran, (d) dichloromethane, (e) chloroform, (f) dimethylformamide and (g) dimethylacetamide (Casasola *et al*., 2014).

Investigations were undertaken to enhance the properties of scaffold materials through the blending of polylactic acid (PLA) with polybutylene succinate (PBS). A progressive improvement in the flexibility of the composite material was observed with increasing PBS content within the blend, as detailed in Table 2.8

Furthermore, research efforts focused on the incorporation of cellulose (CNF) into PLA/PBS composites. The addition of CNF was reported to further enhance the mechanical performance of electrospun scaffolds. Notably, an increase in both tensile strength and elastic modulus was observed with a rising nanocellulose content. This improvement can be attributed to the reinforcing effect exerted by the CNF, a consequence of strong molecular interactions established between the polymer matrix and the CNF (Abudula et al., 2019).

Table 2.8 Characterization summary of PLA/PBS scaffolds in the different ratio (Abudula *et al.*, 2019)

PLA/ PBS ratio	Fiber diameter (nm)	Elastic modulus (Mpa)	Tensile Strength (Mpa)	Strain at break (%)	Indentation modulus (Mpa)	Water contact angle (°)	Protein Adsorption (μg/mg)
100/0	1019 ± 75	129 ± 5.1	1.68 ± 0.17	62.4 ± 2.3	2525 ± 40	113.7 ± 3.1	60.3 ± 3.3
75/25	948 ± 80	112 ± 3.8	2.42 ± 0.14	71.5 ± 3.5	1825 ± 26	107.7 ± 1.7	98.0 ± 5.6
60/40	631 ± 64	108 ± 2.5	2.52 ± 0.2	76.5 ± 2.6	1619 ± 75	98.6 ± 1.9	120.2 ± 3.0
50/50	409 ± 51	98.6 ± 4.6	2.77 ± 0.23	110.3 ± 1.6	1537 ± 32	83.5 ± 2.3	138.4 ± 1.9
40/60	460 ± 60	58 ± 2.6	2.64 ± 0.15	112.5 ± 1.3	1319 ± 55	91.8 ± 1.8	142.2 ± 2.3
25/75	_	29.7 ± 2.3	2.43 ± 0.15	105.6 ± 2.4	1158 ± 24	109.2 ± 1.2	147.2 ± 3.6
0/100	_	11 ± 2.3	1.54 ± 0.1	115.3 ± 1.8	210 ± 11	113.8 ± 2.1	163.9 ± 1.8

Nanocellulose has been extensively studied for its biomedical applications, with various in vivo studies evaluating their safety profiles. A study on cellulose nanofibrils (CNF) administered to rats over five weeks showed no significant toxic effects, as assessments of hematology, serum markers, and organ histology revealed no adverse changes, suggesting that ingested nanocellulose is likely non-hazardous in small quantities (DeLoid et al., 2019). PLA implants typically induce mild inflammatory responses that resolve over time, though localized acidosis from degradation products remains a concern (Bernardo et al., 2022; Hietala et al., 2001). Similar results occurred for PBS and PBS/PLA, while in the case of PLA, the inflammation was still occurring to some extent (Gigli et al., 2016). However, Numerous in vivo studies on biopolymers have revealed generally favorable biocompatibility profiles with manageable side effects.

2.2.3 Strategies in Tissue Engineering

Tissue engineering integrates principles from biology, engineering, and material science to develop functional tissues for regenerative medicine. Various strategies have been explored to enhance tissue regeneration, including scaffold-based approaches, cell-based therapies, and bioactive molecule delivery (Langer and Vacanti, 1993). Scaffold-based tissue engineering involves the use of biomaterial scaffolds that provide structural support and a microenvironment conducive to cell attachment, proliferation, and differentiation (O'Brien, 2011). These scaffolds can be fabricated from natural polymers such as collagen, alginate, and chitosan or synthetic polymers like poly(lactic-co-glycolic acid) (PLGA) and polycaprolactone (PCL) (Murphy et al., 2010).

Cell-based strategies, particularly the use of stem cells, have gained significant attention due to their ability to self-renew and differentiate into multiple cell types (Zakrzewski et al., 2019). Mesenchymal stem cells (MSCs) and induced pluripotent stem cells (iPSCs) have been widely used for tissue repair and regeneration due to their regenerative potential and immunomodulatory properties (Chen et al., 2019). Advances in genetic engineering and cell reprogramming have further improved the efficiency of stem cell-based therapies in tissue regeneration (Takahashi and Yamanaka, 2016).

Another critical strategy in tissue engineering is the delivery of bioactive molecules, such as growth factors, peptides, and small molecules, to stimulate cell behavior and promote tissue regeneration (Mooney and Vandenburgh, 2008). Controlled release systems, including nanoparticles, hydrogels, and microspheres, have been developed to enhance the stability and bioavailability of these molecules (Lee et al., 2011). Advancements also include applying 3D bioprinting and biofabrication techniques, which enable the precise spatial arrangement of cells and biomaterials to create complex tissue constructs (Murphy and Atala, 2014).

Despite these advancements, challenges such as vascularization, immune response, and long-term functionality of engineered tissues remain critical areas for further research (Pashuck and Stevens, 2012). Future efforts aim to integrate advanced biomaterials, smart drug delivery systems, and bioprinting technologies to improve tissue engineering outcomes and facilitate clinical translation.

2.2.4 Challenges and Future Directions

Despite significant advancements, tissue engineering faces several challenges that hinder its clinical translation and widespread application. One of the primary obstacles is vascularization, as engineered tissues require an adequate blood supply to sustain cell viability and function (Zhao et al., 2016). The lack of functional capillary networks in larger tissue constructs limits nutrient and oxygen diffusion, leading to necrosis in the core regions of engineered grafts (Novosel et al., 2011). Current strategies, including the use of angiogenic growth factors, endothelial cell seeding, and 3D bioprinting, aim to address this issue, but achieving fully integrated vascular networks remains a challenge (Zhang et al., 2021).

Another major limitation is immune response and biocompatibility. The host immune system often reacts to implanted scaffolds, cells, or bioactive molecules, leading to inflammation, fibrosis, or rejection (Anderson et al., 2008). The development of immune-evasive biomaterials, immunomodulatory strategies, and patient-specific cell therapies holds promise for overcoming these barriers (De Vries et al., 2019). Additionally, stem cell-based tissue engineering faces challenges related to cell sourcing, differentiation efficiency, and long-term functionality. Ensuring consistent differentiation and integration of stem cells into host tissues remains a crucial hurdle (Trounson and McDonald, 2015).

Scaffold degradation and mechanical stability also present critical concerns. The degradation rate of biomaterial scaffolds must be synchronized with new tissue formation to prevent premature collapse or excessive persistence that hinders remodeling (O'Brien, 2011). Balancing mechanical properties with biodegradability remains a key focus in scaffold design. Furthermore, large-scale manufacturing and standardization pose challenges in translating lab-scale successes to clinical applications. Regulatory approvals, cost-effective production, and reproducibility of tissue-engineered products require significant advancements in biofabrication techniques (Murphy and Atala, 2014).

Looking ahead, the future of tissue engineering lies in emerging technologies such as 3D bioprinting, gene editing, and smart biomaterials. 3D bioprinting enables precise fabrication of complex tissue architectures, incorporating multiple cell types and growth factors (Groll et al., 2016). Gene editing tools like

CRISPR-Cas9 offer potential for genetic modifications to enhance cell functionality and immune tolerance (Hendriks et al., 2023). Additionally, bioactive and responsive biomaterials that can adapt to dynamic physiological environments will revolutionize tissue engineering applications (Sant et al., 2021). Addressing these challenges through interdisciplinary collaboration and technological advancements will drive the next generation of regenerative medicine and organ bioengineering.

CHAPTER III

MATERIALS AND METHODS

3.1 Nanocellulose preparation

Sugarcane bagasse was obtained from Mitr Phol Company in Thailand. The cellulose extraction process involved pretreating the bagasse with a 4% sodium hydroxide solution (1:15 w/v ratio) for 24 hours at 60°C. The pretreated bagasse was then washed with RO water until reaching a neutral pH. To remove color from the sample, a 15% hydrogen peroxide solution (1:10 ratio) was used at 80°C for 2 hours, followed by another RO water wash until a pH of 7 was achieved. The wet cellulose was dried overnight at 50°C in a tray dryer, then mashed and sieved through a 50 µm sieve. A 1% cellulose mixture was prepared by sieving the cellulose with RO water before size reduction.

A hydraulic pilot-scale homogenizer (Microfluidics, M-110EH-30, USA) was shown in figure 3.1 and operated under various pressure conditions (10,000 - 30,000 psi) in combination with an enzymatic process for nanocellulose production. Commercial cocktail enzyme (Novozymes, C-Tech 2, Denmark) was added to the cellulose powder at 1-7% w/w, and the mixture was incubated at 50°C for 96 hours to promote size reduction. Enzymatic hydrolysis was stopped by boiling for 5 minutes. The resulting nanocellulose was then centrifuged at 8,000 rpm for 30 minutes at 25°C and washed three times before being transferred to the mini spray dryer (fig 3.2).

Finally, the nanocellulose was dried using a mini spray dryer (Buchi, B-250, Switzerland) with an inlet temperature of 130°C and the following conditions: 470 L/h air flow rate, 3.5 mL/min feeding rate, 1.4 mm nozzle size, and -50 mbar aspirator pressure drop.

Figure 3.1 Hydraulic pilot-scale homogenizer (Microfluidics, M-110EH-30, USA)

Figure 3.2 Mini spray dryer (Buchi, B-250, Switzerland)

3.2 Production of Nanocellulose based biopolymer scaffold

Design-Expert software version 13 was used to optimize the polymer ratio using the mixture design model. The model operated under the following constraints: (65% ≤ PLA ≤ 90%), (PBS ≤ 35%), (cellulose ≤10%), (PBS + cellulose ≤40%), and (PLA + PBS + cellulose = 100%). The designed experiment was presented in Table 3.1 The responses measured included water contact angle, medium contact angle, and maximum tensile force.

The composite materials were dissolved in N-methyl pyrrolidone (NMP) at 150°C at a total polymer concentration of 30 wt%. Scaffolds were then fabricated using the film

casting technique. Immediately following casting, the scaffolds were immersed in water to remove the solvent. This immersion process was repeated twice. The wet scaffolds were left at room temperature for a few minutes before drying overnight at 50°C. The prepared scaffolds were 8 mm in diameter and were subsequently sterilized using EO (ethylene oxide) gas at the Suranaree University of Technology Hospital.

Table 3.1 The total designed experiment of composited material from Design expert program.

Run	PLA(%)	PBS(%)	nanocellulose (%)
1	77.50	17.50	5.00
2	65.00	26.71	8.29
3	77.50	17.50	5.00
4	65.00	26.71	8.29
5	90.00	7.11	2.89
6	76.30	23.70	0.00
7	90.00	7.11	2.89
8	84.10	11.53	4.37
9	77.50	17.50	5.00
10	65.00	35.00	0.00
11	82.62	7.38	10.00
12	74.69	15.31	10.00
13	82.53	17.47	0.00
14	88.58	1.42	10.00
15	70.14	28.99	0.87
16	77.50	17.50	5.00
17	82.53	17.47	0.00
18	69.24	20.76	10.00
19	88.58	1.42	10.00

3.3 hWJ-MSC isolation and culture

Human umbilical cords (n=2) were obtained from Maharat Nakhon Ratchasima Hospital (Nakhon Ratchasima, Thailand), for which informed consent was obtained from

the mothers in accordance with the Ethics Committee for Research Involving Human Subjects of Suranaree University of Technology (EC-64-125). The cords were approximately 7–10 cm long and were washed with phosphate buffered saline (-) (PBS(-)). hWJ-MSCs were isolated from the umbilical cords and cultured as described previously (Tanthaisong et al., 2017) Briefly, gelatinous Wharton's Jelly tissues were collected and sliced into small pieces (2–5 mm^2), placed in 90-mm × 15-mm culture dishes, and grown in the alpha modification of Eagle's medium (α-MEM) enriched with 2 mM L-glutamine, 100 U/ml penicillin, 100 µg/ml streptomycin, and 10% fetal bovine serum (FBS). The MSCs were expanded until passage 3, cryopreserved with 10% dimethyl sulfoxide (DMSO) in culture media, and then stored in liquid nitrogen.

Human Wharton's Jelly mesenchymal stem cells (hWJ-MSCs) were cultured in collaboration with the Embryo Technology and Stem Cell Research Center, Suranaree University of Technology.

For cell seeding, approximately 1.0 x 10^5 hWJ-MSCs were plated on 4-well dishes (Nunc, Roskilde, Denmark) pre-coated with 0.1% gelatin. The cells were cultured in a complete medium (α-MEM supplemented with 10% FBS).

In the following hepatogenic differentiation protocol as shown in figure 3.3., the optimal scaffold was incorporated at the beginning of the process, cells were first cultured in serum-free IMDM (Iscove's Modified Dulbecco's Medium) supplemented with 10 ng/mL bFGF (human basic fibroblast growth factor), 20 ng/mL EGF (epidermal growth factor), 100 µg/mL streptomycin, 100 U/mL penicillin, and 1 mM NaBu (Sodium butyrate) for 3 days (pre-treatment step). Subsequently, the cells were induced to differentiate into the hepatic lineage using serum-free IMDM supplemented with 10 ng/mL bFGF, 40 ng/mL HGF (hepatocyte growth factor), and 5 mM nicotinamide for 7 days (differentiation step). Finally, the cells underwent a maturation step in serum-free IMDM supplemented with 10 ng/mL OSM, 10 nM dexamethasone, and 1% ITS-X for 7 days. The culture medium was changed twice weekly throughout the differentiation process (Panta, et al., 2019).

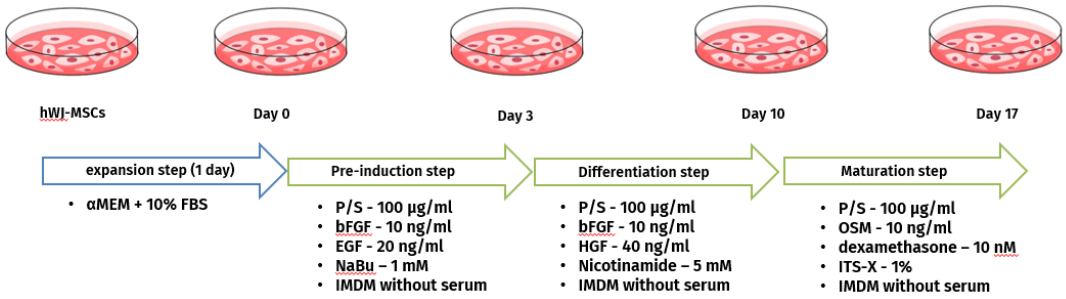

Figure 3.3 Hepatogenic differentiation protocol

3.4 Characterizations

3.4.1 Particle analysis

The average size, zeta potential, and polydispersity index of the nanocellulose samples were characterized using a Zetasizer nano zs instrument (Malvern,UK). The Zetasizer nano zs instrument was shown in figure 3.4.

Figure 3.4 Zetasizer nano zs instrument (Malvern,UK)

3.4.2 Fourier Transform Infrared Spectrometer (FT-IR)

The nanocellulose powder was prepared using a Diamond compression cell (S.T. Japan Europe, Germany) equipped with two disks and a diamond window with a diameter of 3 mm. A thin layer of nanocellulose was added to the window using a needle, followed by compact closure with the two disks.

Synchrotron radiation-based FT-IR spectroscopy was appeared in figure 3.5 and employed to analyze chemical modifications in the nanocellulose. This technique utilizes a synchrotron infrared source at beamline 4.1 of the Thai Synchrotron National Lab, operated in conjunction with a Bruker VEXTEX 70 vacuum FTIR spectroscopy system

linked to a Bruker Hyperion 2000 IR microscope (Bruker Optics, Ettlingen, Germany). The microscope was equipped with a 36X objective and a mercury cadmium telluride (MCT) detector cooled with liquid nitrogen. The nanocellulose sample was measured in transmission mode using a spot size of 20 x 20 μm^2. Background subtraction was performed, and 64 scans were co-added with a spectral resolution of 4 cm^{-1}. Spectral data collected at beamline 4.1 were then analyzed using OPUS 7.5 software.

Finally, principal component analysis (PCA) of the FT-IR spectra was conducted in the wavenumber ranges of 3630-2770 cm^{-1} and 1720-900 cm^{-1} by second derivative analysis. This analysis utilized the Savitzky-Golay smoothing function within the Unscrambler X version 10.4 software.

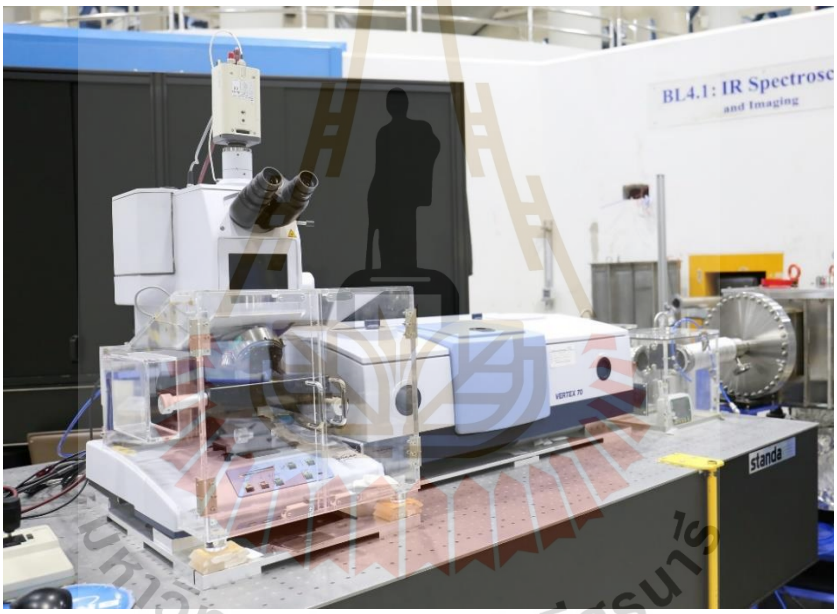

Figure 3.5 Bruker VEXTEX 70 vacuum FTIR spectroscopy system linked to a Bruker Hyperion 2000 IR microscope (Bruker Optics, Ettlingen, Germany) at beamline 4.1 of the Synchrotron Light Research Institute (Public Organization), Thailand.

3.4.3 Wide-Angle X-ray Scattering (WAXS)

Wide-Angle X-ray Scattering (WAXS) experiments were performed at Beamline 1.3W of the Synchrotron Light Research Institute (Public Organization), Thailand (figure 3.6). The samples were exposed to X-rays with a wavelength of 0.137 nm for 600 seconds at room temperature. The sample-to-detector distance (SDD) was set to 167 mm. The raw data were preprocessed using the SAXSIT program, developed by SLRI staff, to generate the 1D WAXS curve. This curve was then further analyzed using the pseudo-

Voigt function within the SAXSIT software to determine the crystallinity index of the nanocellulose.

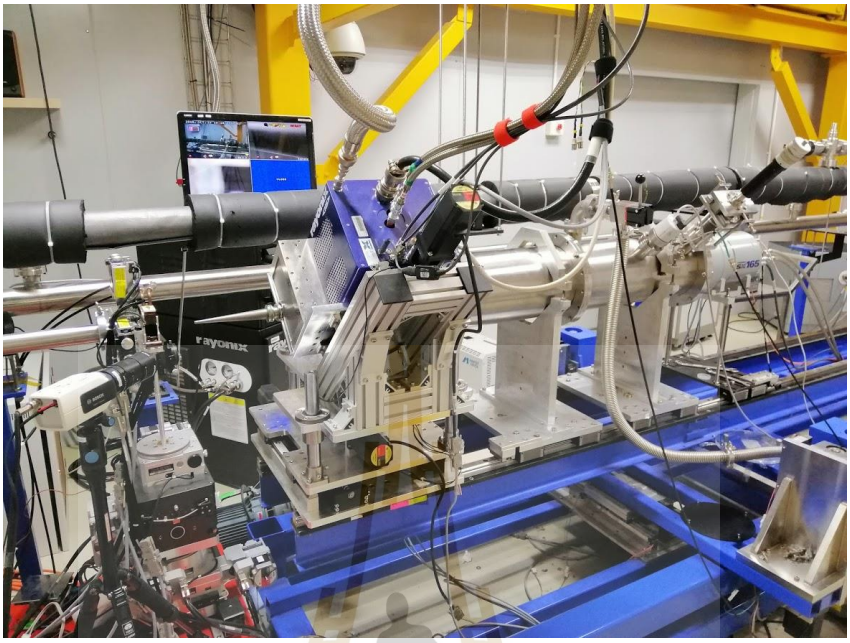

Figure 3.6 Wide-Angle X-ray Scattering (WAXS) instrument at Beamline 1.3W of the Synchrotron Light Research Institute (Public Organization), Thailand.

3.4.4 Thermal characterizations

The thermal stability of the samples was evaluated using thermogravimetric analysis (TGA) under an inert nitrogen atmosphere (flow rate of 30 mL/min) with a TGA instrument (TGA/DSC1, Mettler Toledo, USA) (fig 3.7). Approximately 2 mg of each sample was loaded onto a sample pan and heated from 30 °C to 500 °C at a constant heating rate of 10 °C/min. The onset temperature of weight loss and the temperature corresponding to the maximum degradation rate were determined.

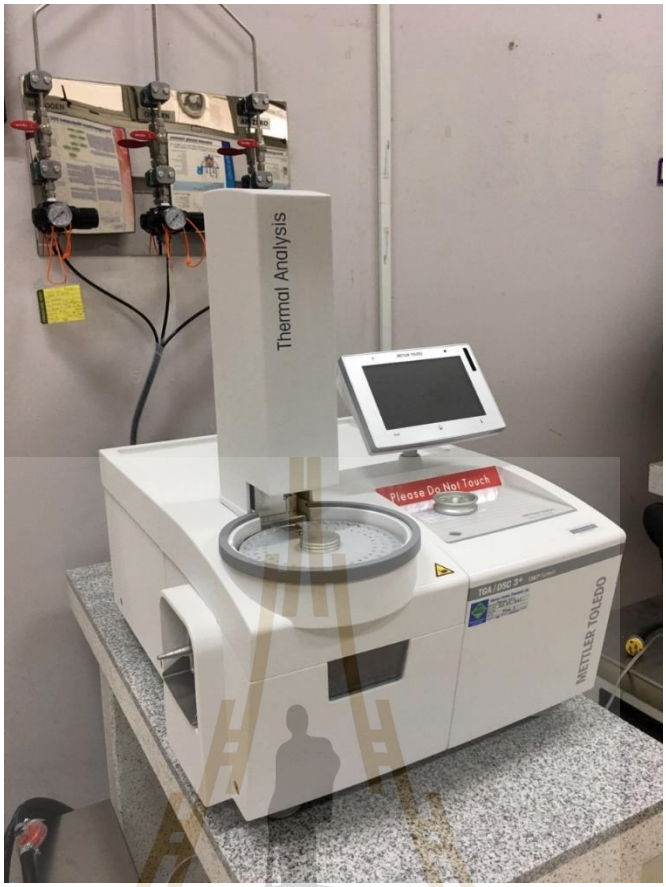

Figure 3.7 TGA instrument (TGA/DSC1, Mettler Toledo, USA)

The thermal properties of the samples were analyzed using differential scanning calorimetry (DSC) (DSC 204F1, NETZSCH, Germany) (fig 3.8) under a nitrogen atmosphere at a heating rate of 10 °C/min. The samples were heated from 20 °C to 250 °C. The glass transition temperature (Tg), melting temperature (Tm), and melting enthalpy (Hm) were determined from the instrument. The degree of crystallinity (X_c) of PLA and PBS in the scaffold was then calculated from the melting enthalpy values according to the following equation:

$$X_c(\%) = \frac{\Delta H_m}{f_p \times \Delta H_m^\circ} \times 100\%$$

where:

- ΔH_m (J/g) is the melting enthalpy of the polymer matrix measured by DSC.
- f_p is the weight fraction of PLA or PBS in the sample.
- ΔH_m° (J/g) is the melting enthalpy of pure crystalline PLA (93 J/g) or PBS (200 J/g) [Hu, & et al., 2018].

Figure 3.8 Differential scanning calorimetry (DSC) (DSC 204F1, NETZSCH, Germany)

3.4.5 Tensile force measurement

Uniaxial tensile testing was performed at ambient temperature to characterize the mechanical properties of the scaffold samples. A TA.XT Plus SMS Stable Micro Systems Texture Analyzer (Stable Microsystems Ltd., Surrey, England) appeared in figure 3.9 and equipped with Texture Expert software was employed for the analysis. The scaffold specimens measured 0.1 mm in width, 50 mm in height, and 20 mm in length. The testing protocol involved subjecting the specimens to a controlled tensile load. The specific parameters for the test were as follows: pre-test speed of 1.0 mm/s, test speed of 1.5 mm/s, post-test speed of 10.0 mm/s, trigger type set to auto-5g, and tare mode disabled.

Figure 3.9 A TA.XT Plus SMS Stable Micro Systems Texture Analyzer (Stable Microsystems Ltd., Surrey, England)

3.4.6 Contact angle measurement

The scaffold was analyzed for the contact angles of ultrapure water and cell culture medium by the sessile drop method in Agriculture and Bioplasma Technology Center, Thailand. Equilibrium contact angles (considered at 60 s) were measured for 5 μL droplet volumes. Determinations were made on 5 different locations for each condition.

3.4.7 Microscopies

The structural surface morphology of the nanocellulose samples and cell adhesion on the scaffold were investigated using field emission scanning electron microscopy (FESEM) (Zeiss, AURIGA, Germany) to assess surface features, FESEM was shown in figure 3.10. Transmission electron microscopy (TEM) (FEI, Tecnai G2 20 TEM, USA) was appeared in figure 3.11 and employed to image the nanocellulose at the microscopy laboratory, Suranaree University of Technology.

Figure 3.10 field emission scanning electron microscopy (FESEM) (Zeiss, AURIGA, Germany)

Figure 3.11 Transmission electron microscopy (TEM) (FEI, Tecnai G2 20 TEM, USA)

3.4.8 Analysis of cytotoxicity

One thousand hWJ-MSCs were replated in 96-well culture plates (SPL Life Sciences, Gyeonggi-do, Korea) and cultured in a culture medium for 24 hours to allow attachment. The cytotoxicity of the optimal scaffold was evaluated by adding it to the culture medium. All cultures were maintained at 37°C for 48 hours in a humidified atmosphere with 5% CO2. The effects of scaffold on cell viability were quantified using a 3-(4,5-dimethylthiazol-2-yl)-2,5-diphenyl tetrazolium bromide (MTT) assay. The microplate reader (Varioskan LUX, Thermo Scientific, USA) was used to measure absorbance at 540 nm, as shown in Figure 3.12.

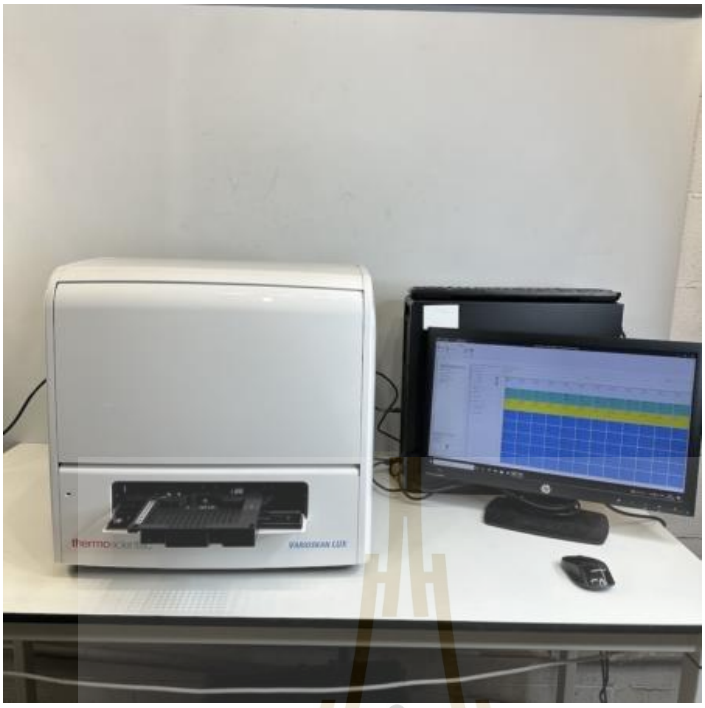

Figure 3.12 microplate reader (Varioskan LUX, Thermo Scientific, USA)

3.4.9 Immunofluorescence staining

Immunofluorescence staining was employed to evaluate protein expression profiles in cells undergoing a 17-day differentiation process on the scaffold. Cells were harvested on day 17 and fixed with 4% paraformaldehyde (PFA) for 15 minutes. Subsequently, a blocking and permeabilization step was performed using a solution containing BSA, normal goat serum, sodium azide, and Triton-X 100 for 2 hours at 37°C. The cells were then incubated overnight at 4°C with a panel of primary antibodies targeting specific proteins of interest, including alpha-fetoprotein (AFP), cytokeratin 18 (CK18), and albumin (ALB). Following incubation, the cells were washed and subsequently exposed to corresponding secondary antibodies for 2 hours. Nuclei were visualized using DAPI staining, and protein expression was observed using a Confocal Laser Scanning Microscope (CLSM-Upright Ni-E, Nikon, Japan), which instrument appeared in figure 3.13.

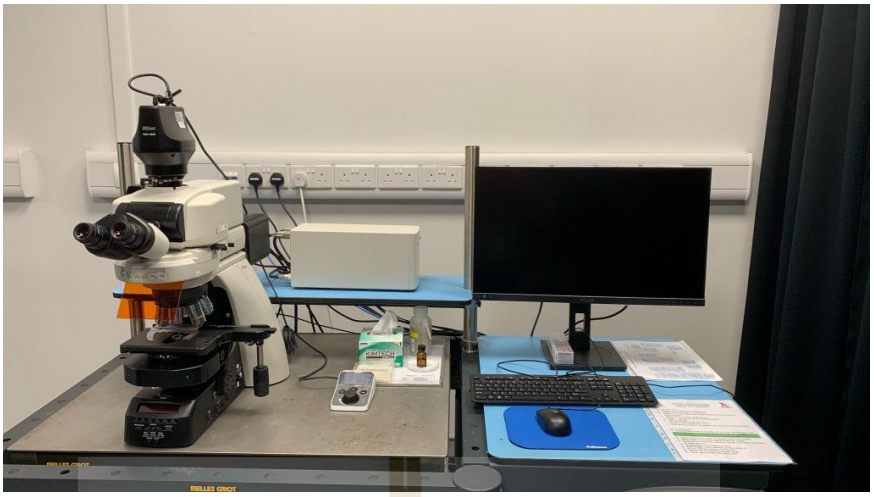

Figure 3.13 Confocal Laser Scanning Microscope (CLSM-Upright Ni-E, Nikon, Japan)

CHAPTER IV
RESULTS AND DISCUSSIONS

4.1 Nanocellulose analysis

4.1.1 Nanocellulose characterization

Characterization of the dried cellulose revealed a primary composition of cellulose fibers with a lignin content of 0.53% and a hemicellulose content of 6.63%, as determined through chemical analysis. Field emission scanning electron microscopy (FESEM) was employed to investigate the cellulose morphology, which is presented in Figure 4.1.

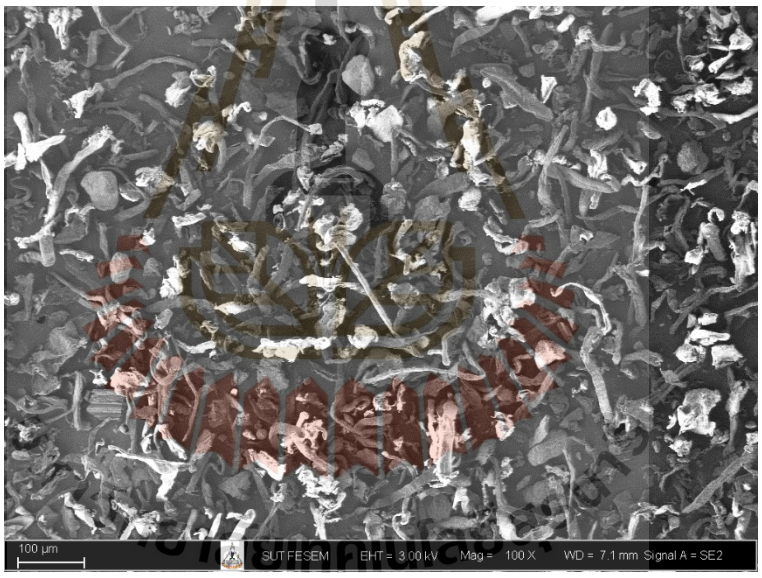

Figure 4.1 FESEM image of sieved cellulose.

The initial cellulose mixture possessed an average particle size of 43 µm before undergoing high-pressure homogenization. All three samples, the homogenized mixture, the enzyme-treated product, and the nanocellulose powder depicted in Figure 4.2 were subjected to analysis to determine their average particle sizes (Figure 4.3). The optimal particle size reduction of 278.9 nm was achieved using high-pressure homogenization at 30,000 psi for 15 passes with the addition of a 7% enzyme cocktail. These findings suggest

that the enzyme cocktail played a substantial role in facilitating size reduction, with high-pressure homogenization further augmenting this effect.

The cellulose nanofibers (CNF) were examined in PBS for tissue engineering scaffolds and reported that CNFs with lengths of 500-800 nm and diameters below 50 nm resulted in the best combination of mechanical strength and cell attachment properties(Lin et al., 2011). In addition, biocompatibility aspects of nanocellulose were studied in various polymers and found that for biomedical implants, CNFs with aspect ratios (length/diameter) between 70-100 showed reduced inflammatory responses while maintaining mechanical advantages (Endes et al., 2016). The optimal size of nanocellulose for biomedical applications remains unclear. This is because nanocellulose size significantly influences the mechanical properties of the composite. However, the ideal size depends on the specific biomedical application and its intended purpose.

Figure 4.2 image of sample in nanocellulose preparation a) dried cellulose, b) homogenized cellulose mixture, c) enzyme-containing product (homogenized cellulose mixture was added by enzyme) and d) nanocellulose powder.

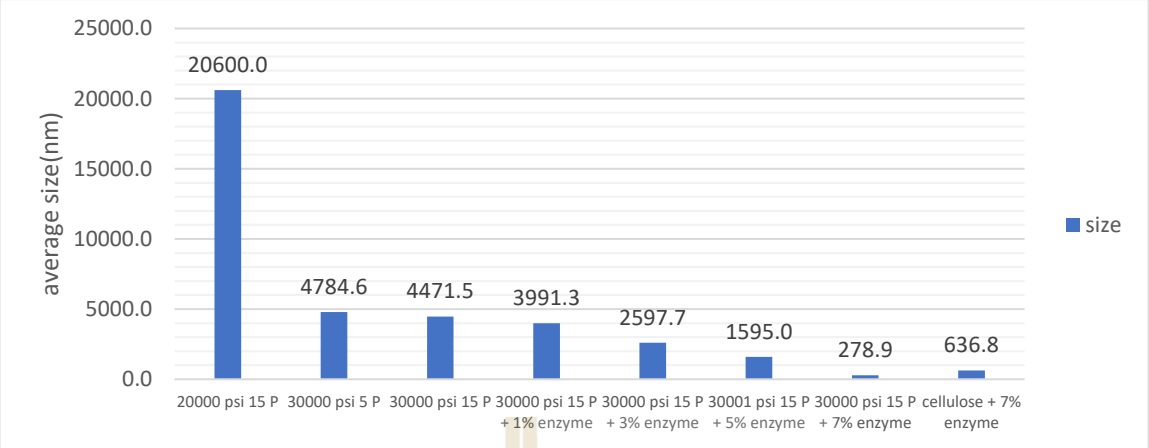

Figure 4.3 average size (nm) of nanocellulose with different conditions.

The polydispersity index (PDI) served as a metric to evaluate the distribution of particle sizes within the nanocellulose samples. The PDI values for nanocellulose produced under various processing conditions were presented in Table 4.1 The structural modifications induced by high-pressure homogenization were hypothesized to render the cellulose fibrils more amenable to enzymatic degradation during subsequent hydrolysis. This enhanced susceptibility to enzymatic hydrolysis can be attributed to the substantial shortening of the fibrils observed following enzymatic treatment. As a direct consequence, the incorporation of enzymes resulted in a significant elevation of the PDI of the nanocellulose. The enzyme cocktail functions synergistically, though each enzyme follows a distinct action pattern, further contributing to size heterogeneity. The increased PDI indicates a broader particle size distribution after enzymatic treatment. While the average particle size may decrease, the resulting population becomes more diverse, comprising both very small fragments from regions highly susceptible to enzymatic attack and larger fragments from more resistant regions.

Table 4.1 Polydispersity index (PDI) of nanocellulose with different conditions.

sample	PDI
20000 psi 15 P	0.554
30000 psi 5 P	0.390
30000 psi 15 P	0.462
30000 psi 15 P + 1% enzyme	0.567
30000 psi 15 P + 3% enzyme	0.616
30001 psi 15 P + 5% enzyme	0.669
30000 psi 15 P + 7% enzyme	0.752
cellulose + 7% enzyme	0.720

Zeta potential, a physicochemical property quantifying the electrostatic potential at the interface between a solid particle and a surrounding liquid, was presented for the nanocellulose samples in Figure 4.4 Intriguingly, the zeta potential of the nanocellulose exhibited a significant reduction to approximately -20 mV following high-pressure homogenization at 30,000 psi for 15 cycles. This observation suggests a pressure-dependent decline in zeta potential magnitude during homogenization. The observed decrease can potentially be attributed to the exposure of anionic functional groups on the nanocellulose surface. This phenomenon may result from cellulose fiber release or surface chemistry alterations induced by the mechanical stress of homogenization, as previously reported (Wu et al., 2020). Conversely, the enzymatic treatment is not recognized to introduce negatively charged groups onto the surface of the nanocellulose. Notably, materials with lower negative zeta potential values are generally considered more favorable for specific biomedical applications (Squinca et al., 2020).

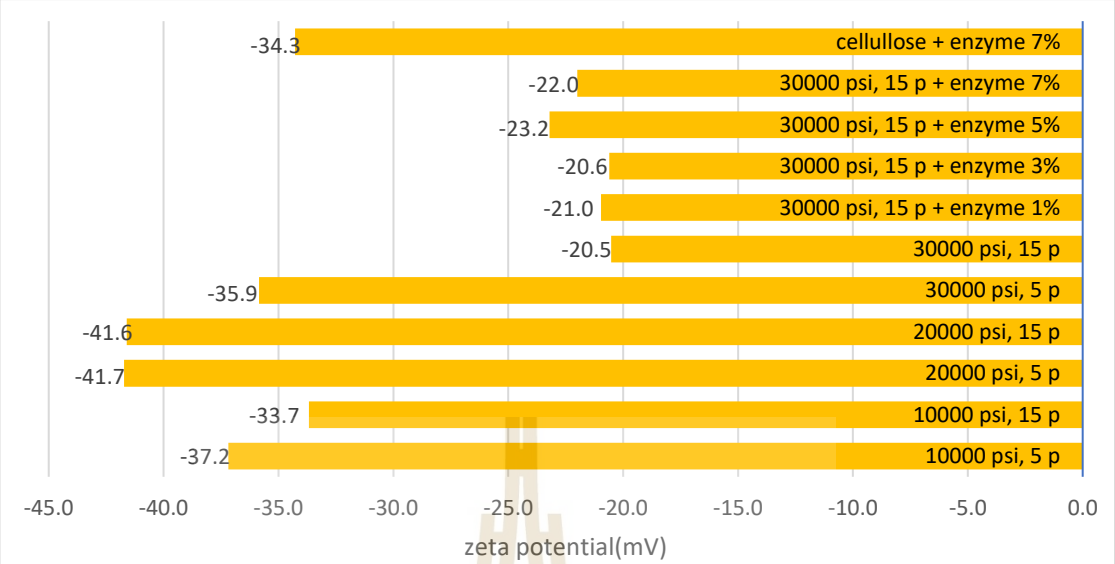

Figure 4.4 zeta potential (mV) of nanocellulose with different conditions.

4.1.2 Morphological analysis

The morphology of cellulose processed solely through mechanical means is illustrated in Figure 4.5(left) The image depicts extensive fibrillation, a consequence of high-pressure homogenization at 10,000 psi for 5 cycles. Conversely, Figure 4.5 (middle) provides a clear visualization of the nanocellulose obtained through the synergistic application of high-pressure homogenization and enzymatic hydrolysis. Notably, the nanocellulose exhibits a markedly reduced particle size compared to cellulose processed solely by the mechanical technique. The enzymatic hydrolysis was postulated to have instigated a cascade of complex reactions, ultimately transforming the cellulose fibril morphology into a more spherical configuration. Moreover, transmission electron microscopy (TEM) was utilized to examine the crystal structure of the nanocellulose derived from the combined methods, as presented in Figure 4.5 (right).

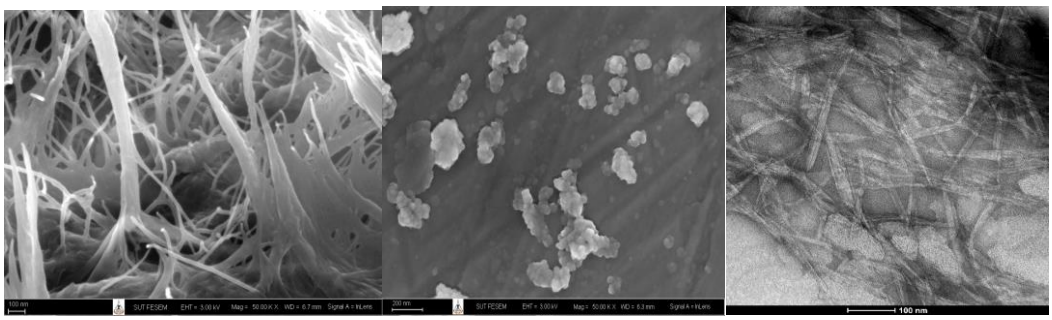

Figure 4.5 FESEM image of cellulose nanofibrils from high pressure homogenization at 10,000 psi 5 pass (left), FESEM image of nanocellulose from high pressure homogenization at 30,000 psi, 15 pass couple with enzymatic process (7% of enzyme) (middle), TEM image cellulose nanocrystal from high pressure homogenization at 30,000 psi, 15 pass couple with enzymatic process (7% of enzyme) (right)

4.1.3 FTIR analysis

Fourier Transform Infrared (FTIR) spectroscopy serves as a well-established analytical technique for elucidating the chemical functionalities and structural characteristics of cellulose. The average spectra obtained for nanocellulose processed under various conditions are presented in Figure 4.6.

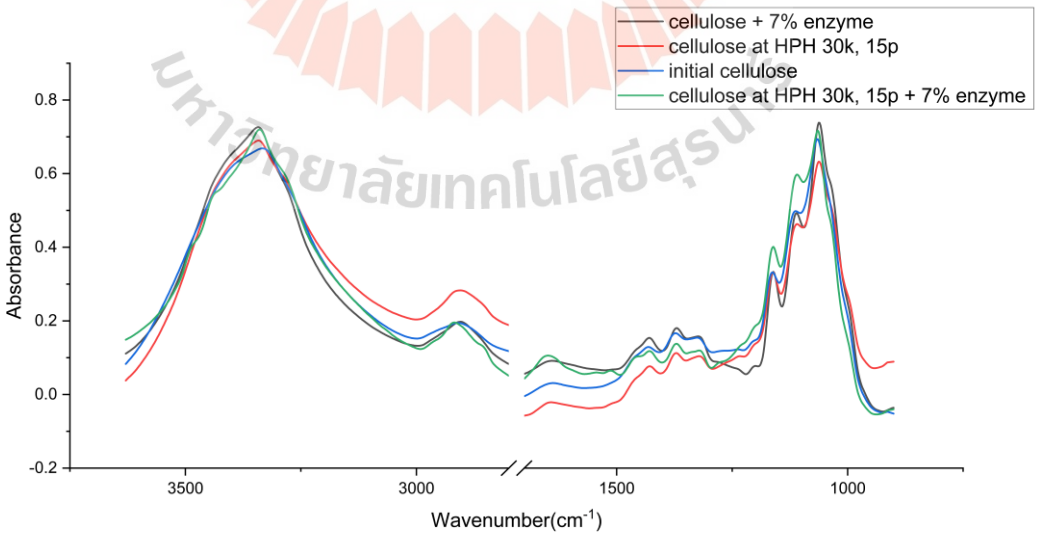

Figure 4.6 The original average FTIR spectra of nanocellulose in different conditions and initial cellulose in wavenumber ranges of 3630-2770 cm^{-1} and 1720-900 cm^{-1}.

Principal component analysis (PCA) represents a multivariate statistical method employed to analyze large datasets. In this study, PCA was utilized to characterize the FTIR spectra of the nanocellulose samples. Typically, PCA applied to spectroscopic data yields two primary types of information including. First, the expression of a group of similar spectra within the dataset was visualized in a scatter plot (Figure 4.7A). This 2D PCA score plot depicts PC-1 (contributing 30% of the variance) versus PC-2 (contributing 6% of the variance). The second type, the loadings corresponded to the influence of specific spectral features on the observed variation. These loadings were presented in Figure 4.7B. The negative loading plot was illustrated in Figure 4.7B (top), which relates to the positive score plot of the initial cellulose by PC-2 (represented by the blue symbol). The FTIR spectral bands were summarized in Table 4.2

Table 4.2 FTIR Spectral Bands and Assignments

Peak (cm^{-1})	Assignment	Reference
3490, 3442	Intramolecular OH (cellulose II)	[Hishikawa et al., 2017, Makarem et al., 2019]
3320	Intramolecular OH (cellulose)	[Hishikawa et al., 2017, Makarem et al., 2019]
3339	Intermolecular OH (cellulose Iα and Iβ)	[Hishikawa et al., 2017, Makarem et al., 2019]
3276	Intermolecular OH (cellulose Iβ)	[Hishikawa et al., 2017, Makarem et al., 2019]
2919	CH stretching vibration	[Hishikawa et al., 2017, Makarem et al., 2019]
2965	CH_2 asymmetric stretching (cellulose)	[Hishikawa et al., 2017, Makarem et al., 2019, Boukir et al.,2019]
2852	CH_2 symmetric stretching (cellulose)	[Hishikawa et al., 2017, Makarem et al., 2019, Boukir et al.,2019]
1511	Aromatic skeletal vibration (lignin)	[Javier-Astete et al., 2021, Salim et al., 2021]
1459, 1373, 1315	CH_2 bending vibration (crystalline cellulose I)	[Makarem et al., 2019, Boukir et al.,2019]
1425	CH_2 asymmetric stretching (amorphous cellulose)	[Makarem et al., 2019, Boukir et al.,2019]
1384	C-H (cellulose)	[Hishikawa et al., 2017, Makarem et al., 2019]

Peak (cm^{-1})	Assignment	Reference
1278	CH deformation (cellulose I and II)	[Makarem et al., 2019, Boukir et al.,2019, Salim et al., 2021]
1174, 1128	C-O-C (cellulose)	[Makarem et al., 2019, Boukir et al.,2019]
1162, 1120	C-O-C asymmetric stretching (cellulose I and II)	[Boukir et al.,2019, Salim et al., 2021, Kudzin et al., 2021]
1072, 1041, 1000	-C-O- (cellulose)	[Makarem et al., 2019, Boukir et al.,2019, Salim et al., 2021, Kudzin et al., 2021]
1062, 1029, 995	C-O vibration and C-O valence vibration (cellulose)	[Oudiani et al., 2017, Parihar et al., 2019]

The negative loadings at peaks 3320 cm^{-1} (intramolecular OH cellulose), 1384 cm^{-1} (C-H in cellulose), 1174 cm^{-1}, and 1128 cm^{-1} (C-O-C in cellulose), 1072 cm^{-1}, 1041 cm^{-1}, and 1000 cm^{-1} (-C-O- in cellulose) indicate a strong association of these wavenumbers with the initial cellulose structure. Conversely, the positive loading plot (Figure 4.7B, bottom) was associated with the negative score plot of the cellulose processed with high-pressure homogenization (HPH) at 30,000 psi for 15 cycles with the addition of 7% enzyme (represented by the green symbol) by PC-2. The positive loadings at peaks 3490 cm^{-1} and 3442 cm^{-1} (intramolecular OH cellulose), 3339 cm^{-1} (intermolecular OH cellulose), 2850 cm^{-1} and 1315 cm^{-1}(CH_2 in cellulose), and 1064 cm^{-1} (C-OH in cellulose) suggest a prominent contribution of these functionalities to the spectral variations observed in the HPH + enzyme treated cellulose. Additionally, the negative loadings at peaks 1064 cm^{-1}, 1020 cm-1, and 991 cm^{-1} (-C-O- in cellulose) imply potential structural modifications in these regions following the combined HPH and enzymatic treatment.

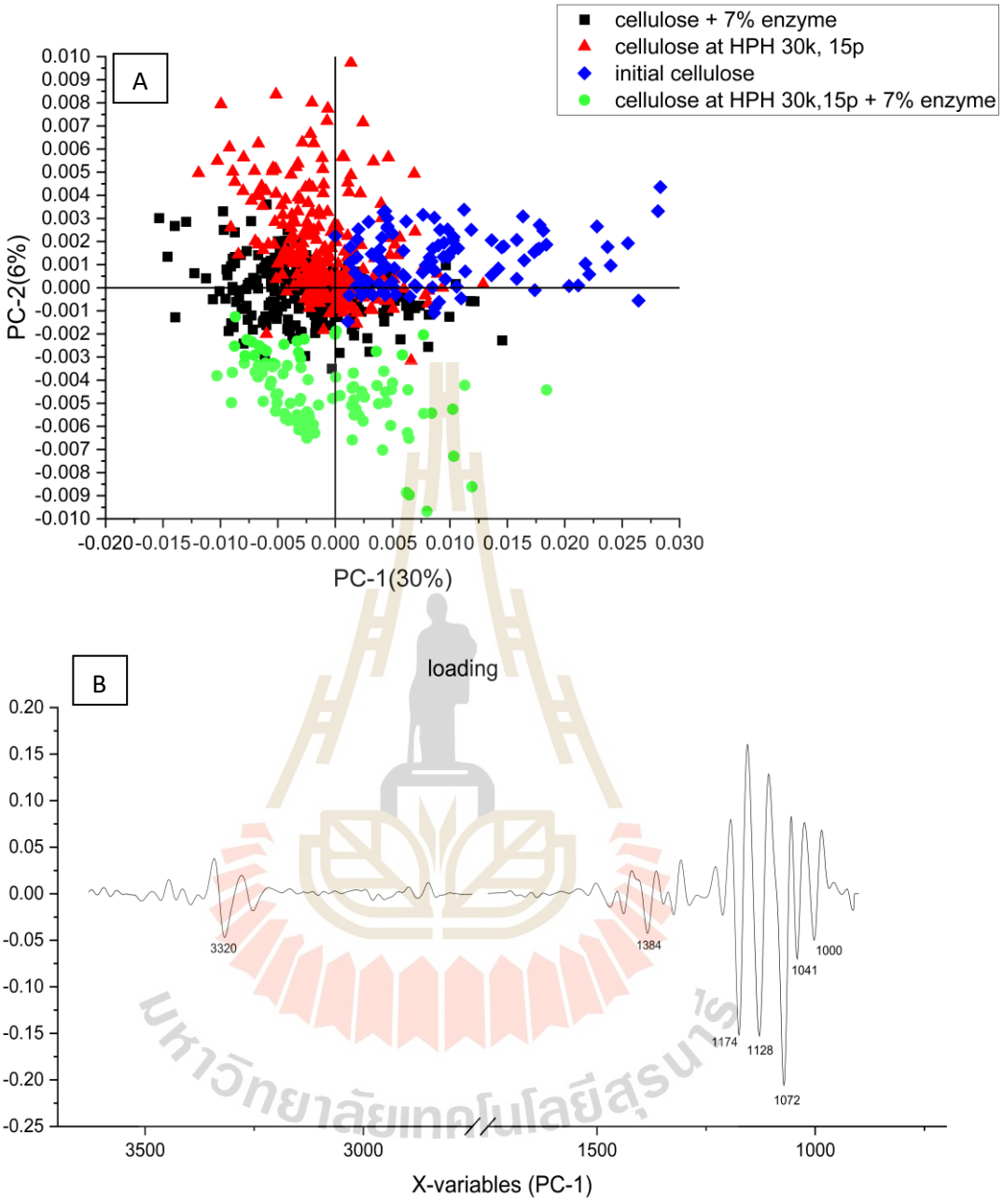
A
cellulose + 7% enzyme
cellulose at HPH 30k, 15p
initial cellulose
cellulose at HPH 30k,15p + 7% enzyme
PC-2(6%)
PC-1(30%)
B
loading
3320
1384
1174
1128
1072
1041
1000
X-variables (PC-1)

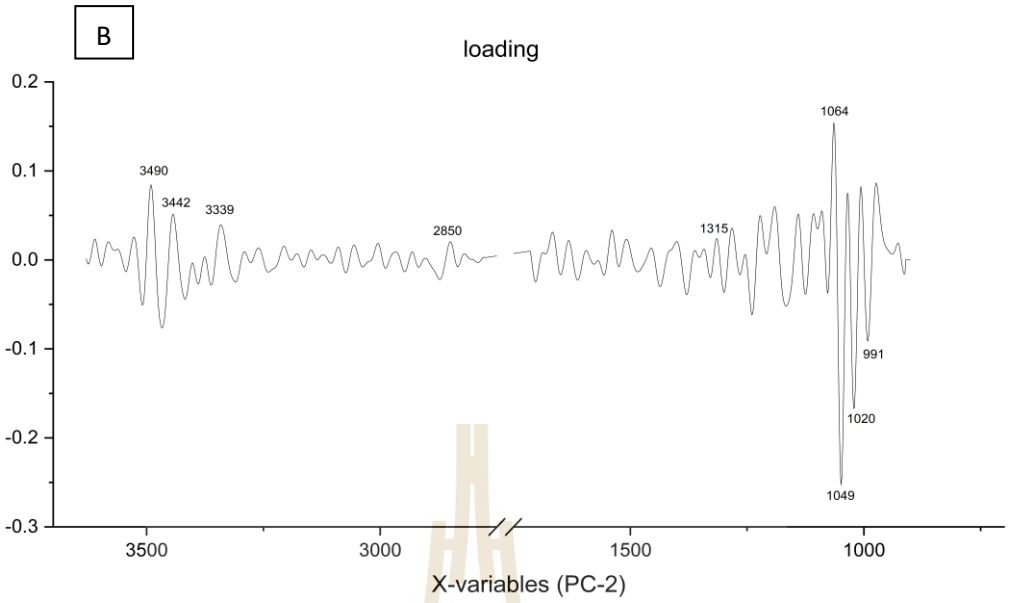

Figure 4.7 The principal component analysis (PCA) score plot of FTIR spectra Principal component analysis score plots (A) and loading plots (B) from 2nd derivative spectra of nanocellulose in different conditions and initial cellulose. Spectra derived using second-derivative processing with the entire biochemical fingerprint region (1800–900 cm^{-1}) and (3500–2800 cm^{-1}).

The second derivative analysis of designated spectral regions within the FTIR spectra, as depicted in Figure 4.8, the band around 3490 cm^{-1} and 3442 cm^{-1} was employed to comparatively assess the nanocellulose samples processed under various conditions with the pristine cellulose. The co-localized band observed at these wavenumbers corresponds to intramolecular hydrogen bonding within cellulose II (Hishikawa et al., 2017; Makarem et al., 2019), whereas the peak at 3339 cm^{-1} is characteristic of intramolecular hydrogen bonding in cellulose Iα and Iβ. The peak at 3276 cm^{-1} is attributed to intermolecular hydrogen bonding in cellulose Iβ. Both the mechanical processing and enzymatic hydrolysis treatments are known to augment the surface area of the cellulose particles, thereby exposing a greater number of hydroxyl (OH) groups. This phenomenon manifests as a more intense and well-defined peak at the OH stretching frequency within the FTIR spectra. The intensity of the intermolecular hydrogen bonding peak (3276 cm^{-1}) serves as an indicator of the crystallinity of cellulose. The observed enhancement in OH stretching intensity associated with intramolecular hydrogen bonding suggests a transformation of the crystalline structure towards a more

amorphous state following the combined application of mechanical and enzymatic treatments.

The band at 2919 cm^{-1} corresponds to CH stretching vibration, while the bands at 2852 cm^{-1} and 2965 cm^{-1} are assigned to CH_2 symmetric and asymmetric stretching vibrations in cellulose, respectively (Doumenq, 2019; Makarem et al., 2019). The presence of the band at 1511 cm^{-1}, attributed to aromatic skeletal vibration in lignin (Javier-Astete et al., 2021; Md Salim et al., 2021), suggests the efficacy of both delignification methods in disrupting the lignin structure.

The peaks at 1459 cm^{-1}, 1373 cm^{-1}, and 1315 cm^{-1} are associated with CH_2 bending vibration in crystalline cellulose I, while the peak at 1425 cm^{-1} corresponds to CH_2 asymmetric stretching vibration in amorphous cellulose (Doumenq, 2019; Makarem et al., 2019). The peak at 1278 cm^{-1} is attributed to CH deformation in both cellulose I and II. The peaks at 1162 cm^{-1} and 1120 cm^{-1} are indicative of C-O-C asymmetric stretching vibration in cellulose I and II (Kudzin et al., 2021; Doumenq, 2019; El Oudiani et al., 2017). Finally, the peaks at 1062 cm^{-1}, 1029 cm^{-1}, and 995 cm^{-1} are assigned to C-O vibration and C-O valence vibration in cellulose (Parihar et al., 2019; El Oudiani et al., 2017).

High-pressure homogenization alters the chemical architecture of cellulose by fragmenting the fibers into nanoscale particles. This process disrupts existing hydrogen bonds within the cellulose fibers and potentially facilitates the formation of new ones. The high pressure and shear forces can also induce mechanical stress, promoting the formation of novel hydrogen bonds between cellulose molecules, resulting in a more densely packed and organized structure. Enzymatic hydrolysis modifies the chemical structure by generating new chemical functionalities on the surface of the cellulose fibers as it cleaves the glycosidic bonds. These modifications can further influence the chemical composition of the resulting nanocellulose.

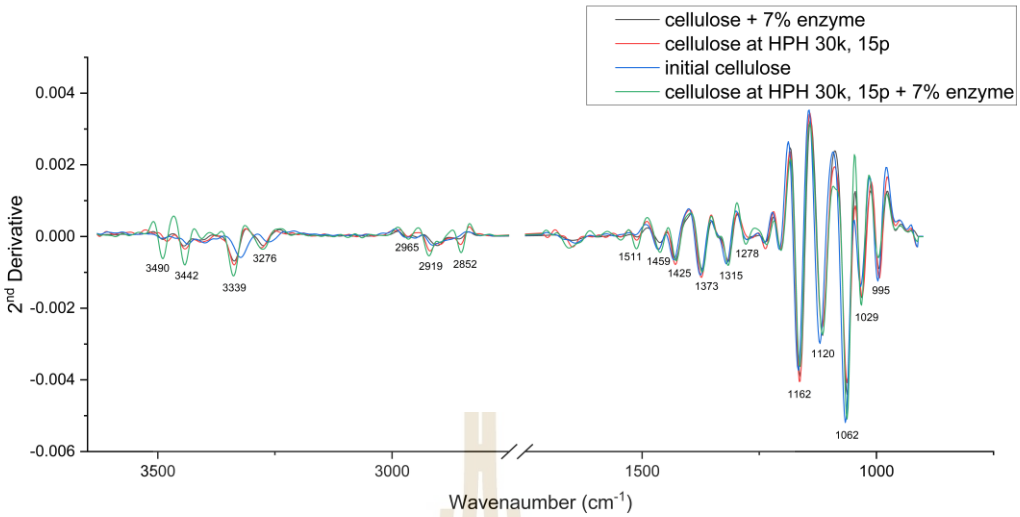

Figure 4.8 The average second derivative spectra obtained from FTIR spectra nanocellulose in different conditions and initial cellulose. The spectra after 13 points of smoothing and normalized with extended multiplicative signal correction over the range of 3630-2770 $cm^{-1}$and 1720-900 cm^{-1}.

4.1.4 WAXS analysis

Wide-angle X-ray scattering (WAXS) analysis is a well-established technique for characterizing crystalline structures. The WAXS patterns of the nanocellulose samples are presented in Figure 4.9. The characteristic scattering peaks for cellulose I were observed at 2θ = 14.8°, 16.3°, 20.6°, 22.4°, and 34.4° (Cheng et al., 2014), while those for cellulose II were identified at 2θ = 12.4°, 20.2°, and 21.8° (Cheng et al., 2014). The peaks at 2θ = 26.5° and 27.8° were attributed to natural graphite (Lionetto et al., 2019) and natural silver chloride (Chen et al., 2014), respectively. The unidentified peaks at 2θ = 36.4° and 39.2° could potentially originate from natural minerals present in the sample.

The crystallinity index (CI) of cellulose was determined using the WAXS deconvolution method implemented in SAXSIT software. This method involves separating the amorphous and crystalline contributions in the WAXS spectrum through curve fitting using Voigt functions. The resulting CI values are shown in Figure 4.10.

The initial cellulose exhibited a high CI of 59.2%. However, high-pressure homogenization led to a decrease in CI, possibly due to the disruption of the crystalline structure by the high-pressure forces. Conversely, enzymatic hydrolysis initially resulted in an increase in CI with increasing enzyme concentration up to 5%. However, CI

decreased to 50% when 7% enzyme was added. During homogenization, the mechanical forces can disrupt hydrogen bonding networks within cellulose crystalline domains (Nechyporchuk et al.,2016), the high shear forces and localized pressure differences randomly create structural defects in the crystalline regions, converting portions of crystalline cellulose to amorphous regions, and amorphous regions were destroyed, leading to the breakdown of the structure and size reduction.

For the enzymatic hydrolysis, the cellulase enzymes initially access and hydrolyze the more accessible amorphous regions (Siqueira et al., 2010, Peciulyte et al., 2015). The selective enzymatic hydrolysis preferentially attacks amorphous regions while leaving crystalline domains intact (Tata et al., 2015). This selective degradation effectively increases the proportion of crystalline material in the remaining cellulose. In another hand, higher enzyme loadings or extended reaction times, enzymes begin attacking the crystalline domains after depleting most accessible amorphous regions (Peng et al., 2015).Excessive enzymatic treatment can penetrate the ordered crystalline structure, creating defects and reducing overall crystallinity (Chen et al., 2016 , Park et al., 2010).

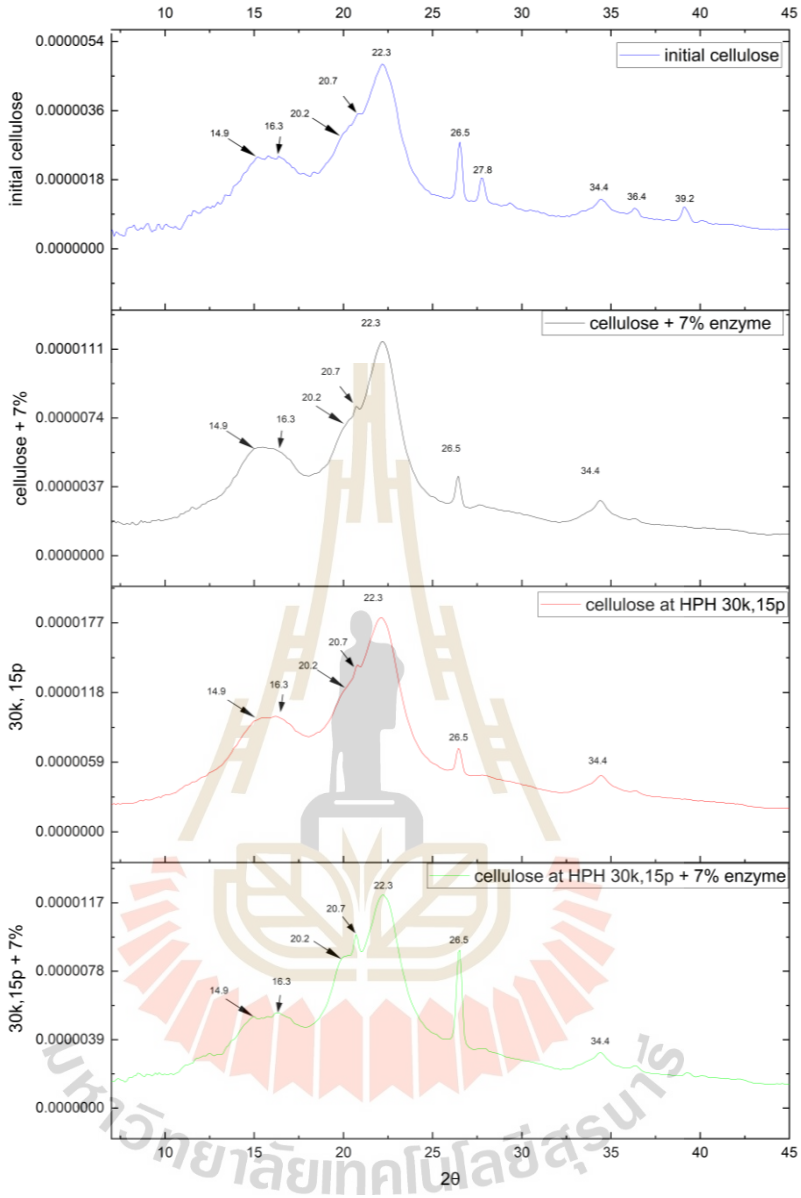

Figure 4.9 WAXS patterns of nanocellulose in different methods compared with initial cellulose.

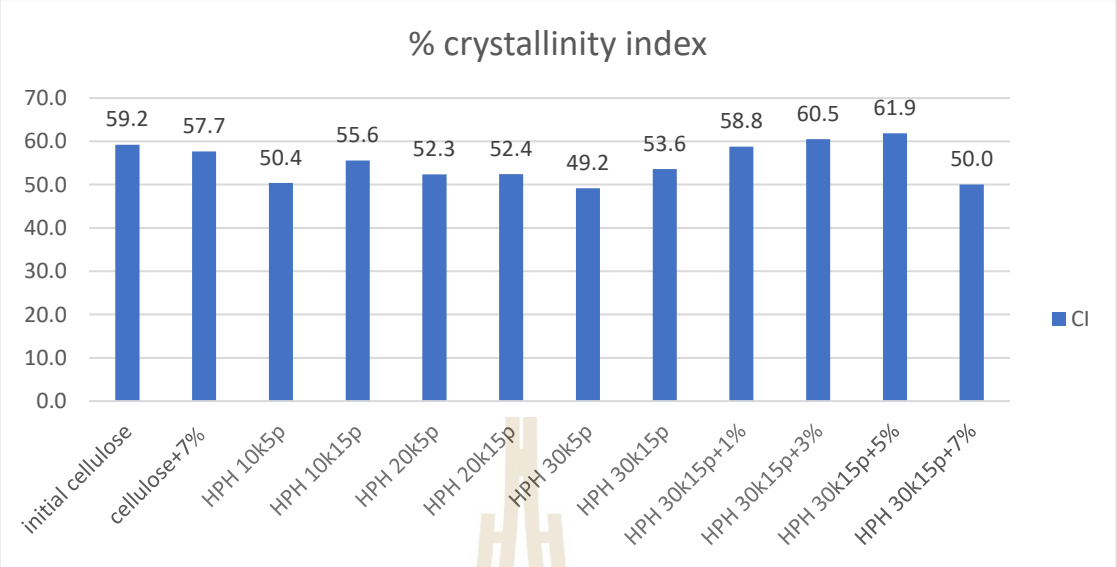

Figure 4.10 crystallinity index of cellulose in different methods.

4.2 Optimal scaffold production and scaffold characterization

4.2.1 Ratio optimization and analysis of scaffold

For the design of cell culture scaffolds, high hydrophilicity and absorption are crucial properties. These characteristics were evaluated by measuring the contact angles of water and cell culture media on the scaffolds. Additionally, the maximum tensile force was analyzed. Experiments were conducted according to the design outlined in Table 4.3, encompassing a total of 19 runs. The water contact angle, cell culture medium contact angle, and maximum tensile force for each run are presented in Table 4.3. To analyze the influence of factors and the relationships between variables, both analysis of variance (ANOVA) and Response Surface Methodology (RSM) were employed. Statistical values including sequential model sum of squares, adjusted coefficient of determination, predicted coefficient of determination, and lack of fit were assessed to determine the suitability of the model.

Table 4.3 mixture designed experiment and results of water contact angle, medium contact angle and maximum tensile force

Run	PLA(%)	PBS(%)	nanocellulose (%)	water contact angle(radius)	medium contact angle(radius)	average maximum tensile force(g)
1	77.50	17.50	5.00	73.29	79.76	1175.40
2	65.00	26.71	8.29	62.20	67.85	956.83
3	77.50	17.50	5.00	71.42	66.10	1175.40
4	65.00	26.71	8.29	64.36	61.43	956.83
5	90.00	7.11	2.89	60.79	60.69	1739.58
6	76.30	23.70	0.00	89.07	79.04	1344.92
7	90.00	7.11	2.89	69.87	62.17	1739.58
8	84.10	11.53	4.37	91.87	82.20	1649.75
9	77.50	17.50	5.00	73.86	73.44	1175.40
10	65.00	35.00	0.00	59.57	63.44	1456.92
11	82.62	7.38	10.00	82.21	74.42	1890.25
12	74.69	15.31	10.00	72.49	82.47	1203.28
13	82.53	17.47	0.00	83.12	82.37	1030.75
14	88.58	1.42	10.00	77.34	76.78	1640.72
15	70.14	28.99	0.87	72.60	62.43	1089.45
16	77.50	17.50	5.00	74.05	82.76	1175.40
17	82.53	17.47	0.00	98.34	113.72	1030.75
18	69.24	20.76	10.00	97.78	72.33	1330.40
19	88.58	1.42	10.00	77.23	76.38	1640.72

Statistical analysis was employed to select a model equation that effectively described the relationship between the water contact angle, maximum tensile force, and the composite material ratio of the cell culture scaffold. A quartic model exhibited the best fit for this relationship, whereas a quadratic model was more appropriate for the contact angle of the cell culture medium and the ratio.

The suitability of the model equations for explaining or predicting experimental outcomes was evaluated using several coefficients (presented in Table 4.4). These coefficients included the coefficient of determination (R^2), adjusted coefficient of determination (adj-R^2), predicted coefficient of determination (pred-R^2), and lack of fit (p-value).

The R^2 values for the water contact angle and maximum tensile force experiments were high (0.8772 and 0.9203, respectively). Generally, a higher R^2 value approaching unity indicates a stronger correlation between the model and the experimental data. In these instances, the close agreement between the model predictions and the experimental observations suggests that the model equations can be used for accurate explanation or prediction.

However, the R^2 value for the cell culture medium contact angle experiment was lower (0.5153), signifying a poor fit. This translates to a substantial discrepancy between the model predictions and the experimental results, thereby diminishing the model's accuracy for explanation and prediction in this context.

For a robust model, the adj-R^2 value should be close to the R^2 value, and a high pred-R^2 value indicates the model's efficacy in predicting response values for novel data points. However, all three experiments exhibited relatively low pred-R^2 values, suggesting that the models are not well-suited for predicting the response of new data.

Furthermore, an analysis of variance (ANOVA) was conducted, and the coefficient of variation (C.V.%) was examined. A lower C.V.% value signifies less variance in the data relative to the mean. The C.V.% values for the water contact angle and maximum tensile force experiments were relatively low (7.12% and 8.41%, respectively), indicating minimal data variation. Conversely, the cell culture medium contact angle experiment exhibited a higher C.V.%, suggesting greater data variance.

A statistically significant p-value for lack of fit indicates that the model inadequately describes the data. The p-values for lack of fit for the water contact angle and cell culture medium contact angle experiments were 0.2203 and 0.4320, respectively, suggesting that the lack of fit is not statistically significant in these cases. However, the p-value for lack of fit in the maximum tensile force experiment was not reported. It is essential to assess this value to definitively determine the model's suitability for this relationship.

Finally, the Water contact angle, The model fits well with a high R^2 and reasonable C.V. The predicted R^2 is low, indicating potential issues in generalizing to new data. Medium contact angle, the model shows moderate fit, but the predicted R^2 is very low, suggesting the model may not generalize well to new data. Maximum Tensile force, the model shows an excellent fit with high R^2 and relatively low C.V., but the low predicted R^2 suggests caution in generalizing the model.

Table 4.4 the data from ANOVA for fitted model

properties	fitted model	sequential P-value	P-value Lack of fit	R^2	adj-R^2	pred-R^2	C.V.(%)
water contact angle	special quartic quadratic	0.0046	0.2203	0.8772	0.779	0.2189	7.12
medium contact angle	quadratic linear	0.0347	0.432	0.5153	0.3288	0.0455	13.55
maximum tensile force	special quartic quadratic	0.0011	-	0.9203	0.8566	0.3237	8.41

Assessment of a model's suitability for variance prediction necessitates residual plot analysis to corroborate the predictions generated by the model equations. Commonly employed plots for this purpose include normal probability plots of residuals, residuals versus predicted values, and predicted versus actual values.

The residual plots for the water contact angle experiment were depicted in Figure 4.11. The data points in the normal probability plot (Figure 4.11A) exhibit a tight distribution around the regression line (red line), signifying minimal deviations from the mean. Similarly, the residuals in the residual versus predicted plot (Figure 4.11B) cluster around the zero line (black line) with no observations exceeding the control lines (red lines). This indicates a favorable distribution of data devoid of outliers. Finally, the predicted versus actual plot (Figure 4.11C) demonstrates that the data points concentrate around the diagonal line (black line), suggesting low errors relative to the predicted

values. Based on this residual analysis, the model appears well-suited for predicting the water contact angle.

However, the residual plots for the cell culture medium contact angle (Figure 4.12) and maximum tensile force (Figure 4.13) experiments reveal some limitations. In the normal probability plots (Figures 4.12A and 4.13A), certain data points (circled) deviate considerably from the regression line, indicating substantial deviations from the mean. Furthermore, while most data points in the residual versus predicted plots (Figures 4.12B and 4.13B) cluster near the zero line, a solitary circled data point falls outside the control lines, suggesting the presence of an outlier. Although most data points in the predicted versus actual plots (Figures 4.12C and 4.13C) lie close to the diagonal line, the circled data points exhibit significant errors compared to the predicted values.

These observations gleaned from the residual plots for the cell culture medium contact angle and maximum tensile force experiments suggest potential shortcomings in the model's capacity to predict these outcomes. While the elimination of outlying data points might seem appealing, a critical investigation into the underlying causes of these deviations is paramount. Re-analyzing the data after addressing these issues might enhance the model's predictive capability.

A)

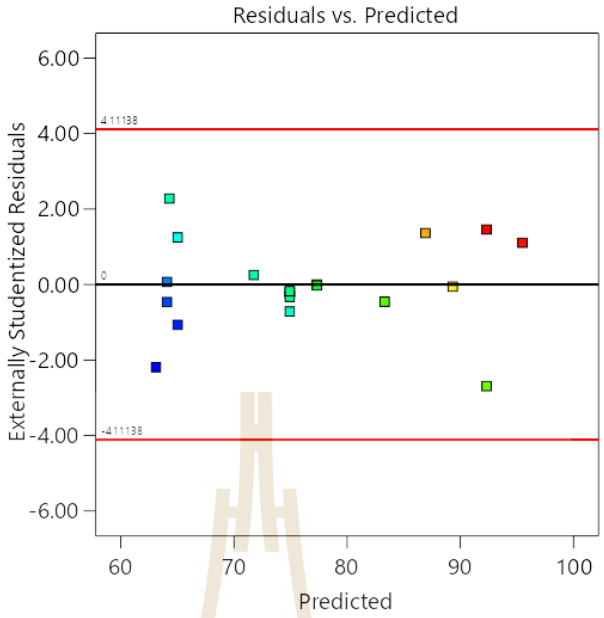

.

B)

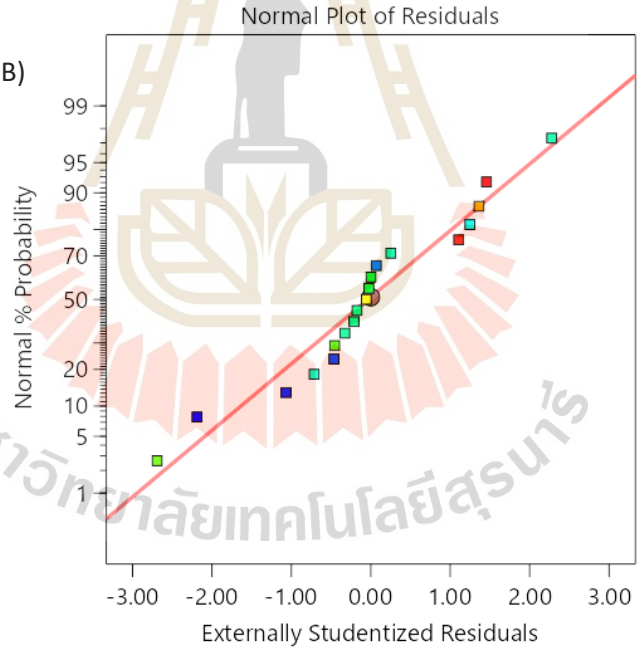

C)

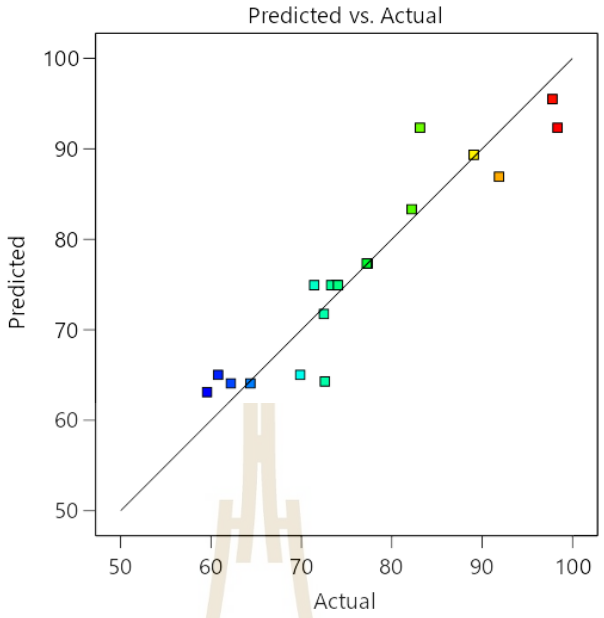

Figure 4.11 verification of the model of the water contact angle experiment : A) Normal plot of Residual, B) Residual Vs. Predicted, C) Predicted Vs. Actual

A)

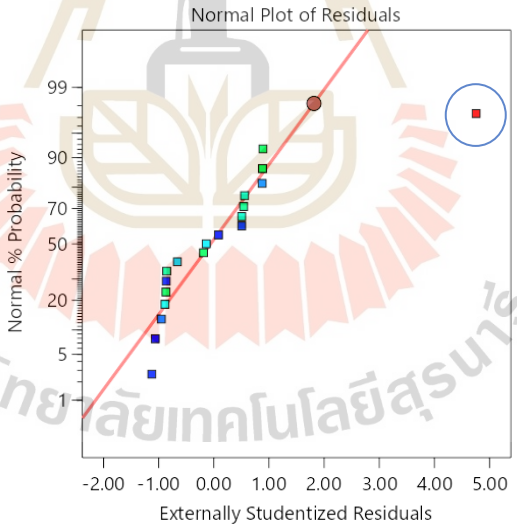

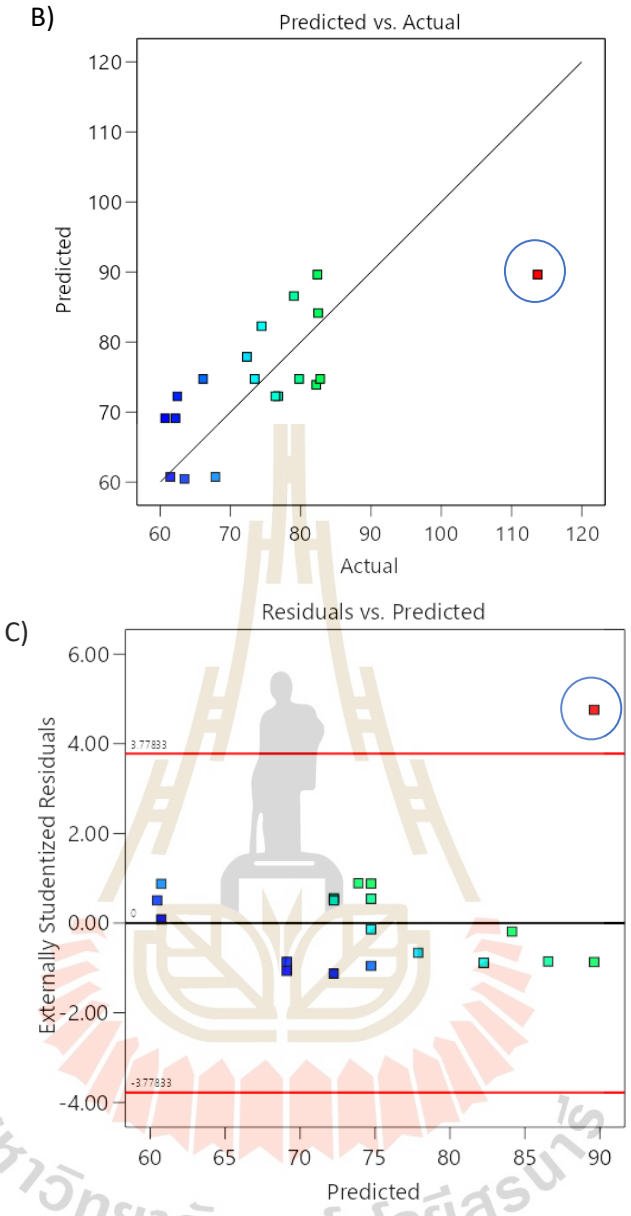

Figure 4.12 verification of the model of the cell culture medium contact angle experiment : A) Normal plot of Residual, B) Residual Vs. Predicted, C) Predicted Vs. Actual

A)

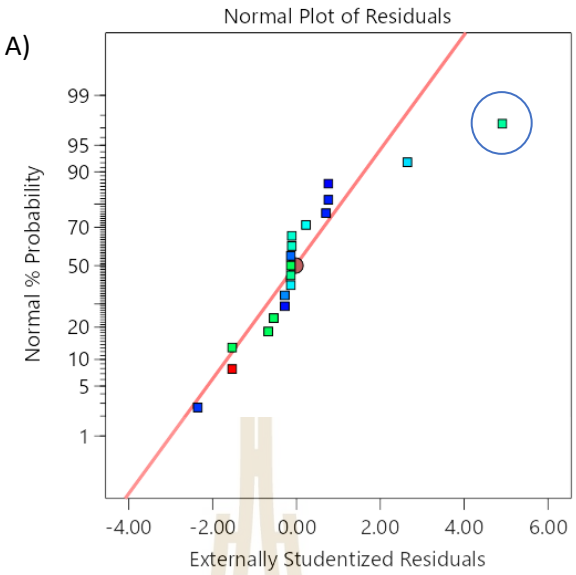

B)

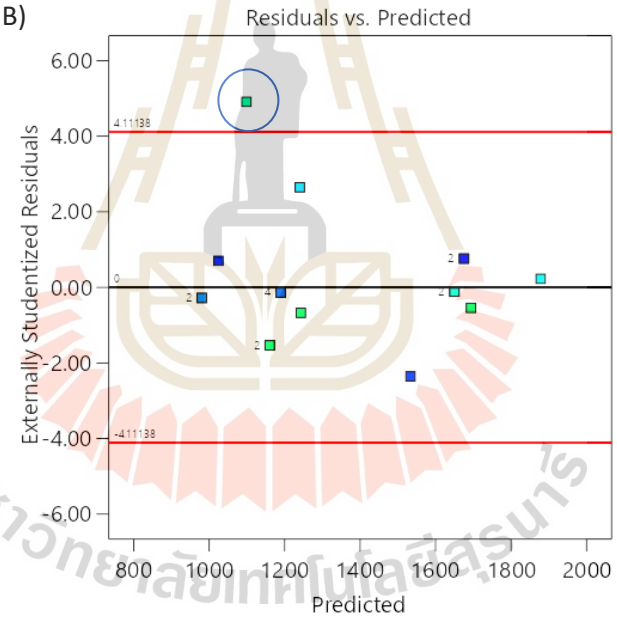

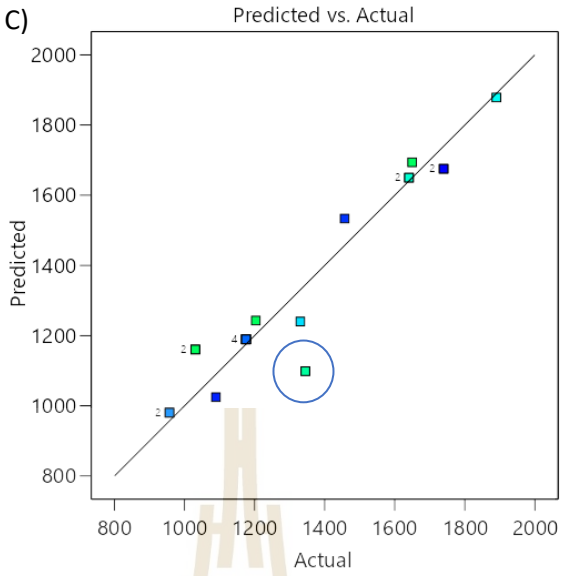

Figure 4.13 verification of the model of the maximum tensile force experiment : A) Normal plot of Residual, B) Residual Vs. Predicted, C) Predicted Vs. Actual

Response Surface Methodology (RSM) constitutes a statistical approach for optimizing production processes. It achieves this by generating a mathematical model that elucidates the interactions between various experimental variables. RSM can be employed to visually represent the relationships between variables through contour plots. Figure 4.14 exemplifies this concept. Within these plots, red areas signify the highest observed values, yellow and green areas represent intermediate values, and blue areas depict the lowest values.

In the water contact angle experiment, the red area is localized within the region of high PLA concentration. This observation implies that PLA addition leads to an increase in the water contact angle of the scaffold, which translates to a reduction in material hydrophilicity. Conversely, the incorporation of PBS and nanocellulose appears to enhance the hydrophilicity of the material.

The cell culture medium contact angle experiment, as illustrated in Figure 16B, exhibits trends analogous to those observed in the water contact angle experiment. In this case, the maximum tensile force demonstrates an increase with the addition of both PLA and nanocellulose, but exhibits a decrease with the addition of PBS.

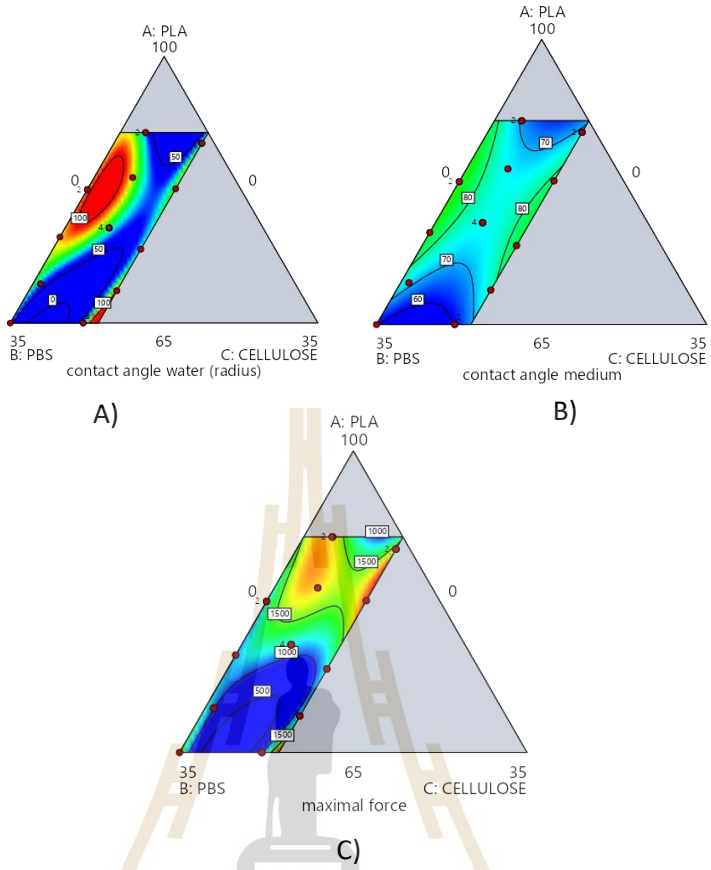

Figure 4.14 Contour plot obtained after optimization (RSM): A) contact angle of water, B) contact angle of cell culture medium and C) maximum tensile force

Response Surface Methodology (RSM) was implemented to optimize the ratio of composite materials under the following constraints, PLA content: 65% to 90% (65% ≤ PLA ≤ 90%), PBS content: maximum 35% (PBS ≤ 35%), Nanocellulose content: maximum 10% (nanocellulose ≤ 10%), Combined PBS and nanocellulose content: maximum 40% (PBS + nanocellulose ≤ 40%), Total content of 100% (PLA + PBS + nanocellulose = 100%)

Analysis via RSM revealed the optimal ratio for cell culture scaffold production to be 65% PLA, 26.814% PBS, and 8.186% nanocellulose. Subsequently, this ratio was validated through the fabrication of cell culture scaffolds with the aforementioned composition. The fabricated scaffolds were then subjected to characterization for water contact angle, cell culture medium contact angle, and maximum tensile force to corroborate their suitability.

As depicted in Figure 4.15, the water contact angle and cell culture medium contact angle of the scaffolds produced under the optimal conditions were 67.72 degrees and 65.61 degrees, respectively. Furthermore, the maximum tensile force was measured to be 651.425 g.

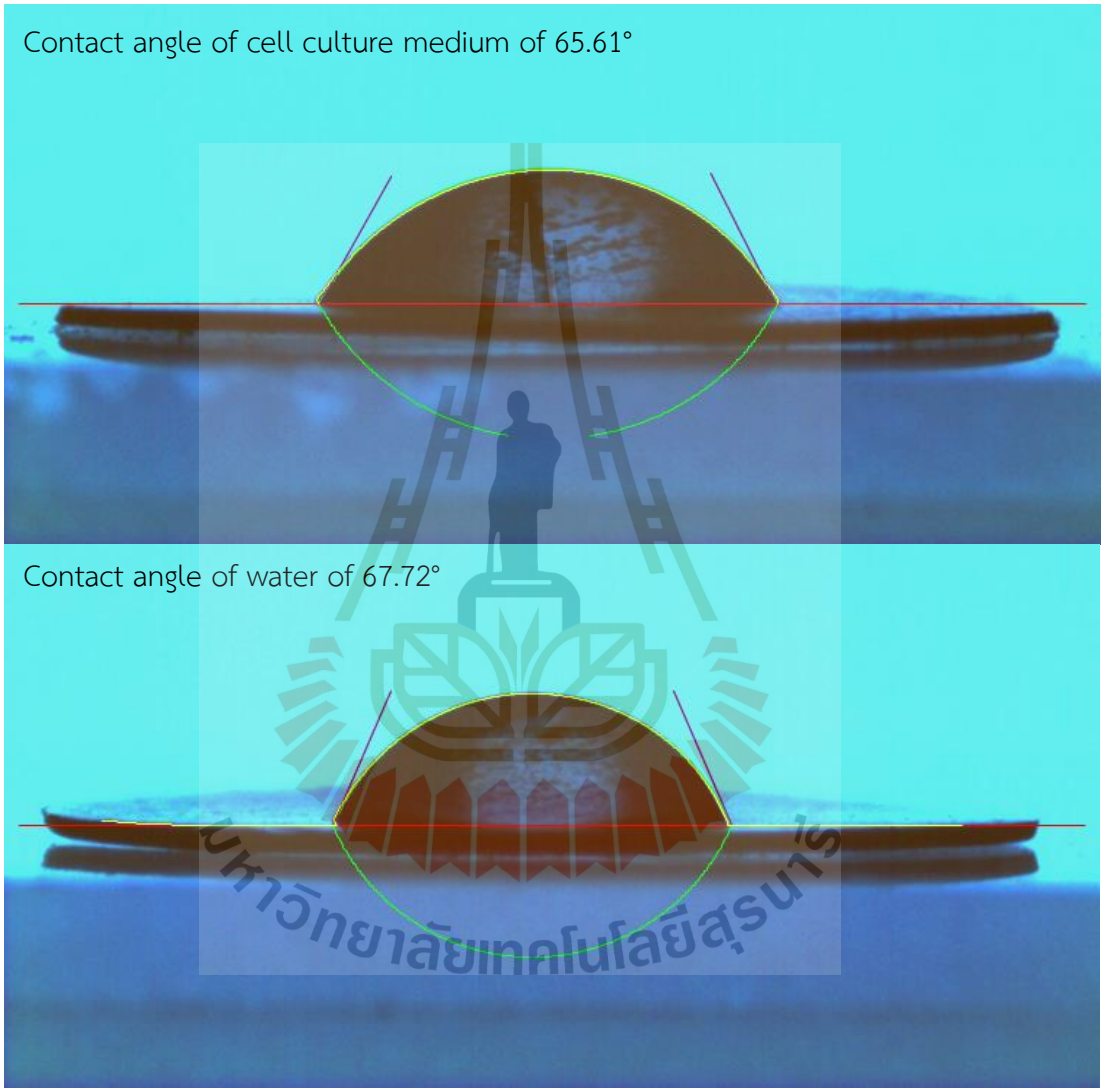

Figure 4.15 contact angle images of cell culture medium (up) and water (bottom) on optimal scaffold

4.2.2 Thermal stability analysis

Thermogravimetric analysis (TGA) was employed to investigate the thermal degradation profiles of nanocellulose, PLA, PBS, PLA/PBS and the composite scaffold, as illustrated in Figure 4.16. The TGA results for nanocellulose exhibited a two-stage weight

loss pattern. The initial stage, likely attributable to the decomposition of inherent natural components, occurred at approximately 180 °C. Notably, the final decomposition temperature of nanocellulose yielded the highest residual weight (29.64%) compared to the other materials. Conversely, the residual weights of PLA, PBS, PLA/PBS, and the scaffold were 10.67%, 6.26%, 1.59%, and 1.57%, respectively. Nanocellulose retains the highest residual weight (29.64%), indicating superior thermal stability due to its crystalline structure and the formation of carbonaceous residues that resist further degradation. In contrast, PLA (10.67%) and PBS (6.26%) decompose more extensively, with PBS exhibiting lower thermal stability than PLA. The PLA/PBS blend (1.59%) and the scaffold (1.57%) show the lowest residual weights, This suggests potential interactions between materials in the blend that may reduce overall thermal stability. The high biodegradability of PLA/PBS and the scaffold is advantageous for biomedical applications such as tissue engineering, where controlled degradation supports tissue regeneration.

Table 4.5 summarizes the critical parameters associated with thermal stability, including the onset decomposition temperature, the peak decomposition temperature, and the final decomposition temperature. It is noteworthy that the thermal degradation of the scaffold exhibited a decrease relative to the individual components. This observation suggests that the blending process might have induced a chemical restructuring within the composite materials.

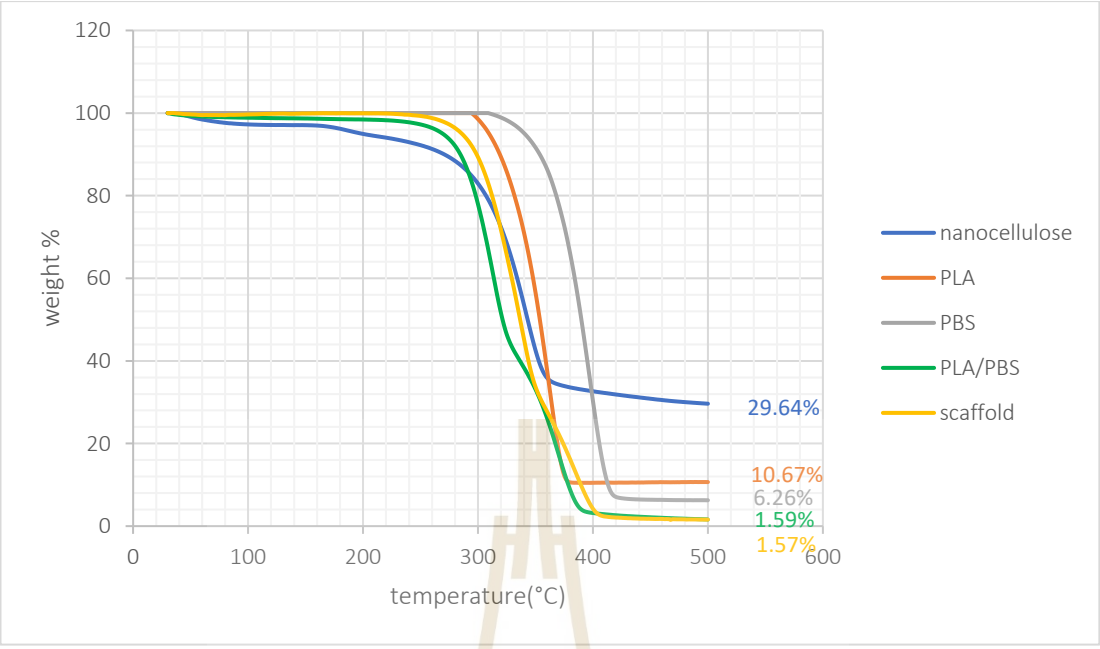

Figure 4.16 weight loss of nanocellulose, PLA, PBS and scaffold (PLA 65%, PBS 26.82%, nanocellulose 8.18%) at temperature of 20 ℃ to 500 ℃

Table 4.5 TGA results of nanocellulose, PLA, PBS and scaffold (PLA 65%, PBS 26.82%, nanocellulose 8.18%)

sample	Starting decomposition temperature	Maximum decomposition temperature	Ending decomposition temperature
nanocellulose	290	340	381
PLA	297	359	390
PBS	320	376	427
PLA/PBS	260	311	409
Scaffold	260	334	415

4.2.3 Thermal properties analysis

Differential scanning calorimetry (DSC) analysis was employed to investigate the thermal properties of PLA, PBS, nanocellulose, and the composite scaffold. The findings, as depicted in Figure 4.17 and summarized in Table 4.6, provide valuable insights into the material behavior of the scaffold.

The DSC thermogram of the nanocellulose revealed a distinct endothermic peak at 187.6 °C, attributable to the evaporation of inherent moisture content. Interestingly, the glass transition temperature (Tg) and melting temperature (Tm) of the PLA fraction exhibited a slight reduction within both the PLA/PBS blend and the composite scaffold compared to pure PLA. The PLA/PBS blend displayed a Tg peak at approximately 64.7 °C and a Tm peak at 149.5 °C. The scaffold exhibited a Tg peak of around 62.3 °C and a Tm peak of 150.4 °C. Notably, the PBS fraction within both the blend and the scaffold displayed distinct Tm peaks at 113.9 °C and 111.7 °C, respectively.

Furthermore, the crystallinity of both the PLA and PBS fractions within the scaffold displayed an enhancement with the incorporation of nanocellulose. This observation suggests that nanocellulose may facilitate the rearrangement of ordered PLA and PBS molecular chains during the blending process. In this context, nanocellulose can be considered analogous to a nucleating agent, acting to promote the crystallization process within the composite scaffold.

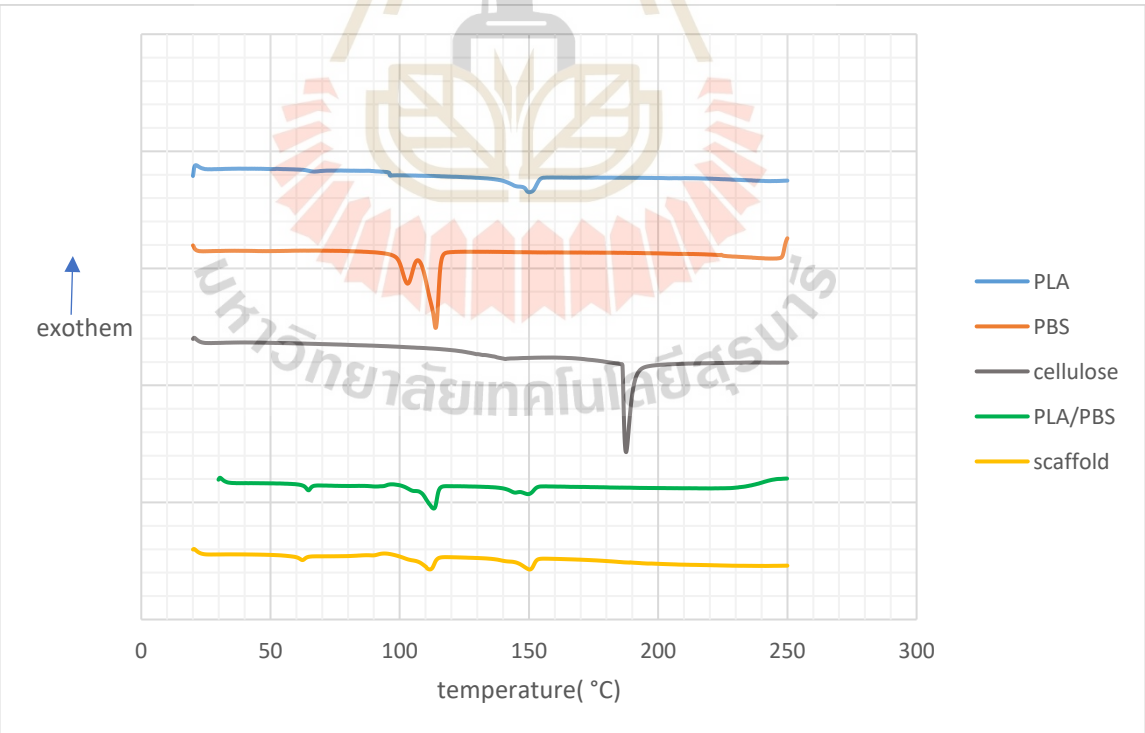

Figure 4.17 DSC results of nanocellulose, PLA, PBS PLA/PBS (PLA 60%, PBS 40%) and scaffold (PLA 65%, PBS 26.82%, nanocellulose 8.18%)

Table 4.6 DSC results of nanocellulose, PLA, PBS, PLA/PBS (PLA 60%, PBS 40%) and scaffold (PLA 65%, PBS 26.82%, nanocellulose 8.18%)

samples	PLA fraction				PBS fraction			
	T_g(°C)	T_m(°C)	H_m (J/g)	X_c(%)	T_g(°C)	T_m(°C)	H_m (J/g)	X_c(%)
PLA	67.1	150.4	31.88	34.27	-	-	-	-
PBS	-	-	-	-	-	113.9	129.3	64.65
PLA/PBS	64.7	149.5	16.23	29.09	-	113.9	37.45	46.81
Scaffold	62.3	150.4	19.87	32.87	-	111.7	27.04	50.41

4.2.4 Morphological analysis

Field-emission scanning electron microscopy (FESEM) was employed to investigate the morphological features of the surface of the nanocellulose-based biopolymer scaffold (comprised of 65 wt% PLA, 26.82 wt% PBS, and 8.18 wt% nanocellulose). The FESEM image, presented in Figure 4.18, depicts a surface topography characterized by abundant miniature pores and a striated texture. The presence of these pores suggests that the scaffold possesses a porous microstructure, which is a crucial characteristic for applications in tissue engineering, as it facilitates cell adhesion, proliferation, and nutrient transport (Lutzweiler et al., 2020). The striated texture observed on the surface may be attributed to phase separation between PLA and PBS, as these polymers have different miscibility and crystallization behaviors (Jompang et al., 2013). The incorporation of nanocellulose likely influences surface morphology by acting as a nucleating agent, leading to the formation of a more structured and interconnected network.

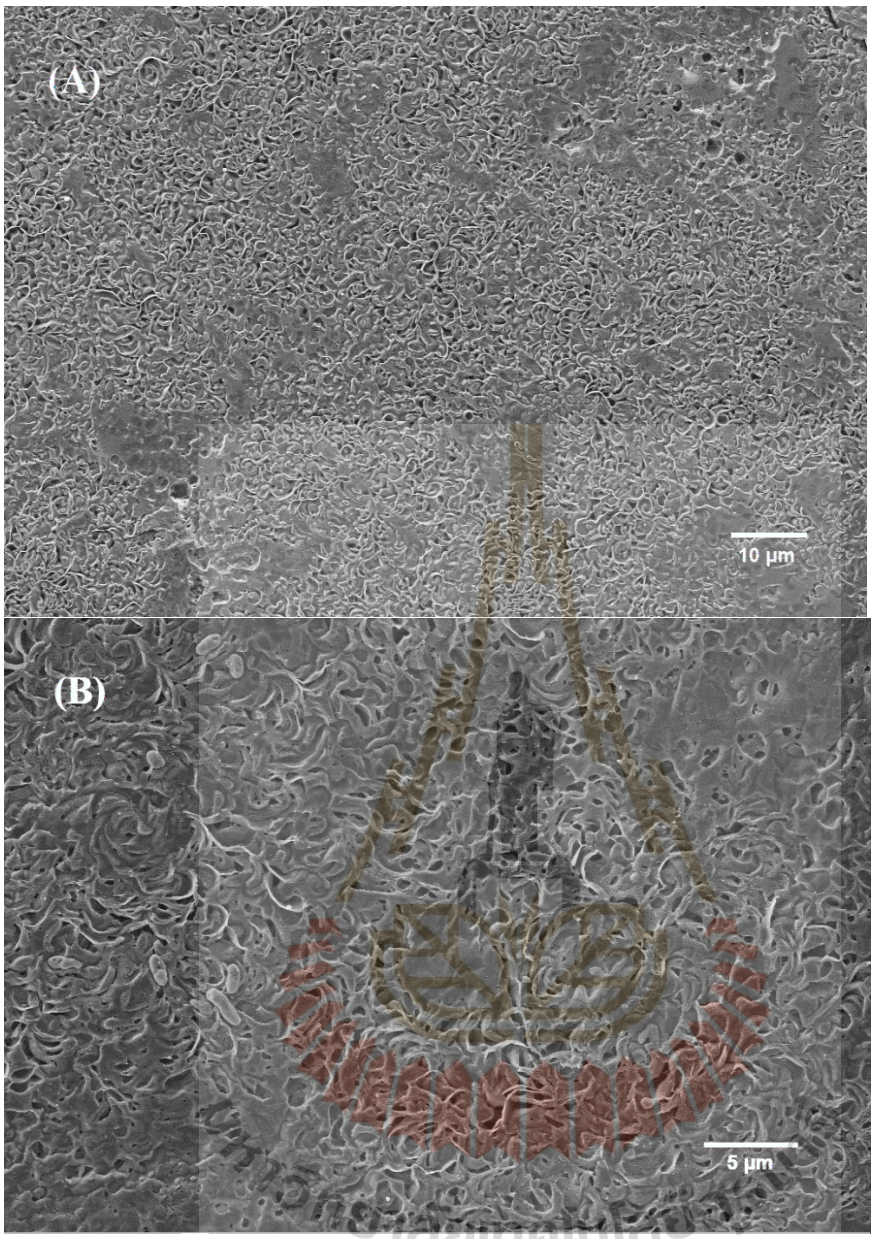
(A)
10 µm
(B)
5 µm

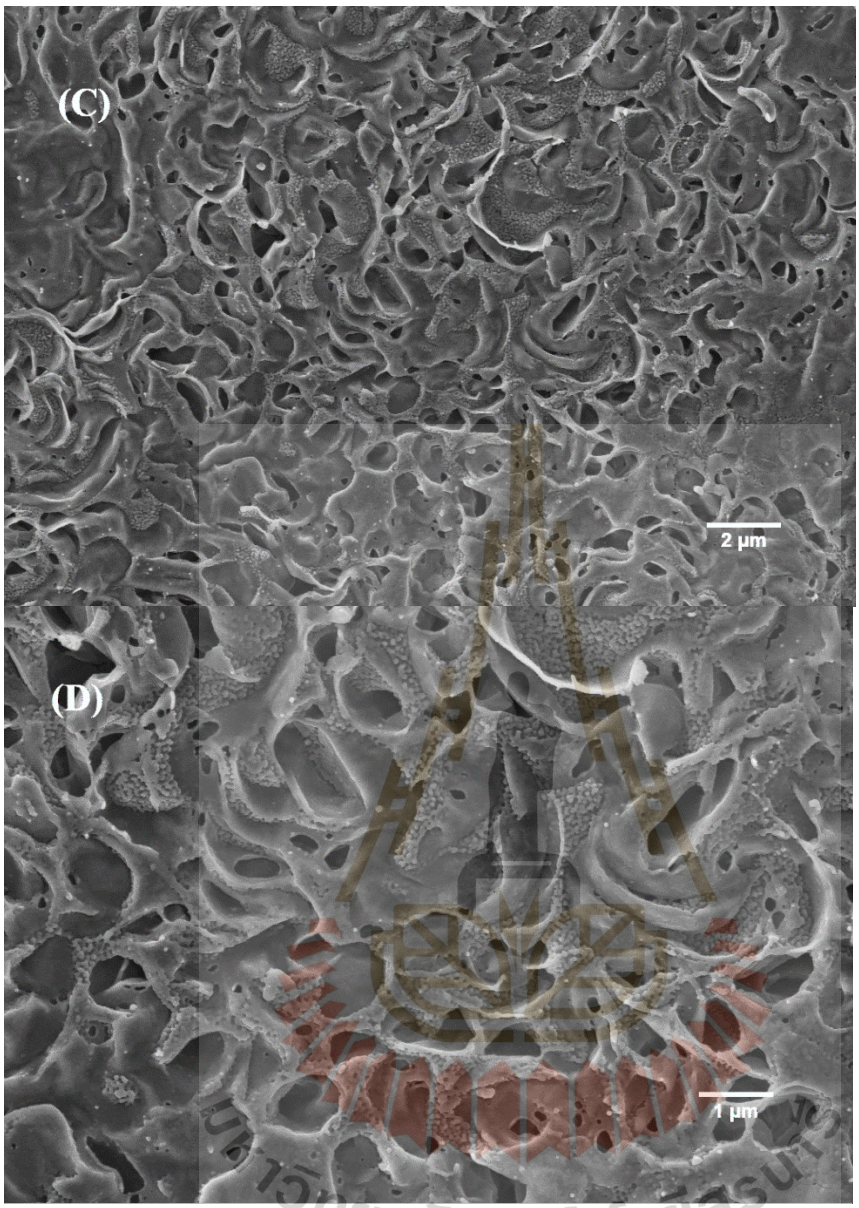

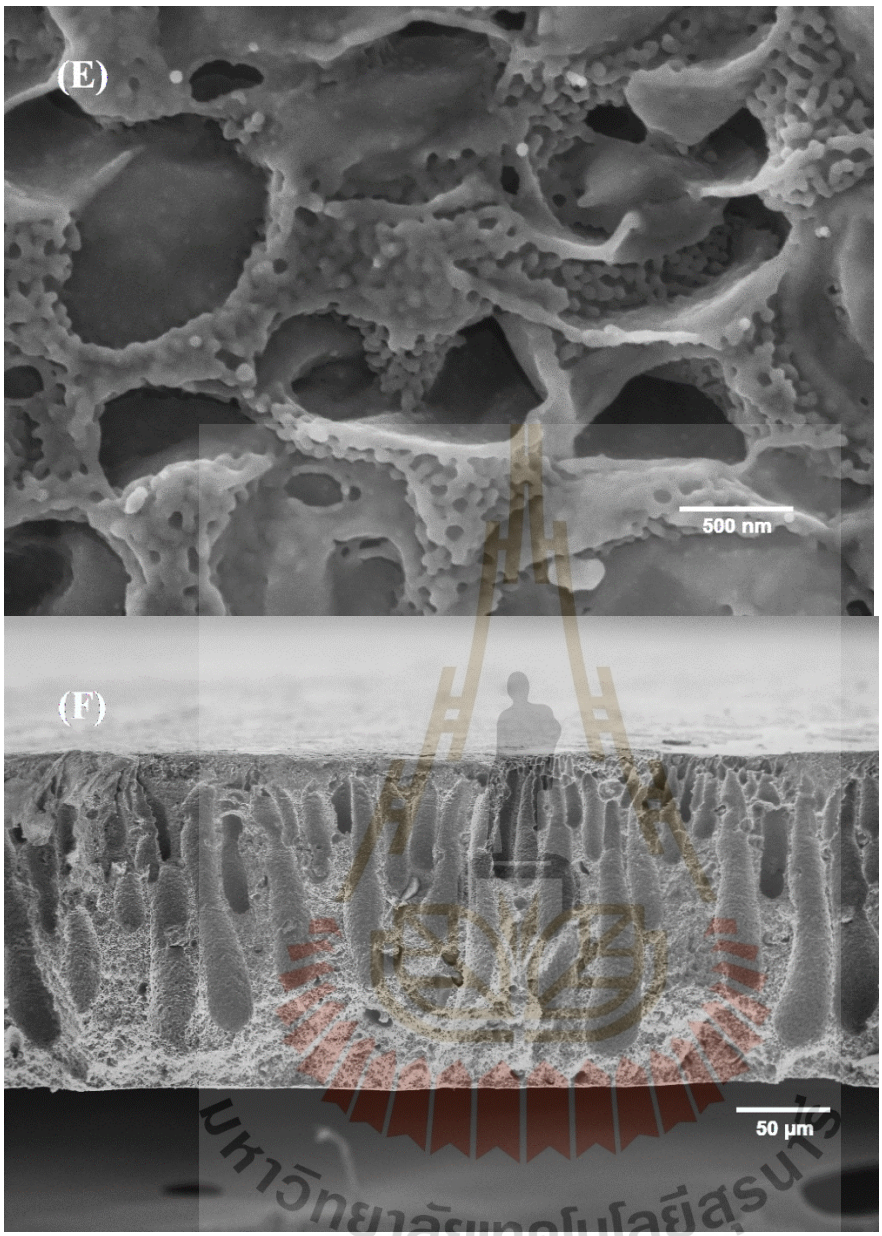

Figure 4.18 morphology of surface structure of nanocellulose based biopolymer scaffold (65% of PLA, 26.82% of PBS and 8.18% of nanocellulose) under FESEM : (A) scale bar of 10 µm, (B) scale bar of 5 µm, (C) scale bar of 2 µm, (D) scale bar of 1 µm (E) scale bar of 500 nm, and (F) cross-sectional area of scaffold, scale of 50 µm.

4.3 Cell culture analysis

4.3.1 Mesenchymal stem cells(hWJ-MSCs) viability on scaffold

An in vitro cytotoxicity evaluation of the scaffold was conducted. Human Wharton's Jelly Mesenchymal Stem Cells (hWJ-MSCs) were co-cultured with the scaffold

material within a complete medium for 72 hours. Subsequently, cell viability was quantitatively assessed using the MTT assay. The experiment was performed in triplicate to ensure data reproducibility. The analysis revealed an average cell viability of 96.65%.

4.3.2 Hepatogenic differentiation of hWJ-MSCs

The process of hepatogenic differentiation in hWJ-MSCs was evaluated microscopically on days 3, 6, 8, 10, 13, 15, and 17 as shown in figure 4.19. Light microscopy observations revealed morphological alterations indicative of hWJ-MSCs transitioning towards a hepatocyte-like morphology. Specifically, no substantial changes in cellular morphology were observed on days 3 and 6. However, on day 8, the cells commenced exhibiting shape transformations, which progressively continued towards the acquisition of a polygonal morphology by day 17.

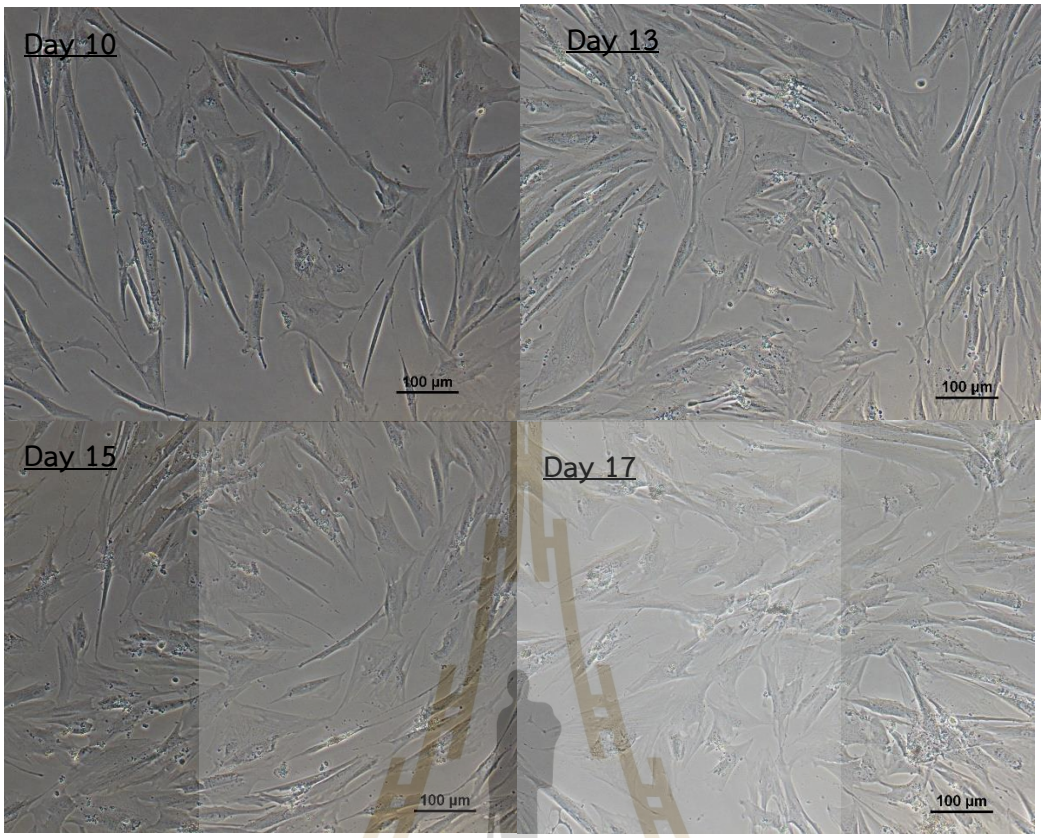

Figure 4.19 morphological change of Hepatogenic differentiation of Human Wharton's jelly – derived mesenchymal stem cells(hWJ-MSCs) for 17 days, scale bar of 100 µm.

4.3.3 Hepatogenic differentiation of Human Wharton's jelly – derived mesenchymal stem cells (hWJ-MSCs) on scaffold

Human Wharton's Jelly Mesenchymal Stem Cells (hWJ-MSCs) were seeded onto the scaffold as shown in Figure 4.20 (upper) to promote their differentiation towards a hepatocyte lineage. The findings, depicted in Figure 4.20 (bottom), corroborate the successful differentiation of hWJ-MSCs into hepatocyte-like cells on the aforementioned nanocellulose-based biopolymer scaffold (comprised of 65 wt% PLA, 26.82 wt% PBS, and 8.18 wt% nanocellulose).

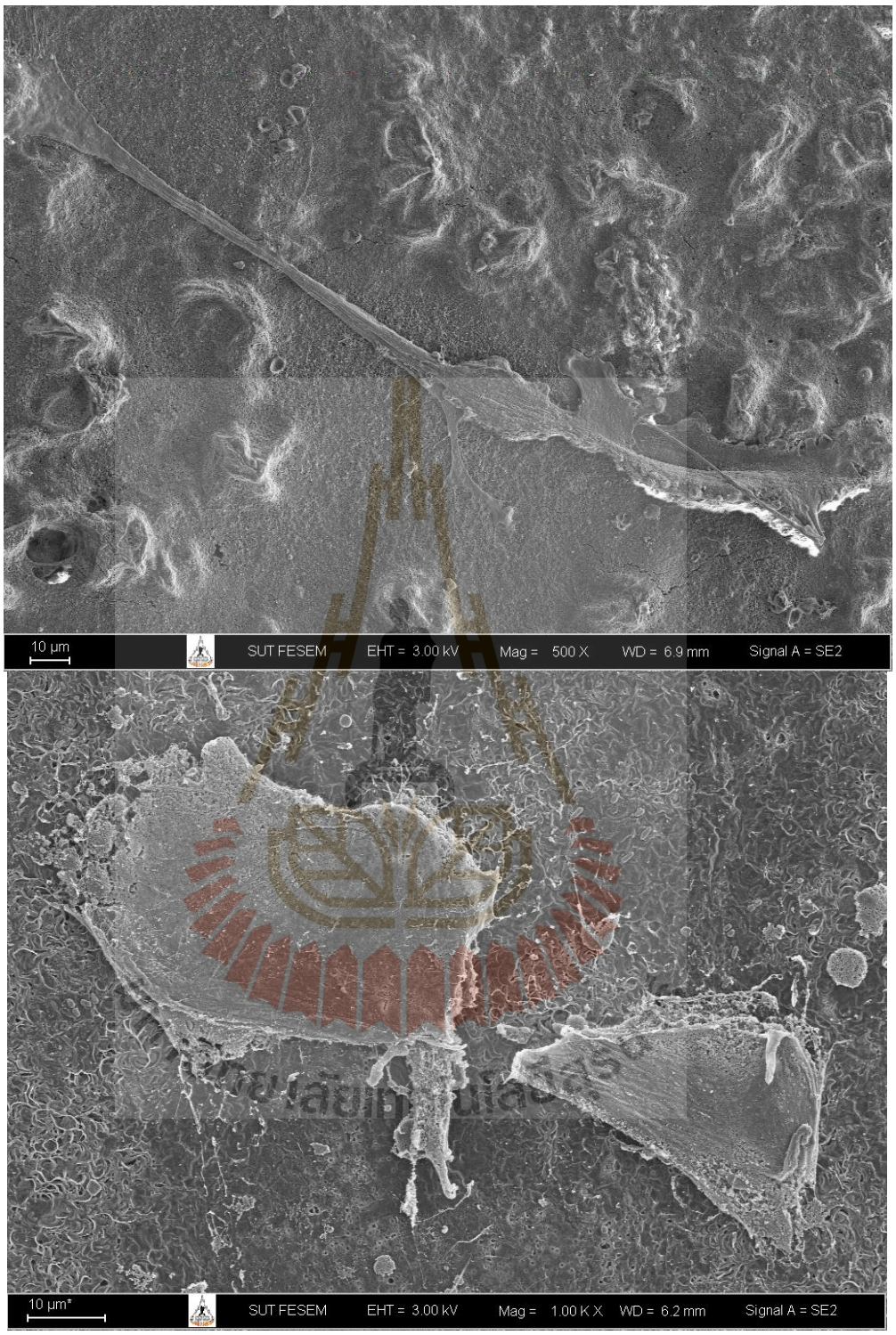

Figure 4.20 FESEM image of Human Wharton's jelly – derived mesenchymal stem cells (hWJ-MSCs) on nanocellulose based biopolymer scaffold (upper) and FESEM image of hepatocyte on nanocellulose based biopolymer scaffold (bottom), Human Wharton's jelly – derived mesenchymal stem cells (hWJ-MSCs) were induced into hepatocyte on scaffold using modified protocol for 17 days.

4.3.4 Immunofluorescence staining

The expression of hepatic markers (AFP, CK18, and ALB) in hepatogenic differentiated cells was investigated. Immunocytochemical analysis of hWJ-MSCs differentiated on the scaffold for hepatic lineage revealed the presence of all three hepatic markers as shown in figure 4.21. This finding supports the successful differentiation of hWJ-MSCs towards a hepatocyte-like phenotype on the scaffold.

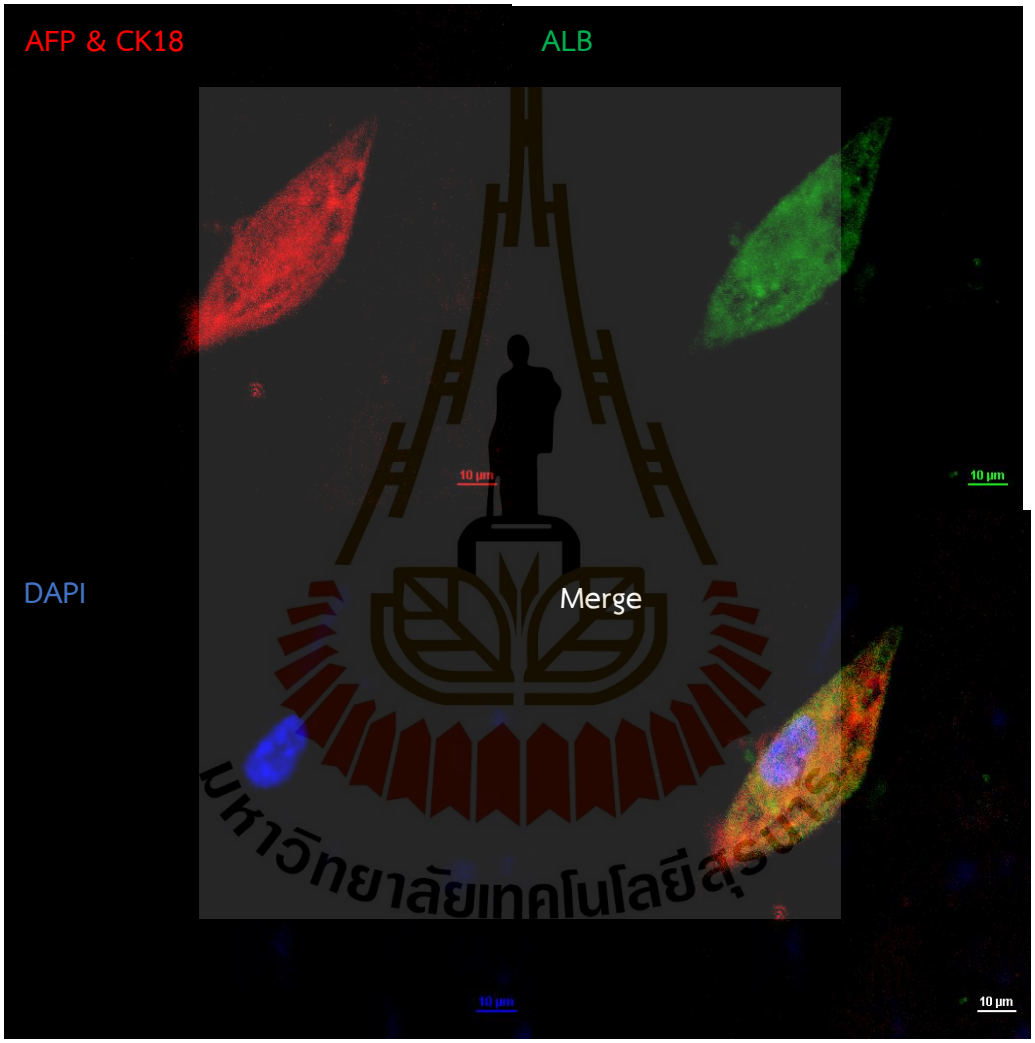

Figure 4.21 immunofluorescence analysis, AFP, CK18 = red, ALB = green and DAPI = blue; nucleus, scale bar = 10 µm.

CHAPTER V
CONCLUSIONS

Nanocellulose was fabricated using a synergistic approach that combines high-pressure homogenization and enzymatic digestion, resulting in the smallest nanocellulose with an average size of 278.9 nm. The optimal scaffold composition consisted of 65.000 wt% PLA, 26.814 wt% PBS, and 8.186 wt% nanocellulose, exhibiting good hydrophilic properties. Biopolymer scaffolds incorporating nanocellulose demonstrate significant potential for tissue engineering applications due to their biocompatibility and safety profile. The scaffold showed the lowest residual weight (1.57%), suggesting a high degree of biodegradability, which is advantageous for controlled degradation in biomedical applications. Additionally, Cells exhibit strong adhesion at multiple sites on the scaffold and demonstrate effective hepatogenic differentiation. This study represents the initial phase in the development of scaffolds that could encourage enhanced cellular adhesion and lay the foundation for advancements in the field of tissue engineering.

Future in vivo studies will be essential to validate these promising in vitro results and thoroughly evaluate the scaffold's performance within a living organism, ultimately paving the way for potential clinical translation. However, this study has some limitations, particularly concerning the translation of these 2D findings into complex 3D structures, which are often required for functional tissue regeneration. The next steps in scaffold refinement involve not only optimizing the scaffold's mechanical properties and degradation rate but also focusing on the fabrication of 3D scaffolds with controlled architecture and porosity, potentially using techniques like 3D bioprinting, to better mimic the native tissue environment and enhance tissue formation.

REFERENCES

Abudula, T., Saeed, U., Memic, A., Kalamegam, G., Hussain, M., & Al-Turaif, H. (2019). Electrospun cellulose Nano fibril reinforced PLA/PBS composite scaffold for vascular tissue engineering. *Journal of Polymer Research, 26*. doi:10.1007/s10965-019-1772-y

Akbar, D. A., Kusmono, Wildan, M. W., & Ilman, M. N. (2020). Extraction and Characterization of Nanocrystalline Cellulose (NCC) from Ramie Fiber by Hydrochloric Acid Hydrolysis. Key Engineering Materials, 867, 109–116. https://doi.org/10.4028/www.scientific.net/kem.867.109

Aliotta, L., Seggiani, M., Lazzeri, A., Gigante, V., & Cinelli, P. (2022). A Brief Review of Poly (Butylene Succinate) (PBS) and Its Main Copolymers: Synthesis, Blends, Composites, Biodegradability, and Applications. *Polymers, 14*(4), 844. Retrieved from https://www.mdpi.com/2073-4360/14/4/844

Alvira, P., Tomás-Pejó, E., Ballesteros, M., & Negro, M. J. (2010). Pretreatment technologies for an efficient bioethanol production process based on enzymatic hydrolysis: A review. *Bioresource Technology*, 101(13), 4851-4861.

Anderson, J. M. (2012). 9.19 - Biocompatibility. In K. Matyjaszewski & M. Möller (Eds.), *Polymer Science: A Comprehensive Reference* (pp. 363-383). Amsterdam: Elsevier.

Anderson, J. M., Rodriguez, A., & Chang, D. T. (2008). Foreign body reaction to biomaterials. *Seminars in Immunology, 20*(2), 86-100.

Badylak, S. F., Taylor, D., & Uygun, K. (2011). Whole-organ tissue engineering: Decellularization and recellularization of three-dimensional matrix scaffolds. *Annual Review of Biomedical Engineering, 13*(1), 27-53.

Bernardo, M. P., da Silva, B. C. R., Hamouda, A. E. I., de Toledo, M. A. S., Schalla, C., Rütten, S., Goetzke, R., Mattoso, L. H. C., Zenke, M., & Sechi, A. (2022). PLA/Hydroxyapatite scaffolds exhibit in vitro immunological inertness and promote robust osteogenic differentiation of human mesenchymal stem cells without osteogenic stimuli. *Scientific Reports*, 12(1), 2333.

Bianco, P., Cao, X., Frenette, P. S., Mao, J. J., Robey, P. G., Simmons, P. J., & Wang, C. Y. (2013). The meaning, the sense, and the significance of mesenchymal stem cells in medicine. *Nature Medicine, 19*(1), 35-42.

Boerjan, W., Ralph, J., & Baucher, M. (2003). Lignin biosynthesis. *Annual Review of Plant Biology*, 54(1), 519-546.

Bondancia, T. J., de Aguiar, J., Batista, G., Cruz, A. J. G., Marconcini, J. M., Mattoso, L. H. C., & Farinas, C. S. (2020). Production of Nanocellulose Using Citric Acid in a Biorefinery Concept: Effect of the Hydrolysis Reaction Time and Techno-Economic

Brethauer, S., R. Shahab and M. Studer (2020). "Impacts of biofilms on the conversion of cellulose." Applied Microbiology and Biotechnology **104**.

Carlström, I. E., Rashad, A., Campodoni, E., Sandri, M., Syverud, K., Bolstad, A. I., & Mustafa, K. (2020). Cross-linked gelatin-nanocellulose scaffolds for bone tissue engineering. *Materials Letters, 264*, 127326. doi:https://doi.org/10.1016/j.matlet.2020.127326

Casasola, R., Thomas, N. L., Trybala, A., & Georgiadou, S. (2014). Electrospun poly lactic acid (PLA) fibres: Effect of different solvent systems on fibre morphology and diameter. *Polymer, 55*(18), 4728-4737. doi:https://doi.org/10.1016/j.polymer.2014.06.032

Castañeda-Rodríguez, S., González-Torres, M., Ribas-Aparicio, R. M., Del Prado-Audelo, M. L., Leyva-Gómez, G., Gürer, E. S., & Sharifi-Rad, J. (2023). Recent advances in modified poly (lactic acid) as tissue engineering materials. *Journal of Biological Engineering, 17*(1), 21. doi:10.1186/s13036-023-00338-8

Chandel, A., da Silva, S., Carvalho, W., & Singh, O. (2012). Sugarcane bagasse and leaves: Foreseeable biomass of biofuel and bio-products. *Journal of Chemical Technology and Biotechnology, 87*. doi:10.1002/jctb.2742

Chandra, R., Takeuchi, H., Hasegawa, T., & Kumar, R. (2007). Improving biodegradability and enzymatic hydrolysis of woody biomass through pretreatment by ammonia fiber explosion (AFEX) and steam explosion. *Bioresource Technology*, 98(8), 1599-1609.

Chen, F. M., Liu, X. (2019). Advancing biomaterials of human origin for tissue engineering. *Progress in Polymer Science, 38*(4), 1637-1655.

Chen, F. M., Zhang, M., & Wu, Z. F. (2007). Toward delivery of multiple growth factors in tissue engineering. *Biomaterials, 28*(2), 346-358.

Chen, L., Zhu, J. Y., Baez, C., Kitin, P., & Elder, T. (2016). Highly thermal-stable and functional cellulose nanocrystals and nanofibrils produced using fully recyclable organic acids. *Green Chemistry*, 13(8), 3835-3843.

Cheng, G., Zhang, X., Simmons, B., & Singh, S. (2014). Theory, practice and prospects of X-ray and neutron scattering for lignocellulosic biomass characterization: Towards understanding biomass pretreatment. *Energy & Environmental Science, 8*. doi:10.1039/C4EE03147D

Chinga-Carrasco, G. (2018). Potential and limitations of nanocellulose-based materials for biomedical applications. *Journal of Nanotechnology*, 2018, 1-13.

Corujo, V. F., Cerrutti, P., Foresti, M. L., & Vázquez, A. (2016). Chapter 2 - Production of Bacterial Nanocellulose From Non-Conventional Fermentation Media. In D. Puglia, E. Fortunati, & J. M. Kenny (Eds.), *Multifunctional Polymeric Nanocomposites Based on Cellulosic Reinforcements* (pp. 39-59): William Andrew Publishing.

Data Page: Sugar cane production, part of the following publication: Hannah Ritchie and Pablo Rosado (2023) - "Agricultural Production". Data adapted from Food and Agriculture Organization of the United Nations. Retrieved from https://ourworldindata.org/grapher/sugar-cane-production [online resource]

de Aguiar, J., Bondancia, T. J., Claro, P. I. C., Mattoso, L. H. C., Farinas, C. S., & Marconcini, J. M. (2020). Enzymatic Deconstruction of Sugarcane Bagasse and Straw to Obtain Cellulose Nanomaterials. *ACS Sustainable Chemistry & Engineering, 8*(5), 2287-2299. doi:10.1021/acssuschemeng.9b06806

De Vries, M. R., Quax, P. H. A., & Van Keulen, J. K. (2019). Immunomodulatory strategies to improve tissue engineering. *Trends in Biotechnology, 37*(7), 759-770.

DeLoid, G. M., Cao, X., Molina, R. M., Silva, D. I., Bhattacharya, K., Ng, K. W., Loo, S. C. J., Brain, J. D., & Demokritou, P. (2019). Toxicological effects of ingested nanocellulose in in vitro intestinal epithelium and in vivo rat models. *Environmental Science: Nano*, *6*(7), 2105-2115.

Devarbhavi, H., Asrani, S. K., Arab, J. P., Nartey, Y. A., Pose, E., & Kamath, P. S. (2023). Global burden of liver disease: 2023 update. *Journal of Hepatology, 79*(2), 516-537. doi:https://doi.org/10.1016/j.jhep.2023.03.017

Dias, M. L., Paranhos, B. A., & Goldenberg, R. (2022). Liver scaffolds obtained by decellularization: A transplant perspective in liver bioengineering. *J Tissue Eng, 13*, 20417314221105305. doi:10.1177/20417314221105305

Ding, D. C., Shyu, W. C., & Lin, S. Z. (2011). Mesenchymal stem cells. *Cell Transplant, 20*(1), 5-14. doi:10.3727/096368910x

Doumenq, A. (2019). The effect of natural degradation process on the cellulose structure of Moroccan hardwood fiber: a survey on spectroscopy and structural properties. Mediterranean Journal of Chemistry, 8, 179-190. doi:10.13171/10.13171/mjc8319050801ab

Dufresne, A. (2012). Nanocellulose: From nature to high-performance tailored materials. *De Gruyter*.

Dufresne, A. (2012). Nanocellulose: From nature to high-performance tailored materials. *De Gruyter*.

Dvir, T., Timko, B. P., Kohane, D. S., & Langer, R. (2011). Nanotechnological strategies for engineering complex tissues. *Nature Nanotechnology, 6*(1), 13-22.

Ebringerová, A. (2006). Structural diversity and application potential of hemicelluloses. *Macromolecular Symposia*, 232(1), 1-12.

El Oudiani, A., Msahli, S., & Sakli, F. (2017). In-depth study of agave fiber structure using Fourier transform infrared spectroscopy. *Carbohydrate Polymers, 164*, 242-248. doi:https://doi.org/10.1016/j.carbpol.2017.01.091

Endes, C., Camarero-Espinosa, S., Mueller, S., Foster, E. J., Petri-Fink, A., Rothen-Rutishauser, B., Weder, C., & Clift, M. J. D. (2016). A critical review of the current knowledge regarding the biological impact of nanocellulose. *Journal of Nanobiotechnology*, 14(1), 78.

Fortunati, E., Armentano, I., Zhou, Q., Puglia, D., Terenzi, A., Berglund, L. A., & Kenny, J. M. (2012). Microstructure and nonisothermal cold crystallization of PLA composites based on silver nanoparticles and nanocrystalline cellulose. *Polymer Degradation and Stability*, 97(10), 2027-2036.

Gigli, M., Fabbri, M., Lotti, N., Gamberini, R., Rimini, B., & Munari, A. (2016). Poly(butylene succinate)-based polyesters for biomedical applications: A review. *European Polymer Journal*, 75, 431-460.

Groll, J., Boland, T., Blunk, T., Burdick, J. A., Cho, D. W., Dalton, P. D., ... & Malda, J. (2016). Biofabrication: Reappraising the definition of an evolving field. *Biofabrication, 8*(1), 013001.

Habibi, Y., Lucia, L. A., & Rojas, O. J. (2010). Cellulose nanocrystals: Chemistry, self-assembly, and applications. *Chemical Reviews*, 110(6), 3479-3500.

Hastuti, N., Kanomata, K., & Kitaoka, T. (2019). Characteristics of TEMPO-oxidized cellulose nanofibers from oil palm empty fruit bunches produced by different amounts of oxidant. *IOP Conference Series: Earth and Environmental Science, 359*, 012008. doi:10.1088/1755-1315/359/1/012008

Hendriks, W. T., Warren, C. R., Cowan, C. A., & Woltjen, K. (2023). Genome editing in stem cells for regenerative medicine. *Nature Reviews Genetics, 24*(1), 31-48.

Hernández-Varela, J. D., Chanona Pérez, J. J., Gallegos-Cerda, S. D., et al. (2021). High-resolution study of garlic and agave cellulose nanoparticles crystalline structures using transmission electron microscopy (TEM). *MRS Advances*, 6, 941–946.

Hietala, E.-M., Salminen, U.-S., Ståhls, A., Välimaa, T., Maasilta, P., Törmälä, P., Nieminen, M. S., & Harjula, A. L. J. (2001). Biodegradation of the Copolymeric Polylactide Stent: Long-Term Follow-Up in a Rabbit Aorta Model. *Journal of Vascular Research*, 38(4), 361-369.

Himmel, M. E., Ding, S. Y., Johnson, D. K., Adney, W. S., Nimlos, M. R., Brady, J. W., & Foust, T. D. (2007). Biomass recalcitrance: Engineering plants and enzymes for biofuels production. *Science*, 315(5813), 804-807.

Hishikawa, Y., Togawa, E., & Kondo, T. (2017). Characterization of Individual Hydrogen Bonds in Crystalline Regenerated Cellulose Using Resolved Polarized FTIR Spectra. *ACS Omega, 2*(4), 1469-1476. doi:10.1021/acsomega.6b00364

Hollister, S. J. (2009). Porous scaffold design for tissue engineering. *Nature Materials, 4*(7), 518-524.

Hu, X., Su, T., Li, P., & Wang, Z. (2018). Blending modification of PBS/PLA and its enzymatic degradation. *Polymer Bulletin, 75*(2), 533-546. doi:10.1007/s00289-017-2054-7

Hutmacher, D. W. (2000). Scaffolds in tissue engineering bone and cartilage. *Biomaterials, 21*(24), 2529-2543.

Jakab, K., Norotte, C., Marga, F., Murphy, K., Vunjak-Novakovic, G., & Forgacs, G. (2010). Tissue engineering by self-assembly of cells printed into topologically defined structures. *Tissue Engineering Part A, 16*(12), 3721-3732.

Javier-Astete, R., & Zolla, G. (2021). Determination of hemicellulose, cellulose, holocellulose and lignin content using FTIR in Calycophyllum spruceanum (Benth.) K. Schum. and Guazuma crinita Lam. *PLOS ONE, 16*. doi:10.1371/journal.pone.0256559

Jompang, L., Thumsorn, S., On, J. W., Surin, P., Apawet, C., Chaichalermwong, T., Kaabbuathong, N., O-Charoen, N., & Srisawat, N. (2013). Poly(Lactic Acid) and Poly(Butylene Succinate) blend fibers prepared by melt spinning technique. *Energy Procedia*, 34, 493-499.

Jonoobi, M., Harun, J., Mathew, A. P., & Oksman, K. (2010). Mechanical properties of cellulose nanofiber (CNF) reinforced polylactic acid (PLA) prepared by twin screw extrusion. *Composites Science and Technology*, 70(12), 1742-1747.

Kanmaz, D., Karahan Toprakci, H. A., Olmez, H., & Toprakçı, O. (2018). Electrospun Polylactic Acid Based Nanofibers for Biomedical Applications. *Material Science Research India, 15*, 224-240. doi:10.13005/msri/150304

Kiran Pulidindi, H. P. (2020). Nanocellulose market size by product (nano fibrillated cellulose, nanocrystalline cellulose), by application (composites, paper processing, food & beverages, paints & coatings, oil & gas, personal care). *Industry Analysis Report, Regional Outlook, Growth Potential, Price Trend, Competitive Market Share & Forecast*, *2026*.

Klemm, D., Heublein, B., Fink, H. P., & Bohn, A. (2005). Cellulose: Fascinating biopolymer and sustainable raw material. *Angewandte Chemie International Edition*, 44(22), 3358-3393.

Kudzin, M., Mrozińska, Z., & Urbaniak, P. (2021). Vapor Phosphorylation of Cellulose by Phosphorus Trichlo-Ride: Selective Phosphorylation of 6-Hydroxyl Function—The Synthesis of New Antimicrobial Cellulose 6-Phosphate(III)-Copper Complexes. *Antibiotics, 10*, 203. doi:10.3390/antibiotics10020203

Kushan, E. (2020). Liquid to Soft Solid Transition of Cellulose Nanocrystal Suspensions in Presence of Micelle Forming Surfactants.

Lam, N. T., Chollakup, R., Smitthipong, W., Nimchua, T., & Sukyai, P. (2017). Utilizing cellulose from sugarcane bagasse mixed with poly(vinyl alcohol) for tissue engineering scaffold fabrication. *Industrial Crops and Products, 100*, 183-197.

Langer, R., & Tirrell, D. A. (2004). Designing materials for biology and medicine. *Nature, 428*(6982), 487-492.

Langer, R., & Vacanti, J. P. (1993). Tissue engineering. *Science, 260*(5110), 920-926.

Laurichesse, S., & Avérous, L. (2014). Chemical modification of lignins: Towards biobased polymers. *Progress in Polymer Science*, 39(7), 1266-1290.

Lee, K. Y., & Mooney, D. J. (2011). Alginate: Properties and biomedical applications. *Progress in Polymer Science, 37*(1), 106-126.

Li, X., Weng, J. K., & Chapple, C. (2014). Improvement of biomass through lignin modification. *The Plant Journal*, 78(4), 631-641.

Lin, N., Huang, J., Chang, P. R., Feng, J., & Yu, J. (2011). Surface acetylation of cellulose nanocrystal and its reinforcing function in poly(lactic acid). *Carbohydrate Polymers*, 83(4), 1834-1842.

Lin, N., Yu, J., Chang, P., Li, J., & Huang, J. (2011). Poly(butylene succinate)-Based Biocomposites Filled With Polysaccharide Nanocrystals: Structure and Properties. *Polymer Composites*, 32, 472-482.

Lionetto F, López-Muñoz R, Espinoza-González C, Mis-Fernández R, Rodríguez-Fernández O, Maffezzoli A. A Study on exfoliation of Expanded Graphite Stacks in Candelilla Wax. Materials (Basel). 2019 Aug 8;12(16):2530. doi: 10.3390/ma12162530. PMID: 31398950; PMCID: PMC6721147.

Liu, X., Holzwarth, J. M., & Ma, P. X. (2016). Functionalized synthetic biodegradable polymer scaffolds for tissue engineering. *Macromolecular Bioscience, 12*(7), 911-919.

Luo, H., Cha, R., Li, J., Hao, W., Zhang, Y., & Zhou, F. (2019). Advances in tissue engineering of nanocellulose-based scaffolds: A review. *Carbohydrate Polymers, 224*, 115144. doi:https://doi.org/10.1016/j.carbpol.2019.115144

Lutolf, M. P., & Hubbell, J. A. (2005). Synthetic biomaterials as instructive extracellular microenvironments for morphogenesis in tissue engineering. *Nature Biotechnology, 23*(1), 47-55.

Lutzweiler, G., Ndreu Halili, A., & Vrana, N. E. (2020). The overview of porous, bioactive scaffolds as instructive biomaterials for tissue regeneration and their clinical translation. *Pharmaceutics*, 12(7), 602.

Luzi, F., Fortunati, E., Jiménez, A., Puglia, D., Pezzolla, D., Gigliotti, G., . . . Torre, L. (2016). Production and characterization of PLA_PBS biodegradable blends reinforced with cellulose nanocrystals extracted from hemp fibres. *Industrial Crops and Products, 93*. doi:10.1016/j.indcrop.2016.01.045

Lynd, L. R., van Zyl, W. H., McBride, J. E., & Laser, M. (2008). Consolidated bioprocessing of cellulosic biomass: An update. *Current Opinion in Biotechnology*, 19(3), 259-264.

MacNeil, S. (2007). Progress and opportunities for tissue-engineered skin. *Nature, 445*(7130), 874-880.

Mahmood, Z., M. Yameen, M. Jahangeer, M. Riaz, A. Ghaffar and I. Javid (2018). Lignin as Natural Antioxidant Capacity.

Makarem, M., Lee, C. M., Kafle, K., Huang, S., Chae, I., Yang, H., . . . Kim, S. H. (2019). Probing cellulose structures with vibrational spectroscopy. *Cellulose, 26*(1), 35-79. doi:10.1007/s10570-018-2199-z

Marrinan, H. J., & Mann, J. (1956). Infrared spectra of cellulose and related polysaccharides. *Journal of the American Chemical Society*, 78(12), 3121-3125.

Martelli-Tosi, M., Torricillas, M. d. S., Martins, M. A., Assis, O. B. G. d., & Tapia-Blácido, D. R. (2016). Using commercial enzymes to produce cellulose nanofibers from soybean straw. *Journal of Nanomaterials, 2016*, 8106814. doi:10.1155/2016/8106814

Md Salim, R., Asik, J., & Sarjadi, M. (2021). Chemical functional groups of extractives, cellulose and lignin extracted from native Leucaena leucocephala bark. *Wood Science and Technology, 55*. doi:10.1007/s00226-020-01258-2

Molina-Cortés, A., Quimbaya, M., Toro-Gomez, A., & Tobar-Tosse, F. (2023). Bioactive compounds as an alternative for the sugarcane industry: Towards an integrative approach. *Heliyon, 9*(2), e13276. doi:https://doi.org/10.1016/j.heliyon.2023.e13276

Mood, S. H., Golfeshan, A. H., Tabatabaei, M., Jouzani, G. S., Najafi, G. H., Gholami, M., & Ardjmand, M. (2013). Lignocellulosic biomass to bioethanol, a comprehensive

review with a focus on pretreatment. *Renewable and Sustainable Energy Reviews*, 27, 77-93.

Moon, R. J., Martini, A., Nairn, J., Simonsen, J., & Youngblood, J. (2011). Cellulose nanomaterials review: Structure, properties, and nanocomposites. *Chemical Society Reviews*, 40(7), 3941-3994.

Mooney, D. J., & Vandenburgh, H. (2008). Cell delivery mechanisms for tissue repair. *Cell Stem Cell, 2*(3), 205-213.

Mosier, N., Wyman, C., Dale, B., Elander, R., Lee, Y. Y., Holtzapple, M., & Ladisch, M. (2005). Features of promising technologies for pretreatment of lignocellulosic biomass. *Bioresource Technology*, 96(6), 673-686.

Murphy, S. V., & Atala, A. (2010). Strategies for tissue and organ regeneration. *Nature Reviews Materials, 3*(6), 77-91.

Murphy, S. V., & Atala, A. (2014). 3D bioprinting of tissues and organs. *Nature Biotechnology, 32*(8), 773-785.

Nair, D. G., & Weiskirchen, R. (2024). Recent Advances in Liver Tissue Engineering as an Alternative and Complementary Approach for Liver Transplantation. *Current Issues in Molecular Biology, 46*(1), 262-278. Retrieved from https://www.mdpi.com/1467-3045/46/1/18

National Renewable Energy Laboratory. (2024). *Biomass Energy Basics*. Retrieved from https://www2.nrel.gov/research/re-biomass

Nechyporchuk, M., Belgacem, M. N., & Bras, J. (2016). Production of cellulose nanofibrils: A review of recent advances. *Industrial Crops and Products*, 93(6), 2-25.

Ng, W. H., Zhang, Y., & Wen, J. H. (2021). Advances in hepatic tissue engineering: Biomaterials and biofabrication techniques. *Acta Biomaterialia, 134*(4), 112-130.

Niklason, L. E., & Langer, R. (2001). Prospects for organ and tissue replacement. *JAMA, 285*(5), 573-576.

Nishiyama, Y., Langan, P., & Chanzy, H. (2002). Crystal structure of cellulose Iβ. *Journal of the American Chemical Society*, 124(31), 9074-9082.

Novosel, E. C., Kleinhans, C., & Kluger, P. J. (2011). Vascularization is the key challenge in tissue engineering. *Advanced Drug Delivery Reviews, 63*(4), 300-311.

O'Brien, F. J. (2011). Biomaterials & scaffolds for tissue engineering. *Materials Today, 14*(3), 88-95.

Okolie, J.A., Nanda, S., Dalai, A.K. *et al.* Chemistry and Specialty Industrial Applications of Lignocellulosic Biomass. *Waste Biomass Valor* **12**, 2145–2169 (2021). https://doi.org/10.1007/s12649-020-01123-0

O'Sullivan, A. C. (1997). Cellulose: The structure slowly unravels. *Cellulose*, 4(3), 173-207.

Panta, W.; Imsoonthornruksa, S.; Yoisungnern, T.; Suksaweang, S.; Ketudat-Cairns, M.; Parnpai, R., Enhanced Hepatogenic Differentiation of Human Wharton's Jelly–Derived Mesenchymal Stem Cells by Using Three-Step Protocol. Int. J. Mol. Sci. 2019;20(12): 3016. https://doi.org/10.3390/ijms20123016

Parihar A, Vongsvivut J, Bhattacharya S. Synchrotron-Based Infra-Red Spectroscopic Insights on Thermo-Catalytic Conversion of Cellulosic Feedstock to Levoglucosenone and Furans. ACS Omega. 2019 May 23;4(5):8747-8757. doi: 10.1021/acsomega.8b03681. PMID: 31459964; PMCID: PMC6648375.

Park, S., Baker, J. O., Himmel, M. E., Parilla, P. A., & Johnson, D. K. (2010). Cellulose crystallinity index: measurement techniques and their impact on interpreting cellulase performance. *Biotechnology for Biofuels, 3*(1), 10. doi:10.1186/1754-6834-3-10

Parry, A. (2016). Nanocellulose and its Composites for Biomedical Applications. *Current medicinal chemistry, 23*. doi:10.2174/0929867323666161014124008

Pashuck, E. T., & Stevens, M. M. (2012). Designing regenerative biomaterial therapies for the clinic. *Science Translational Medicine, 4*(160), 160sr4.

Peciulyte, A., Karlström, K., Larsson, P. T., & Olsson, L. (2015). Impact of the supramolecular structure of cellulose on the efficiency of enzymatic hydrolysis. *Biotechnology for Biofuels, 8*(1), 56. doi:10.1186/s13068-015-0236-9

Peciulyte, A., Karlström, K., Larsson, P. T., & Olsson, L. (2015). Impact of the supramolecular structure of cellulose on the efficiency of enzymatic hydrolysis. *Biotechnology for Biofuels*, 8(1), 56.

Peng, F., Ren, J. L., Xu, F., & Sun, R. C. (2012). Fractional isolation and structural characterization of hemicelluloses from bamboo. *Carbohydrate Polymers*, 87(1), 189-195.

Peng, Y., Gardner, D. J., & Han, Y. (2015). Characterization of mechanical and morphological properties of cellulose reinforced polyamide 6 composites. *Cellulose*, 22, 3199–3215.

Pennsylvania State University. (2024). Hemicellulose structure and role in biomass conversion. *EGEE 439: Alternative Fuels from Biomass*. Retrieved from https://www.e-education.psu.edu/egee439/node/664

Perdoch, W., Mazela, B., Pepliński, B., & Zieliński, M. (2020). Influence of Chemical Pre-Treatments and ultrasonication on the dimensions and appearance of cellulose fibers. *Materials, 13.* doi:10.3390/ma13225274

Phanthong, P., Guan, G., Ma, Y., Hao, X., & Abudula, A. (2016). Effect of ball milling on the production of nanocellulose using mild acid hydrolysis method. *Journal of the Taiwan Institute of Chemical Engineers, 60*, 617-622. doi:https://doi.org/10.1016/j.jtice.2015.11.001

Phanthong, P., Reubroycharoen, P., Hao, X., Xu, G., Abudula, A., & Guan, G. (2018). Nanocellulose: extraction and application. *carbon resources conversion, 1*(1), 32-43. doi:https://doi.org/10.1016/j.crcon.2018.05.004

Pittenger, M. F., Mackay, A. M., Beck, S. C., Jaiswal, R. K., Douglas, R., Mosca, J. D., ... & Marshak, D. R. (1999). Multilineage potential of adult human mesenchymal stem cells. *Science, 284*(5411), 143-147.

Rafiqah, S. A., Khalina, A., Harmaen, A. S., Tawakkal, I. A., Zaman, K., Asim, M., . . . Lee, C. H. (2021). A Review on Properties and Application of Bio-Based Poly(Butylene Succinate). *Polymers, 13*(9), 1436. Retrieved from https://www.mdpi.com/2073-4360/13/9/1436

Ragauskas, A. J., Williams, C. K., Davison, B. H., Britovsek, G., Cairney, J., Eckert, C. A., ... & Tschaplinski, T. (2006). The path forward for biofuels and biomaterials. *Science*, 311(5760), 484-489.

Rahikainen, J., Evans, J. D., Mikander, S., Kalliola, A., Puranen, T., Tamminen, T., & Kruus, K. (2013). Cellulase-lignin interactions—The role of carbohydrate-binding module and pH in nonproductive binding. *Enzyme and Microbial Technology*, 53(5), 315-321.

Ralph, J., Lapierre, C., & Boerjan, W. (2004). Lignin structure and its engineering. *Current Opinion in Biotechnology*, 15(2), 144-152.

Ranakoti, L., Gangil, B., Mishra, S. K., Singh, T., Sharma, S., Ilyas, R. A., & El-Khatib, S. (2022). Critical Review on Polylactic Acid: Properties, Structure, Processing,

Biocomposites, and Nanocomposites. *Materials (Basel), 15*(12). doi:10.3390/ma15124312

Sant, S., Hancock, M. J., Donnelly, J. P., & Khademhosseini, A. (2021). Biomimetic gradient hydrogels for tissue engineering. *Biotechnology Advances, 53*(3), 107724.

Scheller, H. V., & Ulvskov, P. (2010). Hemicelluloses. *Annual Review of Plant Biology*, 61, 263-289.

Singh, A. K., Srivastava, P., & Srivastava, P. (2021). Stem cells: Advances and applications. *International Journal of Biological Sciences, 17*(4), 1121-1135.

Siqueira, G., Bras, J., & Dufresne, A. (2010). Cellulosic bionanocomposites: A review of preparation, properties and applications. *Polymers*, 2(4), 728-765.

Song, R., Murphy, M., Li, C., Ting, K., Soo, C., & Zheng, Z. (2018). Current Development of Biodegradable Polymeric Materials for Biomedical Applications. *Drug Design, Development and Therapy, Volume 12*, 3117-3145. doi:10.2147/DDDT.S165440

Squinca, P., Bilatto, S., Badino, A. C., & Farinas, C. S. (2020). Nanocellulose Production in Future Biorefineries: An Integrated Approach Using Tailor-Made Enzymes. *ACS Sustainable Chemistry & Engineering, 8*(5), 2277-2286. doi:10.1021/acssuschemeng.9b06790

Sridhar, R., Venugopal, J. R., Sundarrajan, S., Ravichandran, R., Ramalingam, B., & Ramakrishna, S. (2011). Electrospun nanofibers for pharmaceutical and medical applications. *Journal of Drug Delivery Science and Technology, 21*(6), 451-468. doi:https://doi.org/10.1016/S1773-2247(11)50075-9

Su, S., Kopitzky, R., Tolga, S., & Kabasci, S. (2019). Polylactide (PLA) and Its Blends with Poly(butylene succinate) (PBS): A Brief Review. *Polymers, 11*(7), 1193. Retrieved from https://www.mdpi.com/2073-4360/11/7/1193

Sugiyama, J., Vuong, R., & Chanzy, H. (1991). Electron diffraction study on the two crystalline phases of native cellulose. *Macromolecules*, 24(14), 4168-4175.

Sun, Y., & Cheng, J. (2002). Hydrolysis of lignocellulosic materials for ethanol production: A review. *Bioresource Technology*, 83(1), 1-11.

Takahashi, K., & Yamanaka, S. (2006). Induction of pluripotent stem cells from mouse embryonic and adult fibroblast cultures by defined factors. *Cell, 126*(4), 663-676.

Tąta, A., Sokołowska, K., Świder, J., Konieczna-Molenda, A., Proniewicz, E., & Witek, E. (2015). Study of cellulolytic enzyme immobilization on copolymers of N-

vinylformamide. *Spectrochimica Acta Part A: Molecular and Biomolecular Spectroscopy*, 149, 494-504.

Thomson, J. A., Itskovitz-Eldor, J., Shapiro, S. S., Waknitz, M. A., Swiergiel, J. J., Marshall, V. S., & Jones, J. M. (1998). Embryonic stem cell lines derived from human blastocysts. *Science, 282*(5391), 1145-1147.

Trache, D., Tarchoun, A. F., Derradji, M., Hamidon, T. S., Masruchin, N., Brosse, N., & Hussin, M. H. (2020). Nanocellulose: From Fundamentals to Advanced Applications. *Frontiers in Chemistry, 8*(392). doi:10.3389/fchem.2020.00392

Trounson, A., & McDonald, C. (2015). Stem cell therapies in clinical trials: Progress and challenges. *Cell Stem Cell, 17*(1), 11-22.

U.S. Department of Energy. (2024). *Biomass Resources*. Retrieved from https://www.energy.gov/eere/bioenergy/biomass-resources

Ullah, I., Subbarao, R. B., & Rho, G. J. (2015). Human mesenchymal stem cells - current trends and future prospective. *Biosci Rep, 35*(2). doi:10.1042/bsr20150025

Wang, B., & Drzal, L. T. (2012). Cellulose nanofiber-reinforced poly(lactic acid) composites prepared by a water-based approach. *ACS Applied Materials & Interfaces*, 4(10), 5079-5085.

Wu, C., McClements, D. J., He, M., Zheng, L., Tian, T., Teng, F., & Li, Y. (2020). Preparation and characterization of okara nanocellulose fabricated using sonication or high-pressure homogenization treatments. *Carbohydrate Polymers*, 117364. doi:https://doi.org/10.1016/j.carbpol.2020.117364

Wulandari, W. T., Rochliadi, A., & Arcana, I. M. (2016). Nanocellulose prepared by acid hydrolysis of isolated cellulose from sugarcane bagasse. *IOP Conference Series: Materials Science and Engineering, 107*, 012045. doi:10.1088/1757-899x/107/1/012045

Xie, J., Willerth, S. M., Li, X., Macewan, M. R., Rader, A., Sakiyama-Elbert, S. E., & Xia, Y. (2010). The differentiation of embryonic stem cells into neural progenitor cells inside electrospun nanofibers. *Biomaterials, 31*(3), 354-362.

Xu, J., & Guo, B.-H. (2010). Poly(butylene succinate) and its copolymers: Research, development and industrialization. *Biotechnology Journal, 5*(11), 1149-1163. doi:https://doi.org/10.1002/biot.201000136

Xu, X., Liu, F., Jiang, L., Zhu, J. Y., Haagenson, D., & Wiesenborn, D. P. (2016). Cellulose nanocrystals vs. cellulose nanofibrils: A comparative study on their microstructures and effects as polymer reinforcing agents. *ACS Applied Materials & Interfaces*, 8(4), 2349-2359.

Yoo, J. J., Lee, S. J., Atala, A. (2011). Biomedical applications of 3D printing. *Journal of Clinical and Translational Research, 12*(3), 23-30.

Zakrzewski, W., Dobrzyński, M., Szymonowicz, M., & Rybak, Z. (2019). Stem cells: Past, present, and future. *Stem Cell Research & Therapy, 10*(1), 68.

Zhang, J., Xue, C., Wang, H., Zhang, X., & Wang, G. (2021). Conductive biomaterials for neural tissue engineering. *Acta Biomaterialia, 134*(5), 12-32.

Zhao, X., Liu, S., Yildirimer, L., Zhao, H., Ding, R., Wang, H., & Cui, W. (2016). Injectable stem cell-laden photocrosslinkable microspheres fabricated using microfluidics for rapid tissue regeneration. *Small, 12*(6), 614-626.

Zhao, X., Zhang, L., & Liu, D. (2012). Biomass recalcitrance: A bottleneck for efficient bioethanol production from lignocellulosic biomass. *BioResources*, 7(3), 3452-3470.

Zoghlami, A., & Paës, G. (2019). Lignocellulosic biomass: Understanding recalcitrance and predicting hydrolysis. *Frontiers in Chemistry*, 7, 874.

BIOGRAPHY

Mister Pongsatorn Poopisut was born on June 1, 1992 in Nakhon Ratchasima, Thailand. He graduated with a Bachelor of Chemical engineering from Suranaree University of Technology in 2016. Then, He worked with Assoc. Prof. Dr. Apichat Boontawan before he studied Master of Science in school of Biotechnology, Institute of Agricultural Technology, Suranaree University of Technology (SUT) with Assoc. Prof. Dr. Apichat Boontawan. He received a Graduate scholarship from SUT to support him tuition and fee. In 2017, His research consisted of process optimization of fast pyrolysis of yeast oil for the biofuel production.

Presentations

Pongsatorn Poopisut, Chotika Gosalawit , Mariena Ketudat-Cairns, Apichat Boontawan 2019 (Oral presentation) Fermentation of an Oleaginous Yeast *Rhodosporidium paludigenum* for biofuels production. 2019 International conference on on green energy systems (ICGES 2019); 2019 oct 9-11; Bangkok, Thailand.

Pongsatorn Poopisut, Apichat Boontawan 2023 (Oral presentation) Production of nanocellulose from sugarcane bagasse for biopolymer composite scaffolds. The 35 th Annual Meeting of the Thai Society for Biotechnology and International Conference "Sustainable Development through Bio-Circular Green (BCG) Economy Model"(TSB 2023); November 26-29, 2023, Greenery Khoa Yai, NaKorn Ratchasima, Thailand

Publications

Pongsatorn Poopisut, Chotika Gosalawit , Mariena Ketudat-Cairns, Apichat Boontawan 2019. Fermentation of an Oleaginous Yeast *Rhodosporidium paludigenum* for biofuels production. *International Journal of Smart Grid and Clean*, v9, n 6, November 2020.

Poopisut, Pongsatorn, Pasama Boonyanan, Pailin Boontawan, Ekarong Sukjit, Nuttapan Promsampao, Nuwong Chollacoop, Mariena Ketudat-Cairns, Adisak Pattiya, and Apichat Boontawan. "Oleaginous Yeast, Rhodotorula Paludigena Cm33, Platform for Bio-Oil and Biochar Productions Via Fast Pyrolysis." *Biotechnology for Biofuels and Bioproducts.* 16, no. 1, 05 February 2023.